DESIGN OF A CONTINUOUS FLOW UV REACTOR FOR OPAQUE LIQUID FOODS BY USING COMPUTATIONAL FLUID DYNAMICS (CFD)

A Thesis Report Submitted to
the Graduate School of Engineering and Sciences of
İzmir Institute of Technology
in Partial Fulfillment of the Requirements for the Degree of

DOCTOR OF PHILOSOPHY

in Food Engineering

by
Mehmet Reşat ATILGAN

June 2013
İZMİR

We approve the thesis of **Mehmet Reşat ATILGAN**

Examining Committee Members:

Assoc. Prof. Dr. Sevcan ÜNLÜTÜRK
Department of Food Engineering, İzmir Institute of Technology

Assoc. Prof. Dr. Figen TOKATLI
Department of Food Engineering, İzmir Institute of Technology

Assist. Prof. Dr. Ünver ÖZKOL
Department of Mechanical Engineering, İzmir Institute of Technology

Assoc. Prof. Dr. Duygu KIŞLA
Department of Food Engineering, Ege University

Assist. Prof. Dr. Ayşe Handan BAYSAL
Department of Food Engineering, İzmir Institute of Technology

24 May 2013

Assoc. Prof. Dr. Sevcan ÜNLÜTÜRK
Supervisor, Department of Food Engineering
İzmir Institute of Technology

Prof. Dr. Ahmet YEMENİCİOĞLU
Head of Department of Food Engineering

Prof. Dr. Tuğrul SENGER
Dean of the Graduate School of Engineering and Sciences

ACKNOWLEDGEMENTS

The author would like to express his sincere gratitude to his adviser, Assoc. Prof. Dr. Sevcan ÜNLÜTÜRK for her supervision, guidance and assistance through this Ph.D. research. Assoc. Prof. Dr. Sevcan ÜNLÜTÜRK subscribed to a substantial amount of her time and effort on this Ph.D. thesis within her greatly appreciated help.

The author is also very grateful to Assoc. Prof. Dr. Figen TOKATLI and Assist. Prof. Dr. Ünver ÖZKOL for their valuable knowledges and commands during Ph.D. progressing of the research. The author is thankful of Assist. Prof. Mehmet ÜNLÜTÜRK for the great support in user defined functions. The author would like to thank Assist Prof. Dr. Ayşe Handan BAYSAL for her great experience of food microbiology, insurance of microbial stock cultures and devoted the time to serve as the thesis committee.

The author would like to thank specialist Burak SEVİN for his substantial amount of time and great experience in operation of ANSYS software components and computational fluid dynamics aspects. The author is also thankful to Çağrı KURUCU for his great help and support for construction of continuous flow UV reactor.

The author would like to thank to his colleauges Research Assistants Özgür Apaydın TARHAN, Bengi Hakgüder TAZE and Nihan GÖĞÜŞ for deep friendship, sharing the Ph.D. period, great sincere support and motivation to terminate his partial desperation, time by time. The author is also thankful for the suport of his family and his friends.

The author acknowledges IZTECH (Izmir Institute of Technology) for its financial support. This study was supported by the Department of Food Engineering, Izmir Institute of Technology, Izmir, Turkey (2010IYTE09).

This thesis is dedicated to author’s wife, Duygu Kocabaş ATILGAN, author’s father, Yaşar ATILGAN (R.I.P.), his mother, Gülgün ATILGAN and sisters, Berrin and Ayşegül ATILGAN

ABSTRACT

DESIGN OF A CONTINUOUS FLOW UV REACTOR FOR OPAQUE LIQUID FOODS BY USING COMPUTATIONAL FLUID DYNAMICS (CFD)

UV-C radiation is usually applied as an alternative non-thermal process for clear liquid food products in order to achieve microbiologically safe and shelf stable products.

The main objective of this Ph.D. study was to design a UV reactor inorder to provide efficient UV dose/intensity distribution to reach minimum 5 log microbial reduction in opaque liquid foods. For this purpose, a S-shaped, thin film, continuous flow UV reactor was designed and constructed. UV dose/intensity delivered in the UV system was measured and determined by means of biodosimetric, actinometric and computational fluid dynamics (CFD) methods.

Inactivation performance of the UV reactor was assesed by using both clear and freshly squeezed opaque white grape juices. The number of spoilage yeast, lactic acid bacteria and *E.coli* K-12 (ATCC 25253) in opaque grape juice was reduced to 1.604, 4.133 and 5.431 log at UV dose levels of 247.302, 301.113 and 273.520 mJ/cm^2 respectively. For clear grape juice samples inoculated with *S.cerevisiae* and *E.coli* K-12 (ATCC 25253), 6.498 and 5.986 log reductions were achieved at UV dose levels of 1001.618 and 577.245 mJ/cm^2.

The microbial shelf life of freshly squeezed grape juice was extended up to fourteen days which was two times longer compared to untreated samples at refrigerated conditions. The physicochemical properties of UV-C processed grape juice were also evaluated during storage. Although pH, total soluble content (Bix %) and total titratable acidity were not affected from UV treatment, significant changes observed in pH, turbidity, color properties, total soluble content (Brix %), total titratable acidity and ascorbic acid (Vitamin C) content during storage.

ÖZET

YARI SAYDAM SIVI GIDALAR İÇİN SÜREKLİ AKIŞ UV REAKTÖRÜN HESAPLAMALI AKIŞKANLAR DİNAMİĞİ KULLANILARAK DİZAYNI

UV-C ışınlama, alternatif ısıl olmayan bir işlem olarak, mikrobiyolojik kaliteyi ve raf ömrünü arttırmak amacıyla berrak sıvı gıda ürünlerinde sıklıkla kullanılmaktadır.

Bu doktora çalışmasının temel amacı, yarı berrak sıvı gıdalarda 5 logaritmik birim mikrobiyal azalma sağlayabilmek için uygun UV doz/intensite dağılımını sağlayacak bir UV reaktör tasarlamaktır. Bu amaç doğrultusunda bir S-şekilli sürekli akış UV reaktörü tasarlanmış ve montajı gerçekleştirilmiştir. UV sistem içerisinde alınan UV doz/intensite değerleri de biyodozimetrik, aktinometrik ve hesaplamalı akışkanlar dinamiği metotlarıyla ölçülmüş ve belirlenmişlerdir.

UV reaktörün inaktivasyon performansı da hem saydam hem de yarı saydam taze sıkılmış opak üzüm suyu örnekleriyle incelenmiştir. UV inaktivasyon sonucunda, bozulmaya neden olan maya, laktik asit bakterisi ve *E.coli* K-12 (ATCC 25253) bakterisi, opak üzüm suyu içerisinde sırasıyla 1.604, 4.133 ve 5.431 logaritmik birim azaltılmıştır. Bu azalma değerlerine sırasıyla 247.302, 301.113 ve 273.520 mJ/cm^2 UV doz miktarlarında ulaşılmıştır. Öte yandan saydam üzüm suyu içerisine inoküle edilen *S.cerevisiae* mayası ve *E.coli* K-12 bakterisi de sırasıyla 1001.618 ve 577.245 mJ/cm^2 UV doz değerlerinde 6.498 ve 5.986 logaritmik birim azaltılmışlardır.

Bununla birlikte, UV ışınlamaya maruz bırakılan taze sıkılmış üzüm suyu için mikrobiyolojik raf ömrü çalışması yapılmış ve raf ömrünün, buzdolabı koşullarında işlemden geçirilmemiş üzüm suyuna göre iki kat daha uzun (on dört gün) sürdüğü gözlemlenmiştir. Raf ömrü çalışması boyunca, UV ışınlamaya maruz bırakılan taze sıkılmış üzüm suyunun fizikokimyasal özellikleri de incelenmiş ve pH, toplam çözünebilen madde (Brix %) ve toplam asitlik değerlerinin UV ışınlama işlemi ile değişmediği gözlemlenmiştir. Bunun yanında, pH, bulanıklık, renk özellikleri, toplam çözünebilen madde miktarı (Brix %), toplam asitlik ve askorbik asit (C vitamini) miktarı gibi özelliklerin raf ömrü boyunca değiştiği görülmüştür.

TABLE OF CONTENTS

LIST OF FIGURES

LIST OF TABLES

LIST OF SYMBOLS AND ABBREVIATIONS

CFD	Computational fluid dynamics
LAB	Lactic acid bacteria
LFPs	Liquid food products
PCGJ	Pasteurized clear grape juice
FSOGJ	Freshly Squeezed Grape Juice
UDF	User defined function
MPSS	Multiple point source summation
Re	Reynolds number
z	Axial distance of UV reactor (m)
r	Radial distance of UV reactor (m)
z_i	Axial distance at i^{th} position of light source (m)
l_i	Distance from the current location to the i^{th} number of point source (m)
m	Point number of UV light source
A_{254}	Absorbance coefficient (m) at 254 nm
I_0	Incident intensity (mW/cm^2)
I_{ave}	Average intensity (mW/cm^2)
d	UV dose (mJ/cm^2)
L	Length of UV reactor (m)
P	Power of UV light source (W)
Q	Volumetric flow rate (mL/s)
RTD	Residence time distribution (s)
γ	Path length in Beer Lambert law (cm)
t	UV treatment time
N_0	Initial microbial population
N	Survival microbial population at any treatment time
k	Inactivation rate constant (min^{-1}) for Log Linear model
α	Scale parameter in Weibull model
β	Shape parameter (concavity index) in Weibull model
t_R	Reliable time
k_1	Inactivation rate constant (min^{-1}) for modified Chick-Watson Model
k_2	First order UV decay constant (min^{-1}) for modified Chick-Watson Model

k’	Inactivation rate constant (min^{-1}) of Hom model
h	UV penetration rate constant of Hom model
TSA	Tryptic soy agar
PDA	Potato dextrose agar
MRS	De Man Rogosa agar
RMSE	Root mean squared error
OD	Optical density
$[c_{iodide}]$	Initial concentration of iodide (M)
Φ	Quantum yield in chemical actinometry
l	Path length in spectrophotometic measurements
$[c_{triiodide}]$	Concentration of iodide (M) formed by photoreaction
nb	Neighbor cells
a_p, a_{nb}	Linearized source terms
ρ	Density (kg/m^3)
υ	Velocity (m/s)
α_i	Fraction of particles
D_i	Average dose for the i^{th} bin interval
$\vec{J}$	Diffusion Flux
R	Source term (referred to be reaction rate)
C	Concentration (number) of microbial populaton
E (r,z)	Total fluence rate
υ_n	Particle velocity normal to the wall
e_t	Momentum in the direction tangential to the wall
θ_1, θ_2	Reflection angles of particles
κ	ratio of inner diameter to outer diameter
D_{out}	Outer diameter (m)
μ	Apparent viscosity (kg/m.s).
L*	Brightness
a*	Redness-greenness
b*	Yellowness-blueness
ΔE	Total color difference
BI	Browning index
TA	Total acidity

f	Normality factor
E	Miliequivalent weight of citric or tartaric acid
M	Sample volume
c	Ascorbic acid concentration (g/L of sample)

CHAPTER 1

INTRODUCTION

The primary public health concern for liquid food products (LFP) is foodborne diseases, caused by microorganisms such as *Escherichia coli* O157:H7, *Salmonella*, *Listeria*, *Yersinia* or *Campylobacter*, thermophilic *Bacillus* strains and *Alicyclobacillus acidoterrestris* and lactic acid bacterias such as *Lactobacillus and Leoconostoc* (Caminiti et al, 2012; Franz et al, 2009; Geveke, 2008; Lee et al, 2001; Mańas et al, 2003, Matak et al, 2005, 2007; Muriana, 1997; Ngadi et al, 2003; Ponce et al, 1999; Wright et al, 2000; Wrigley and Llorca, 1992) or spoilage yeasts such as *S.cerevisiae* and *Zigosaccharomyces bailii* (Battey et al, 2002; Keyser et al, 2008; Lu et al, 2010; Ochoa-Velasco and Guerrero Beltrán, 2012; Qiu et al, 1998; Tran and Farid, 2004). Pasteurization is the treatment method of foods that does not kill all microorganisms in the food. Instead, it reduces the number of viable pathogens so they are unlikely to cause disease (Lewis and McIndoe, 2004; McDonnel, 2009; Mcdonnel and Purke, 2011). Unlike pasteurization, disinfection is named as the treatment process of which pathogenic microorganisms in the food are eliminated chemically, excluding bacterial spores (Lewis and McIndoe, 2004; McDonnel, 2009). Disinfection can be applied by physical or chemical methods. Chemicals used for disinfection can be named as disinfectants having different target of microbial groups in food materials. Hence, for these kind of products a proper disinfection method needs to be applied in addition to the aseptic processing to overcome this problem.

Pasteurization plays a fundamental role for ready-to-use and shelf stable LFPs for the aim of the elimination of foodborne microorganisms. The most common pasteurization method for LFPs is the thermal treatment used for the inactivation of microorganisms by applying heat for defined periods of time (Muriana, 1997). Although thermal pasteurization is an effective method of killing microorganisms; it causes some undesirable effects on the volume, quality and functional properties of the fruit juices (Baumann et al, 2005; Bermudez-Aguirre and Barbosa-Canovas, 2012; Cheng et al, 2007; Góngora-Nieto et al, 2003; Hermawan et al, 2004; Tiwari et al, 2009a, 2009b; Ugarte-Romero et al, 2006; Wong et al, 2011).

Nowadays, food industry is used non-thermal alternative methods, as opposed to thermal processing, which has high operational cost and negative nutritional and quality effects on foods. Research on non-thermal technologies like high pressure, pulsed electric fields, ultraviolet light, irradiation, and ultrasound have been developed (Garde-Cerdàn et al, 2007; Marsellés-Fontanet and Martín-Belloso, 2007; Marsellés-Fontanet et al, 2009; Ozkan et al, 2004; Torkamani and Niakousari, 2011; Walkling-Ribeiro et al, 2008; Wu et al, 2005). Alternative non-thermal pasteurization methods combined with aseptic packaging are explored to extend the shelf life and minimize disadvantages of thermal processing of LFPs (Ball et al, 1987; Bazhal et al, 2000; Bialka and Demirci, 2007; Caminiti et al, 2012; Choi et al, 2010; Choudhary and Bandla, 2012; Ma et al, 1997; Manas et al, 2003; Montenegro et al, 2002; Plaza et al, 2006; Ponce et al, 1999; Ukuku and Geveke, 2010; Welti-Chanes et al, 2009; Wong et al, 2010; Wrigley and Llorca, 1992).

Moreover, most of these methods have also some disadvantages including substantial changes in the structure of LFPs causing coagulation and denaturation of proteins. UV-C radiation is also used as an alternative non-thermal process for LFPs in order to achieve microbiologically safe and shelf stable products (Bintsis et al, 2000). UV-C irradiation between 200-280 nanometers, has been widely used for disinfection of transparent, semi-transparent liquid foods in addition to solid food surfaces due to its germicidal effect (Bolton and Linden, 2003; Koutchma et al, 2009). For this purpose, UV-C irradiation has been commercialized as a non thermal processing of fruit juices. Moreover, 253-264 nanometer has the peak point in the UV-C light spectrum, generating complete destruction of microorganisms. No negative organoleptic and nutritional effects of UV irradiation on liquid food material are reported. Besides, high operation and separation costs of the other methods can be decreased by application of UV-C irradiation (Garibaldi et al, 2003). Photochemical damage to nucleic acids in cellular structure is the main mechanism of germicidal UV-C light, resulting prevention of cell replication and cell lysis (Bank et al, 1990; Bintsis et al, 2000; Miller et al, 1999).

Use of ultraviolet irradiation was allowed by Food and Drug Administration (FDA) to eliminate foodborne pathogens and other microorganisms in juice products since November 29, 2000. UV disinfection method is mainly applied in wastewater treatment of food and beverages (Blume and Neis, 2004, Chmiel et al, 2002, Green et al, 1995, Hassen et al, 2000), treatment of drinking water (Lehtola et al, 2004; Peldszus et al, 2003), pasteurization of milk and clarified fruit juices (Bandla et al, 2012; Choudhary et al, 2011; Koutchma et al, 2004; Matak et al, 2005). Elimination of heat resistant yeasts and lactic

acid bacteria by UV-C treatment is also another application in the orange juice (Keyser et al, 2008; Otezia et al, 2010; Tran and Farid, 2004) apple juice and cider processing (Basaran et al, 2004; Char et al, 2010; Choi and Nielsen, 2005; Donahue et al, 2004; Gabriel, 2012; Gabriel and Nakano, 2009; Geveke, 2005; Guerrero-Beltrán and Barbosa-Cánovas, 2005; Harrington and Hills, 1968; Murakami et al, 2006; Noci et al, 2008; Palgan et al, 2011; Quintero-Ramos et al, 2004; Wright et al, 2000). It is also applied in tropical fruit juice production such as pitaya, mango, guava-and pineapple, mango and pineapple juices (Gouws et al, 2005; Keyser et al, 2008; Ochoa-Velasco and Guerrero Beltrán, 2013), liquid egg products (Ngadi et al, 2003; Unluturk et al, 2008, 2010) and grape juice processing (Guerrero-Beltrán et al, 2009; Geveke and Torres, 2012). Besides, UV treatment is applied on enzyme inactivation of fruit (Guerrero-Beltrán and Barbosa-Cánovas, 2006; Luse and McLaren, 1963).

Main advantages of UV disinfection process are the reduction of total operational cost without leaving any hazardous chemicals, and being safe process with environmentally friendly system. Hence, UV process can have automatically operating option, in addition to ease of reconstruction and maintenance. UV-C light treatment has also been used in the food industry for different purposes including air sanitation in the meat and vegetable processing, reduction of pathogen microorganisms in red meat, poultry and fish processing (Liltved and Landfald 2000; Wong et al, 1998). Elimination of heat resistant yeasts, moulds, *Bacillus subtilis* and *Bacillus pumilus* spore in the orange juice by means of UV-C treatment is also studied (Tran and Farid 2004). Although UV disinfection method is widely used for water and wastewater treatment as a non-thermal method, application to food industry is recent and limited to transparent liquid foods, and not used efficiently for opaque LFPs. There are some attempts to design a UV reactor for disinfection of opaque liquid foods (Sozzi and Taghipour, 2006; Taghipour, 2004). However, these studies are still under investigation.

Efficiency of UV treatment depends on the determination of applied UV dose/intensity exposed by the food material. The determination of UV dose/intensity received by the fluid elements in continuous flow UV systems is a big challenge. The presence of particles that receive different range of UV dose/intensity due to having different location and residence time during flow motion contributes this challenge. That causes complications for measurement of UV dose distribution throughout a flow volume. There are several methods to determine UV intensity and UV dose distributions on treated fluid foods such as biodosimetry, chemical actinometry and a method based on

computational fluid dynamics (CFD). Biodosimetry is the bioassay method where the liquid food inoculated with a target microorganism is first UV treated by static bench top collimated beam aparatus. The dose response curve is created and inactivation rate of UV treatment is determined by applying an inactivation model. Then same fluid food is UV treated in continuous flow UV reactor and inactivation rate obtained in the UV system is recorded. The dose is determined by matching the inactivation rate and marking the UV dose on UV dose response curve. Chemical actinometry method determines the UV dose distribution based on the photochemical reaction of UV sensitive actinometry chemicals. UV dose and intensity is obtained spectrophotometrically by measuring the absorbance of concentration of the chemicals undergoing to photoreaction. In the method based on computational fluid dynamics, physical geometry and grid structure of the domain is created. Then numerical solution was applied using the integration of flow models, an appropriate UV intensity distribution model and discrete phase model (DPM) in a commercial CFD solver. Results were examined and compared with experimental data.

UV dose (UV intensity x UV exposure time) in biodosimetric method is uniform in the irradiated samples. This is supplied by providing a good mixing and a small liquid volume in a petri dish used in a bench top collimated beam apparatus. Biodosimetry method can provide only single average intensity to calculate UV dose. Besides, the applicability of actinometric methods for measurement of single average UV dose/intensity in colored fruit juice is challenging. On the other hand, there are great variations in UV dose distribution in continuous flow UV treatment systems when multiphase (particle-liquid) fluid foods are irradiated. It is essential to determine the location and residence time distribution of particles found in liquid phase throughout the flow volume and then predict the UV dose/intensity received by each particle. It is more rational to find the distribution of UV intensity/dose in continuous flow UV systems rather than the determination of single value based on biodosimetric method and actinometric method.

The overall objective of this Ph.D. study was to design a UV reactor in such a way that to provide efficient UV dose/intensity distribution in order to reach minimum 5 log microbial reduction in opaque food liquids (i.e., freshly squeezed grape juice, FSOGJ). For this purpose, a S-shaped, thin film, continuous flow UV reactor was designed and constructed. UV dose/intensity delivered in the UV system was measured or determined by means of biodosimetric, actinometric and CFD methods.

In the first part of this study (Chapter 3), UV dose response curves were constructed for UV-C irradiated opaque and clear grape juices inoculated with different

target microorganisms (e.g., yeast, lactic acid bacteria, *E.coli* K-12) by means of biodosimetric method in order to determine the UV dose delivered in the constructed UV system. Additionally, the inactivation efficiency of bench top collimated beam apparatus for freshly squeezed opaque and pasteurized clear grape juice was also investigated and different mathematical models were used for the inactivation kinetics.

In the second part of the Ph.D. study (Chapter 4), the UV intensity and UV dose level in S-shaped continuous flow UV reactor were measured by using chemical actinometric method. Iodide/iodate method was used for actinometry. Two different studies were carried out. The first study was designed to test for comparison of the UV intensity recorded by radiometer and and measured by chemical actinometry in bench top collimated beam apparatus. The second study was conducted to determine the UV intensity in continuous flow UV reactor by the help of triiodide (I_3) formation from the potassium iodide (KI) solution reacting under UV exposure.

In the third part of the Ph.D. study (Chapter 6), a general approach was developed by integrating a flow model, Multiple point summation (MPSS) UV intensity distribution model and Discrete Phase (DPM) model for prediction of UV dose/intensity distribution in opaque grape juice passed through the UV reactor. For this purpose, FLUENT® 14.0 was used as a commercial finite volume CFD solver and grape juice was assumed to be composed of both liquid and particle (micoorganisms) phases. For modeling the liquid flow, continuity equation, equations of momentum and mass were numerically solved. In addition, discrete phase model (DPM) was integrated to flow model to estimate the residence time distribution of microbial particles in model food fluid (opaque grape juice). The integrated MPSS model was used to predict the UV intensity/dose recieved by each particles. The simulated UV dose/intensity data were compared with the experimental data obtained from biodosimetric and iodometric studies.

In the fourth part of Ph.D. study (Chapter 7), UV-C irradiation was investigated as a non-thermal pasteurization process for pasteurized clear and freshly squeezed opaque white grape juices treated with a S-shaped, thin film, continuous flow UV reactor. Three different studies were designed to evaluate the effect of UV-C irradiation on the microbial inactivation and physical properties of grape juices. In the first study, pasteurized clear grape juice (PCGJ) was inoculated with *S.cerevisiae* (NRRL Y-139) as target microorganism. In the second study, freshly squeezed opaque grape juice (FSOGJ) was inoculated with spoilage microorganisms, i.e., yeast and lactic acid bacteria after fermentation process. Inoculated or fermented grape juice samples were exposed to a

UV-C irradiation in the continuous flow UV reactor. In the third study, the efficiency of UV-C irradiation was examined using *E.coli* K-12 (ATCC 25253), which is a nonpathogenic surrogate strain of *E.coli* O157:H7 in both clear and freshly squeezed opaque grape juice. UV dose delivered in continuous flow UV reactor was determined based on biodosimetric method.

In the last part of the Ph.D. study (Chapter 8), the microbial shelf life of UV treated FSOGJ was evaluated. For this purpose, two studies were conducted. The first study was designed to evaluate the microbial stability of UV irradiated FSOGJ at refrigerated storage conditions. The second study was planned to investigate the changes in quality parameters of grape juice (such as absorbance coefficient, turbidity, color, brix (%), pH, vitamin C content and total titratable acidity) that was occured throughout storage period.

CHAPTER 2

UV IRRADIATION OF FOOD MATERIALS

2.1. Principles of UV Irradiation

Ultraviolet (UV) can be described as the electromagnetic radiation which lies in a wavelength shorter than that of visible light, but longer than X-rays in the range of 100-400 nm. These frequencies are invisible to humans (Bolton and Linden, 2003; Shama 2007; Sosnin et al, 2006). UV light can be divided into four distinct spectral areas such as vacuum UV (between 100 to 200 nanometers), UV-C (between 200-280 nanometers), UV-B (between 280-315 nanometers), and UV-A (between 315-400 nanometers). The part of an electromagnetic spectrum lies in wavelengths between 200 nm and 300 nm, which is responsible for germicidal effect on microbial structure, is called UV-C (Shama 2007). The This region between 253.7-264 nm range having the peak germicidal wavelength, at 253.7 is known as the "germicidal spectrum", shown in Figure 2.1.

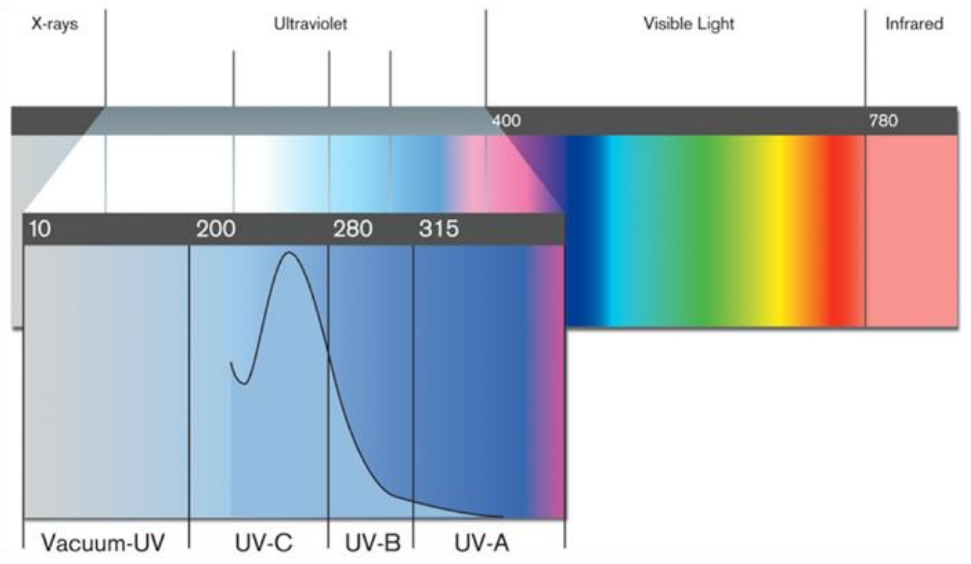

Figure 2.1. UV radiation range groups

(Source: Emperor Aquatics, 2007)

UV treatment is used to eliminate microorganisms from several food materials such as fruit juice, apple cider and milk. It is described as a non thermal disinfection method having no undesirable effect on the organoleptic and nutritional properties on food materials (Bintsis et al, 2000). Photochemical damage to nucleic acids in cellular structure is the main result of the absorption of germicidal UV-C light. The DNA of most living organisms is double stranded, including adenine in one strand and thymine in the other, and linked by one hydrogen bond Then, guanine is paired with cytosine by one hydrogen bond (Bank, 1990; Bintsis, 2000; Cadet et al, 2005; Miller, 1999; Moan, 1998, Tornaletti, 2005). The purine and pyrimidine combinations are called base pairs. When UV light of a germicidal wavelength is absorbed by the pyrimidine bases, the hydrogen bond is ruptured (Cieminis et al, 1987; Tornaletti, 2005). New bonds between adjacent nucleotides are structured with the help of high energy of electromagnetic wavelengths found in UV-C region. This phenomena creates double molecules or dimers (Tornaletti, 2005), shown in Figure 2.2. Dimerization of adjacent pyrimidine molecules is the most common photochemical damage. But in contrast, cytosine-cytosine, cytosine-thymine, and uracil dimerizations are also identified. Hence, the cell replication is interrupted by formation of numerous dimers in the DNA and RNA of microbial structure with the effect of other types of damage such as cosslinking of nucleic acids and proteins is resulted in a cell death (Tornaletti, 2005).

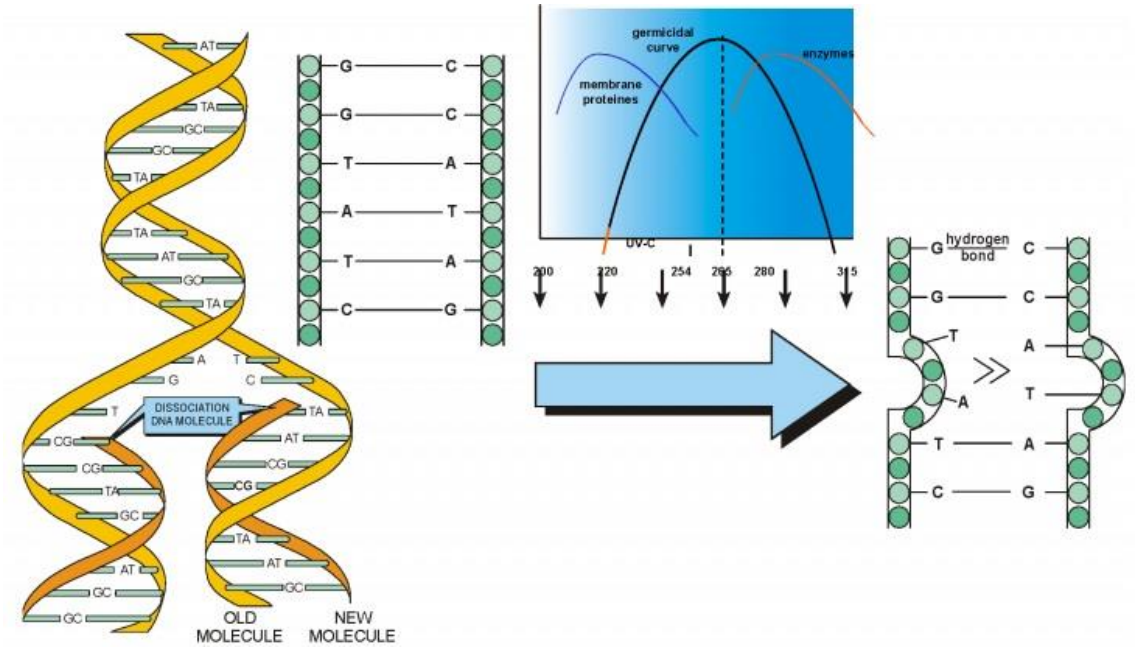

Figure 2.2. Effect of UV-C light on DNA double strand

(Source: Emperor Aquatics, 2007)

The amount of cell damage depends on the dose of UV energy absorbed by the microorganisms and their resistance to UV. UV dose is a product of UV intensity and exposure time and expressed as milli Joules per centimeter square (mJ/cm^2), or milli Watt seconds per centimeter square (mWs/cm^2). UV doses required for 99.9% destruction of various microorganisms are represented in Table 2.1. Non-pathogenic strain is determined to be more resistance than pathogenic microorganisms when exposed to UV-C light (Char et al, 2010; Hijnen et al, 2006; Ukuku and Geveke, 2010; Unluturk et al, 2008, 2010).

Table 2.1. Destruction Levels of UV Doses on Microorganisms

(Source: Wyckomar UV Purification Systems, 2007)

Organisms	**Energy (mJ/cm^2)**
Salmonella enteritidis	7.6
Bacillus subtilis	11
Bacillus subtilis spores	22
Escherichia coli	6.6
Pseudomonas aeruginosa	10.5
S. typhimurium	15.2
Shigella paradysenteriae	3.2
Staphylococcus aureus	6.6
Saccharomyces cerevisiae	13.2
Aspergillus niger	330
Influenza	6.6
Paramecium	200
Penicillium expansum	22

There are various advantages of UV disinfection process including low total operation cost, environmentally friendly applications without hazardous chemicals and safe to use. UV systems are universally accepted disinfection processes especially in food and water disinfection. UV systems are not only operated automatically but maintenance is also made with easy re-installation (Elyasi and Taghipour, 2006; Lazarova et al, 1998; Tchobanoglous et al, 1996). Overall advantages of UV can be represented as;

- UV systems are environmentally friendly.
- Low initial capital cost is a characteristic of UV systems as well as reduced operating expenses according to the similar technologies, such as thermal disinfection of ultrasonic treatment, e.t.c. Their installation is also easy (Lazarova et al, 1998).

- Depending on the food materials, treatment process may be immediately operated without any holding tanks or long retention times (Masschelein et al, 1989; Oppenheimer et al, 1993).
- UV operation is extremely economical that great amount of food material may be treated for a little operating cost with low power consumption (Green et al, 1995).
- Comparing the thermal treatment, no or hardly any change in taste, odor, pH or conductivity is determined in food.
- UV system may be used as a compatible device with other treatment equipments or systems when complete destruction of microbial population is needed (Blume and Neis, 2004; Koivunen and Heinonen-Tanski, 2005).

There are many factors affecting the efficiency of a UV system. Flow regime is one of the main factor that plays an important role in the inactivation of microorganisms using continuous flow UV reactors for treating liquid food products (LFPs). Despite the inhomogenity, UV inactivation in low flow rate treatments improves the efficiency of microbial reduction with higher residence time. Hence, it is possible to maintain high UV dose to disinfect medium. Nevertheless, high flow rate improves homogenity of medium by faster replacement of suspended particles. But in contrast, high velocity of fluid causes low residence time for efficient contact of UV light (Koutchma et al, 2004, 2006). Fluid foods have different physicochemical and optical properties. Physical properties, such as viscosity and density influence the effectiveness of fluid motion and flow pattern. Besides, optical properties such as absorbance coefficient, turbidity and color parameters are described as the main factors effecting the UV light penetration to maintain high efficiency for microbial inactivation. The whole properties of fluid foods help synergistically to construct a well-designed continuous flow UV systems (Koutchma, 2006, 2009; Murakami et al, 2006).

UV treatment method decreases the high operating and separation cost of the other pasteurization methods. (Garibaldi et al, 2003). It is expected that an efficient UV operation must destroy the targeted microorganism in a food material (Lazarova, 1998). Several parameters that affect the design and operating conditions of UV-C radiation device can be categorized as;

- The type of lamp used in the treatment (low-pressure or medium/high-pressure) (Harris et al, 1987, Hassen, 2000).
- The length of the lamp being used (Hassen et al, 2000).

- Physical and optical properties of LFPs being treated (density, viscosity, turbidity, absorbance coefficient, and color) (Parker and Darby, 1995).
- The flow behavior of food material through the UV exposure chamber (Hassen et al, 2000).
- Physical and mechanical design of continuous flow UV reactor, (vertical, horizontal, annulus or single cylindirical within single or multiple UV lamp configuration, positions of inlet and outlet of the reactor based on the flow axis).
- UV-C light resistivity of target microorganism to be inactivated by UV treatment.

Even though UV disinfection method provides several advantages for application in food industry, disadvantages of UV disinfection are also present such as leaving no disinfection residue or lack of a technical database of which defines how a UV irradiation needs to be performed for various food materials (Bolton and Linden, 2003, Koutchma, 2007; Koutchma et al, 2004, 2006, 2009; Murakami et al, 2006). The most fundamental disadvantageous of UV application is the lack of standardized mechanism for measurement, calibration, or certification of UV systems in order to operate without problem after installation.

2.2. Sources of UV Light

Different UV light sources are used for UV technology, based on the power, output, wavelength range and chemicals used for production such as mercury, amalgam or ozone (Bolton and Linden, 2003; Koutchma et al, 2009). Each type has specific strengths and weaknesses (Bolton and Linden, 2003; Bukhari et al, 1999). Many germicidal UV bulbs use special ballasts to regulate electrical current flow to the bulbs (Bukhari et al, 1999).

2.2.1. Mercury Emission Lamps

Mercury emission lamps contain small quantity of elemental mercury (Hg) and inert gas such as argon. Mercury is used due to high volatility that activates the UV lamp even at high temperature (Koutchma et al, 2009). Argon is preferred as filler gas commonly due to optimum emission energy (15.8 eV) that causes mercury ionization activation and emission of lamp. Besides, vaporized mercury has low ionization energy

that drives a chain reaction for electrical discharge when lamp is operated. Mercury lamps can be operated both in low and medium pressures.

Low pressure mercury lamps operate 90.01 to 0.001 mbar range of total gas pressure in order to produce UV light. Carrier gas excess varies from 10 to 100 % that maintains the vapor pressure of liquid mercury at 40 °C of optimum temperature and 1 Pa of optimum mercury vapor pressure in UV lamp. In the operation of UV disinfection with low mercury UV lamps, single or multiple UV bulbs generate the radiation for emitting of UV light by striking an electric arc within low-pressure mercury vapor. This lamp emits a broad spectrum of radiation with intense peaks at germicidal UV wavelengths of 253.7 nanometers (nm) and a peak at 184.9 nm (Koutchma, 2009; Koutchma et al, 2009). The advantage of low pressure mercury lamps is the reversible emission process of a photon by a mercury atom. By this way, emitted photons are absorbed again by another mercury atom when transfered in plasma (Koutchma et al, 2009). Low-pressure UV lamps are high efficient UV bulbs, providing 35 % of UV-C light with low amount of power (Bukhari et al, 1999, Koutchma et al, 2009). Cylindirical shape having 0.9-4 cm of diameter and 10-160 cm of length is common. Lamp contains cathode and anode part at the top and bottom within Faraday dark zone, of which does not emit UV light (Koutchma et al, 2009; Masschelein, 2002). Temperature of the lamp is fundamental during operation that defines the vapor pressure of mercury throughout the lamp. At low temperature, partial condensation of mercury occurs at the inner wall of the lamp. At high temperatures vapor pressure of Hg is high, compared to excessive liquid Hg in the lamp. In order to eliminate cooling effect of Hg, the lamp is placed in a quartz sleeve that maintains air circulation (Koutchma et al, 2009). Aging of the low mercury lamp starts atfer emission drop of first 100-200 hours of operation. After months, solarization occurs on the lamp surface and oxidizing is seen on diodes as black color. The best resonance of low pressure mercury UV lamps lies between 185-253.7 nm of wavelength (monochromatic). At 253.7 nm, approximately 85 % of total UV output is emitted as germicidal for living organisms.

Medium pressure mercury lamps operate at 10^4-10^6 Pa of vapor pressure of Hg. Minimum operation temperature of these lamps is 400 °C and can increase up to 800 °C. Hence an open quartz enclosure of lamp is necessary to prevent direct contact of treated liquid food material with lamp at high temperature during operation. Operating wavelength range of medium pressure mercury lamps is in the range of 250 and 600 nm with several peak emission points (polychromatic). Germicidal effect of these lamps is lower compared to low mercury UV lamps. But in contrast, aging of medium pressure lamps are longer.

Even after 4000 hours, % 80 of emission can be maintained (Koutchma et al, 2009). Medium-pressure UV lamps have lower UV-C output (>10%) compared to low pressure mercury UV lamps (Koutchma, 2009).

In some cases, low pressure mercury lamps produce ozone (O_3) at 185 nm that is effective in photochemical air treatment (Voronov, 2007). Moreover, 0.54 g O_3 is produced for every power (Watt) of low mercury UV source per hour. But since ozone gase is harmful for environment and health, it is not preferred commonly.

2.2.2. Special Lamp Technologies

UV light is powerful enough to produce ozone, hydroxyl, and other free radicals that not only destroy bacteria, but also harmful for food processing (Bolton and Linden, 2003; Koutchma, 2009). Consequently, germicidal wavelength of 253.7 is preferred for disinfection of food materials in industry. Alternative vaporized chemicals are used having less or no harmful effects for human and environment. Instead of using mercury, **amalgam** has been used for low pressure lamps providing long aging and 10 times higher energy output than that of low pressure mercury UV lamps. Amalgam type UV lamps are described as low-pressure lamps, operated with high power (Bolton and Linden, 2003; Koutchma et al, 2009). The optimum operating temperature for amalgam lamps is 90 °C. No transmission loss occurs by quartz sleeve and the constant treatment is provided regardless of aging. Due to high energy output, long aging time, operating teperature and high treatment efficiency, amalgam lamps have been an alternative for medium pressure mercury lamps. Nonetheless, main disadvantage of these lamps for food processing is the accumulation of high temperatures, despite 16.000 hours of complete lifetime (Bolton and Linden, 2003; Koutchma, 2009). Also low efficiency of this lamp type is another disadvantage, compared to traditional low-pressure lamps (30-33% UV-C).

On the other hand the efficiency of a mercury type UV lamp depends on the temperature of lamp surface and vapor pressure of mercury that is hazardous for human health. In order to eliminate temperature dependency, several alternative UV lamp models such as excimer lamps and pulsed UV lamps have been developed (Koutchma, 2009). **Excimer lamps (excilamps)** are operated by the production of rare gas (Rg_2) and halogen excimers (X_2). During the decomposition of these excimers, a single spectral line of UV is produced between 120 and 380 nm.

Pulsed UV lamps produce high intensity UV range. compared to mercury lamps. This type of lamps are useful for treatment of opaque liquid foods for high penetration of UV light (Koutchma et al, 2009). UV emission is produced by stored alternating current in a capacitor that is discharged into a high speed switch for pulse formation (about 100 μs).

2.3. Application of UV Irradiation Using Static and Continuous UV Systems

The U.S. Environmental Protection Agency (EPA) has approved UV disinfection as an emerging technology for water disinfection (The U.S. Environmental Protection Agency). Besides, use of ultraviolet irradiation was allowed by Food and Drug Administration (FDA) to inactivate foodborne pathogens and other microorganisms in juice products by regulation effective since November 29, 2000. UV disinfection is mainly used in air and water purification and sewage treatment, food and beverage processing (Blume and Neis 2004; Chmiel et al, 2002; Green et al, 1995; Hassen et al, 2000) processing of drinking water (Lehtola et al, 2004; Peldszus et al, 2003), milk, liquid egg products and fruit juice production (Bandla et al, 2012; Char et al, 2010; Choudhary et al, 2011; Gabriel, 2012; Gabriel and Nagano, 2009; Geveke, 2008; Guerrero-Beltran et al, 2009; Franz et al, 2009; Keyser et al, 2008; Koutchma et al, 2004; Matak et al, 2005, 2007; Oteiza et al, 2010; Palgan et al, 2011; Walkling-Ribeiro et al, 2008; Ukuku and Geveke, 2010; Unluturk et al, 2008, 2010).

There are many research cited in the literature about the efficacy of UV-C light for the reduction of different microorganisms by using either bench top collimated beam apparatus or continuous flow reactors (Sommer et al, 1998, Lage et al, 2003, Ngadi et al, 2003, Geveke 2008, Unluturk et al, 2010). Most of these works were conducted with drinking and wastewater samples and the microbial inactivation achieved in those studies with lower UV doses than those required for microorganisms suspended in liquid foods such as apple cider and milk (Table 2.2). For example, Lage et al, (2003) treated *E.coli* suspension with UV exposure of 12 mJ/cm^2 UV dose and achieved 3-log reduction (Lage, 2003), whereas Sommer et al, (1998) inoculated water samples of 0.4 cm in depth with three different *E.coli* strains (ATCC 25922, ATCC 11229 and isolated from sewage) and applied 10-50 mJ/cm^2 UV dose to obtain maximum 6-log reduction (Sommer et al, 1998). On the other hand, UV dosages applied by Wright et al, (2000) ranged from 9.4 to 61.5

mJ/cm^2 and the mean log reduction of *E.coli* O157:H7 strain for treated apple cider was found to be 3.81 log CFU/ml in flow through UV reactor (Wright et al, 2000). 5-log reduction of *L. monocytogenes* in milk was achieved when the milk samples treated with UV dose of 15.8±1.6 mJ/cm^2 in continuous flow reactor.

Koutchma and Parisi, (2006) described and compared the performance of three designs of flow-through UV reactors in turbulent flow, thin film and annular laminar systems for the disinfection of a solid-liquid media (apple cider) for elimination of *E.coli* (Koutchma and Parisi (2006). Triassi et al, (2006) studied ultraviolet disinfection of 30 environmental *Legionella* strains from the paediatric and cardiac surgery units (CSU) in hospital environment, hospital water supply and medical devices to prevent Legionnaries' disease (Triassi et al, 2006). Templeton et al, (2006) evaluated UV light efficiency using two viral surrogates (MS2 coliphage and bacteriophage T4) in three types of particles (kaolin clay, humic acid powder, and activated sludge), two coagulants (alum and ferric chloride), two filtration conditions (none and 0.45 mm), and two UV doses (40 and 80 mJ/cm^2 for MS2 coliphage, 2 and 7 mJ/cm^2 for bacteriophage T4) considering in a series of bench-scale UV collimated beam studies conducted at 254 nm. Particle diameter and UV absorbing organic content were found to be critical parameters for the inactivation efficiency of UV irradiation (Templeton et al, 2006). Koutchma et al, (2004) developed a mathematical models such as Dispersed Phase model to describe particle phase flow pattern and particle residence times and the UV intensity distribution model to simulate processing of apple cider in a thin-film UV reactor under 253.7 nm UV light at 60 mW.s/cm^2 UV dose (Koutchma et al, 2004).

Unluturk et al, (2004) studied the effects of UV light efficiency on the destruction of *Escherichia coli* K-12 bacteria in the model fluids using laminar and turbulent flow UV systems interms of the single factor i.e., UV absorbance (Unluturk et al, 2004). Ngadi et al, (2003) evaluated the effect of pH, depth of food medium and UV dose on *E.coli* O157:H7 reduction in egg white and apple juice exposed to UV for 0-16 minutes at 0.315 mW/cm^2 (Ngadi et al, 2003).

Peldszus et al, (2003) investigated the bromate removal from drinking water by irradiation with medium-pressure UV lamps in drinking water at UV dose up to 718 mJ/cm^2. 19% bromate removal was achieved (Peldszus et al, 2003). Chmiel et al, (2002) studied highly contaminated spent process water contamination in food and beverage industries using the combination of membrane bioreactor, UV pre-disinfector and UV disinfection apparatus (Chmiel et al, 2002).

Table 2.2 Summary of UV Inactivation Studies

Author	UV System	Sample	Target m.orgn.	Dose	Time (s)	Log reduction/ml	D_{10}
Harrington & Hills, 1968	Thin film continuous flow	Apple cider	Total microbial count	N/A	0-43.5	2.69	N/A
Wright et al. 2000	Thin film continuous flow	Apple cider	*E.coli* O157:H7	0-0.061 mJ/cm^2	N/A	3.81	N/A
Ngadi et al. 2003	Bench top collimated beam	Egg white Clear apple juice	*E.coli* O157:H7	0-390 mJ/cm^2	0-960	>5.00	N/A
Basaran et al. 2004	Thin film continuous flow	Apple cider	*E.coli* O157:H7	0-14 mJ/cm^2	0-1.9	>5.00	N/A
Donahue et al, 2004	Thin film continuous flow	Apple cider	*E.coli* O157:H7	0-35.11 mJ/cm^2	0-8.12	>5.00	N/A
Tran and Farid, 2004	Thin film continuous flow	Fresh orange juice	Yeast, mould & aerobic plate count	0-120 mJ/cm^2	N/A	2.5 (Yeast and mould) 3.0 (APC)	87.8 mJ/cm^2 (Yeast) 119 mJ/cm^2 (Mould) 123 mJ/cm^2 (APC)
Guerrero-Beltrán, & Barbosa-Cánovas, 2005	Thin film continuous flow	Apple juice	*S.cerevisiae* *L.innocua* *E.coli* (ATCC 11775)	7.5-45 J/cm^2	0-1800	4.0 (*S cerevisiae*) >5.0 (*L.innocua*) >5.0 (*E.coli*)	22.4 min (*S.cerevisiae*) 7.0 min (*L.innocua*) 5.9 min (*E.coli*)
Matak et al, 2005	Thin film continuous flow	Goat's milk	*L.monocytogenes*	0-20 mJ/cm^2	0-18	>5.0	15.8 mJ/cm^2
Murakami et al. 2006	Bench top collimated beam	Apple juice/cider	*E.coli* K-12	0-100 mJ/cm^3	N/A	3.6	N/A
Geveke, 2008	Thin film continuous flow	Liquid egg white	*E.coli* K-12	44 J/ml	0-160	4.3	N/A
Keyser et al, 2008	Thin film continuous flow	Apple juice Guava juice Pineapple juice Mango nectar Strawberry nectar Orange juice	Yeast, mould & aerobic plate count	0-2.066 J/ml	0-1800	4.5 (Yeast and mould) 3.5 (APC)	N/A
Noci et al. 2008	Bench top collimated beam	Fresh apple juice	Total microbial count	N/A	0-1800	2.2	N/A
Unluturk et al, 2008	Bench top collimated beam	Liquid egg white Liquid egg yolk Whole liquid egg	*E.coli* (ATCC 8739) *E.coli* O157:H7 *S.typhimurium*	0-31 mJ/cm^2	0-1200	1.8 (liquid egg white) 0.7 (liquid egg yolk) 0.3 (whole liquid egg)	N/A

(cont. on next page)

Table 2.2. (Cont.)

Gabriel and Nagano, 2009	Bench top collimated beam	Clear apple juice	*E.coli* K-12 *E.coli* O157:H7 *S.enteritidis* *S.typhimurium* *L.monocytogenes*	N/A	0-19.8	N/A	0.55 min (*E.coli* K-12) 0.49 min (*E.coli* O157:H7) 0.61 (*S.enteritidis*) 0.27 (*S.typhimurium)* 1.26 min (*L.monocytogenes*AS-1) 0.44 min (*L.monocytogenes*M24-1)
Guerrero-Beltran et al, 2009	Thin film continuous flow	Grape juice, Cranberry juice, Grapefruit juice	*S.cerevisiae*	7.5-45 J/cm^2	0-1800	0.53 (grape juice) 2.51 (cranberry juice) 2.43 (grapefruit juice)	61.7-113 min (Grape juice) 12.2-40.7 min (Cranberry juice) 12.5-20.7 min (Grapefruit juice)
Franz et al, 2009	Dean flow (continuous)	Cloudy apple juice	*S.cerevisiae* *E.coli* DH5α *L.brevis*	N/A	0-41	4.0 (*S.cerevisiae*) >5.0 (*E.coli* DH5α) 4.0 (*L.brevis*)	N/A
Char et al, 2010	Thin film continuous flow	Clear apple juice Fresh orange juice	*S.cerevisiae* *E.coli*	0-1.87 J/cm^2	0-1200	1.2 (*E.coli* in orange juice) >5.0 (*E.coli* in apple juice) 3.6 (*S.cerevisiae*)	N/A
Oteiza et al, 2010	Bench top collimated beam	Fresh orange juice	*E.coli* O157:H7 Spoilage yeast	0-2 J/cm^2	0-600	> 5.0 (*E.coli* O157:H7) > 5.0 (spoilage yeast)	11 min (*E.coli* O157:H7) 10.55 min (spoilage yeast) for 5 log inactivation
Ukuku & Geveke, 2010	Thin film continuous flow	Clear apple juice	*E.coli* K-12	N/A	0-12	4.0	N/A
Unluturk et al, 2010	Bench top collimated beam	Liquid egg white	*E.coli* K-12 *E.coli* O157:H7 *L.innocua*	0-26.44 mJ/cm^2	0-1200	0.896 (*E.coli* K-12) 1.492 (*E.coli* O157:H7) 0.96 (*L.innocua)*	28.65 min (*E.coli* K-12) 16.26. min (*E.coli* O157:H7) 24.04 min (*L innocua)*
Choudhary et al, 2011	Coiled tube (continuous)	Cow milk & soy milk	*E.coli* W1485 *B.cereus*	0-11.19 mJ/cm^2	0-11.3	>5.0 (*E.coli* W1485) 2.72 (*B.cereus*)	N/A
Bandla et al, 2012	Coiled tube (continuous)	Soy milk	*E.coli* W1485 *B.cereus* endospores	0-11.19 mJ/cm^2	0-11.3	>5.0 (*E.coli* W1485) 3.29 (*B.cereus* endospores)	N/A
Gabriel, 2012	Bench top collimated beam	Clear apple juice	*E.coli* O157:H7 *D.hansenii* *C.lusitaniae* *T.delbrueckii* *P.fermentans* *S.cerevisiae*	N/A	0-480	2.20 (*E.coli* O157:H7) 0.60 (*D.hansenii*) 0.50 (*C.lusitaniae*) 0.80 (*T.delbrueckii*) 0.75 (*P.fermentans*) 0.80 (*S.cerevisiae*)	2.64 min (*E.coli* O157:H7) 8.27 min (*D.hansenii*) 9.78 min (*C.lusitaniae*) 9.39 min(*T.delbrueckii*) 11.04 min (*P.fermentans*) 6.38 min (*S.cerevisiae*)
Geveke & Torres, 2012	Centrifugal flow (continuous)	Grapefruit juice	*E.coli* K-12 *S.cerevisiae*	0-24 mJ/cm^2	0-3.2	>5.0 (*E.coli* K-12) >5.0 (*S.cerevisiae*)	19 mJ/cm^2 (5 log inact. of *E.coli* K-12) 14 mJ/cm^2 (6 log inact. of *S.cerevisiae*)
Ochoa-Velasco & Guerrero Beltrán, 2012	Thin film continuous flow	Pitaya juice	Aerobic mesophyll bacteria Spoilage yeast+mould	0-86 mJ/cm^2	0-1500	2.11 (AMB) 1.14 (yeast+mould)	13.9 min (AMB) 23.5 min (yeast+mould)

Liltved and Landfald, (2000) identified the significant difference of both photoreactivating and photoinactivating process for two fish pathogenic bacteria (*Aeromonas salmonicida* and *Vibro anguillarium*) after exposing to sunlight and artifical (UV) light in their natural river waters using a bench top systems working at 254 nm providing 2-3 mWs/ cm^2 UV dose (Liltved and Landfald, 2000). Giese and Darby, (2000) studied the responses of three coliform bacteria species (*Citrobacter diversus*, *Citrobacter freundii* and *Klebsiella pneumoniae*) when exposed to three wavelengths of UV light (254, 280 and 301 nm) at UV doses ranging from 2.3 to 39 mW s/cm^2 and achieved maximum 3 log inactivation (Giese and Darby, 2000).

Bolton, (2000) calculated the dose distribution and the average dose in an annular UV reactor with either a monochromatic (254 nm) low pressure mercury lamp or a broadband medium-pressure mercury UV lamp (Bolton, 2000). Yaun et al, (2003) defined the UV light treatment and reduced the numbers of multistrain coctails of *Salmonella* and *E.coli* O157:H7 on agar surfaces using a 1 m long UV chamber emitting light at 253.7 nm wavelength by applying 100 mW s/cm^2 UV dose. They achieved 5 log reduction at >8.4 mW/cm^2 and >14.5 mW/cm^2 irradiance average. UV treatment and determination of UV dose delivered for target microorganism were provided using both static bench top collimated beam apparatus and continuous flow UV inactivation (Yaun et al, 2003).

2.3.1. Bench Top Collimated Beam Apparatus (Static UV System)

In order to determine reduction of microorganisms in logarithmic scale when exposed to ultraviolet light, biodosimetry experiments are conducted by collimated beam apparatus (Bolton and Linden, 2003; Ngadi et al, 2006; Unluturk et al, 2008, 2010). UV dose response curve of liquid food product is obtained by using this type of closed bench top ultraviolet system. A bench top collimated beam apparatus is depicted in Figure 2.3. (Bolton and Linden, 2003). The collimated beam apparatus is used to maintain a homogeneous irradiation on a definite surface area. The reflection of UV light on several materials such as glass or plastic is problemmatic. Consequently, the inner surface of the collimating tube is required to be constructed by using a black cardboard and a flatblack paint in order to prevent reflection and minimize the loss of light (Figure 2.3). According to the design, collimating tube or apertures placed at a certain distance from the lamp is constructed to produce parallel radiation from UV light source on irradiated surface

(Bolton and Linden, 2003). It is expected that UV irradiation throughout the aperture hole is to be uniform on the Petri dish or beaker to be irradiated (Atilgan, 2007; Bolton and Linden, 2003; Koutchma et al, 2009). It is fundamental to maintain the appropriate distance between irradiated area and UV light source. It is also essential to provide a homogeneous UV intensity in such a way that all the irradiated microorganisms take the same amount of UV dose. For this purpose, irradiated samples are aseptically placed in Petri dishes or beaker directly below the collimated UV beam and stirred continuously during the irradiation. Bench top collimated beam apparatus consists of a UV source and a platform on which food material or microbial cocktail is placed for UV exposure. The platform is to be easily raised or lowered by tray system to adjust the distance and consequently UV intensity level. A stirrer is used to provide homogeneous UV intensity in liquid medium during UV exposure. Also a shutter is present in front of the lamp to use for blocking or allowing passage of UV light. A cover is kept closed in front of the system during UV experiment to prevent contact of UV light with human skin directly.

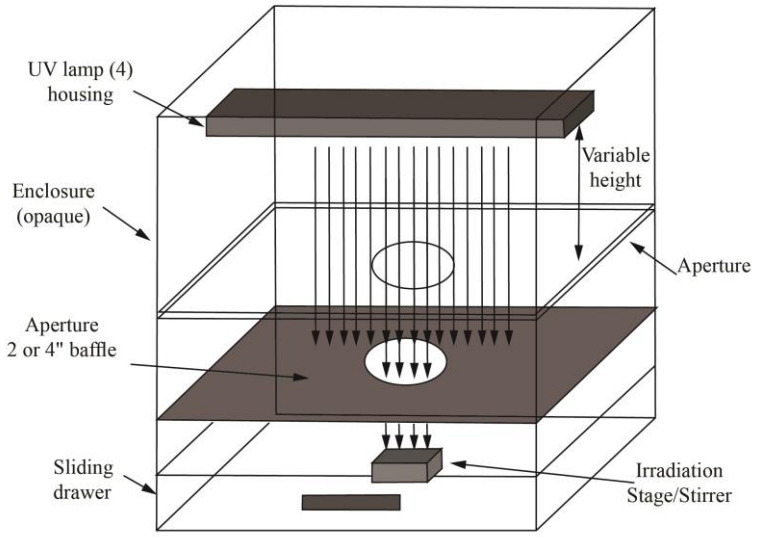

Figure 2.3. Bench top collimated beam apparatus
(Source: Bolton and Linden, 2003)

The UV intensity at the surface of the sample (incident intensity - I_o or irradiance at the surface) is measured using a bench top radiometer. A radiometer includes a sensitive electronic ammeter, equipped with a UV sensor head. Sensor head is used to process a current that is proportional to the incident irradiance on irradiated surface. Units of the radiometer are mW/cm^2, W/m^2 or W/cm^2. In the presence a low pressure UV lamp as a

light source, the radiometer measures the irradiance at the surface of the liquid medium in the petri dish. By this way, the head of radiometer detector is equalized with the the surface of the liquid medium in the container to obtain best calibration (Bolton and Linden, 2003). In order to minimize fluctuations in intensity, light source is switched on for about 30 min prior to UV treatment of the sample. For UV inactivation treatments, inoculated plates are subjected to different doses of UV-C light. The average UV intensity in the stirred sample (I_{avg}) is calculated by an integration of Beer-Lambert law over the sample depth (Morowitz, 1950):

$$I_{avg} = I_0(1 - e^{-A_e\gamma})/A_e\gamma \quad (2.1)$$

where I_o is the incident intensity (mW/cm^2), A_e is the absorbance coefficient given per centimeter and γ is the path length (cm). UV dose can be calculated using these irradiance values from t = 0-t_{end} minutes using the following formula:

$$d = t * I \quad (2.2)$$

where "d" represents UV dose (mJ/cm^2), "t" is time (in minutes) and "I" refers to irradiance in mW / cm^2.

2.3.2. Continuous Flow UV Reactors

The UV reactor technology has been used for disinfection of liquid foods or water (Geveke, 2005, 2008; Koutchma et al, 2009; Koutchma, 2009; Linden and Darby, 1998; Matak et al, 2005; Ngadi et al, 2006; Qualls and Johnson, 1983; Sommer et al, 1998). The efficiency of a continuous flow UV reactor is dependent upon the delivery of uniform dose to fluid. Continuous flow UV reactor system is different from bench top collimated beam apparatus as a basis of design, operation method and equipment characteristics. Additionally, fluid motion plays important role in microbial inactivation and UV light penetration in sample fluid (Geveke, 2005, 2008; Keyser et al, 2008; Koutchma, 2009; Li et al, 2010).

Continous flow UV treatment of semi-transparent (opaque) food materials such as cloudy opaque fruit juices is under investigation (Adhikari et al, 2005; Geveke, 2004,

2008, Keyser et al, 2008; Koutchma, 2009; Matak et al, 2007; Ngadi et al, 2006; Tran and Farid, 2004). The reason of that is the high absorptive properties of opaque fluids, so that the penetration of UV light is limited. Consequently in a design of continuous flow UV treatment system, perfect mixing is required to be well-considered in order to expose the whole fluid to UV light passing throughout UV reactor (Koutchma et al, 2004; Murakami et al, 2006). On the other hand, it is fundamental to make a UV reactor design to have high UV light penetration.

If the microbial population is introduced by poor hydraulic mixing, a significant ratio of the microorganisms can pass throughout the reactor with lack of UV penetration. This means that such a UV reactor does not provide efficient UV dose distribution resulting poor inactivation rate for microorganisms in the irradiated food material. Besides, UV reactor should provide an effective UV dose distribution and high inactivation rate with good hydraulic mixing. By this way, all microorganisms can receive almost the same UV dose (Bolton and Cotton, 2008; Koutchma, 2009). In order to exhibit high inactivation rate, type of UV reactor is important. The main types include anannular thin film UV reactors operated at laminar or turbulent flow regime (Forney and Pierson, 2004; Koutchma et al, 2007; Koutchma and Parisi, 2004; Unluturk et al, 2004; Wright et al, 2000; Ye et al, 2007). On the other hand, several types of UV reactors have been investigated such as Taylor-Couette flow UV reactors (Forney et al, 2004), Dean flow reactors having a helical tube configuration (Koutchma et al, 2007), and other UV reactor types that are designed to increase the UV penetration efficiency by providing good mixing in the treated fluid.

2.3.2.1. Thin Film Annular UV Reactors

Thin film continuous flow UV ractors have been designed in order to eliminate lack of UV penetration throughout disinfected fluid (Koutchma et al, 2006, 2009; Tran and Farid, 2004). In thin film annular UV reactors, disinfected liquid food is pumped through the flow gap between two stationary cylindirical vessel. Thin film reactors provide a thin fluid layer, which is less than 1 mm. This fluid film can be produced by fixed stationary boundaries or by flowing fluid on a single fixed boundary. Thin film reactors are usually operated at laminar flow regime within a parabolic velocity profile. Thin film annular flow type reactors are used for the disinfection of apple juice and cider (Koutchma et al, 2006,

2007; Worobo, 1999) or pulp juices such as mango nectar (Guerrero-Beltrán and Barbosa-Cánovas, 2006). The gap size and length of the reactor is dependent upon the type of treated food, flow rate and flow regime. An example for vertical type annular flow UV reactor is depicted in figure 2.4 (Tran and Farid, 2004). This reactor is constructed by using a single lamp fixed at the center and enclosed by a quartz sleeve to prevent direct contact of irradiated fluid. Fluid flow between quartz sleeve of inner cylinder and outer cylinder is maintained as thin film. An air cooling system is placed to remove excessive heat generated by UV lamp.

In some cases, thin film reactors are operated at turbulent flow regime (Keyser et al, 2008; Unluturk et al, 2004) to maintain proper mixing of irradiated food materials by providing high velocity.

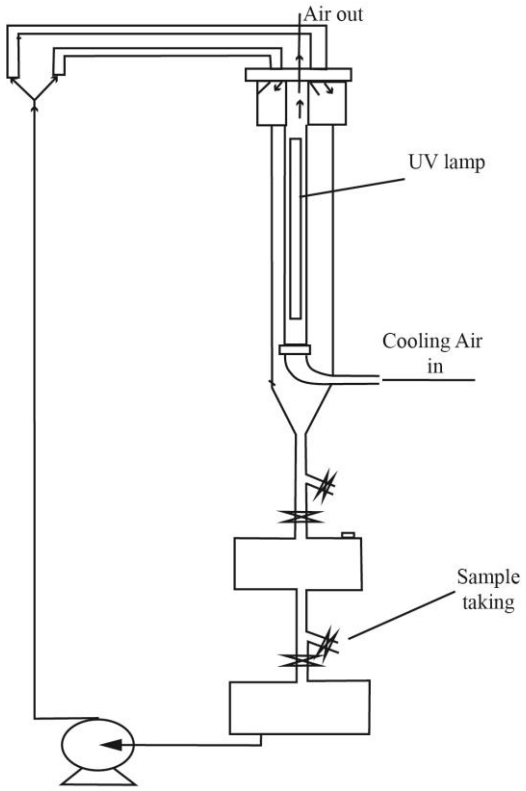

Figure 2.4. Thin film annular flow UV reactor system
(Source: Tran and Farid, 2004)

2.3.2.2. Taylor-Couette Flow UV Reactors

Even though thin film continuous flow UV reactors are effective for UV light emission throughout fluid flow, there are some limitations including a lack of UV penetration due to inappropriate mixing. This may cause inefficient UV treatment. In order to provide efficient disinfection level, turbulent flow regime is applied on fluid by increasing the flow rate and decreasing residence time. Taylor-Couette flow UV reactor maintains the good mixing in annular gap (Forney et al 2003; Koutchma, 2009; Ye et al, 2007). In Taylor-Couette reactor, the inner cylinder is rotated (called rotor) when outer cylinder is kept stationary, and called stator (Figure 2.5). The fluid flows in the gap between the two long concentric cylinders. In order to maintain a good exposure efficiency and ideal mixing of irradiated fluid, UV radiation source is placed around the stationary cylinder. The inner cylinder rotates at low rotational rates. Thus, a laminar flow with vortices can be seen within the annular gap. Moreover, the mixing of irradiated fluid provides a homogeneous UV dose distribution. The flow characteristics of this reactor approached ideal plug flow with a residence time that is examined from the hydrodynamics or boundary layer characteristics (Koutchma et al, 2009).

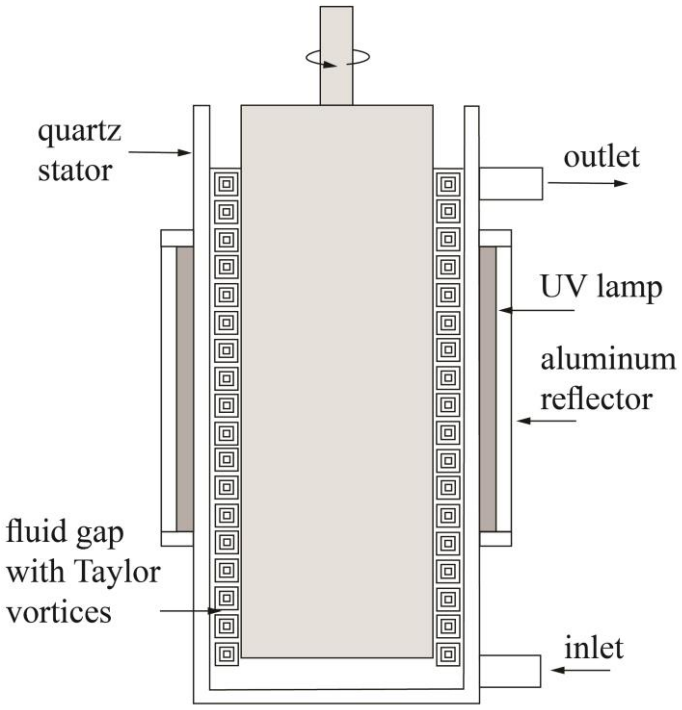

Figure 2.5. Taylor-Couette flow UV reactor
(Source: Koutchma, 2008)

2.3.2.3. Dean Flow UV Reactors

Continuous flow UV reactor with Dean flow is depicted in figure 2.6. UV reactor includes a coiled Teflon tube with UV lamps and reflectors on the inside and outside of the coiled tube. These reflectors are used to increase uniform UV irradiance on fluid food. The coiled tube promotes additional turbulence in liquid flow inside a coiled tube that is named as secondary eddy flow effects (Dean vortices), also known as the Dean effect (Dean, 1927; Schmidt and Kauling, 2007). Consequently, uniform velocity and residence time distribution is observed by radial mixing even in laminar flow (Dean, 1927). Moreover opaque food materials with low UV emissivity such as fruit juices can be treated by homogeneous UV treatment with a minimum energy loss (Franz et al, 2009). There are some studies on using coiled tube UV reactors to promote the additional mixing in milk, fresh apple cider, orange juice and liquid egg white (Bandla et al, 2012; Franz et al, 2009; Geveke 2005, 2008; Keyser et al, 2007; Koutchma et al, 2007; Müller et al, 2005).

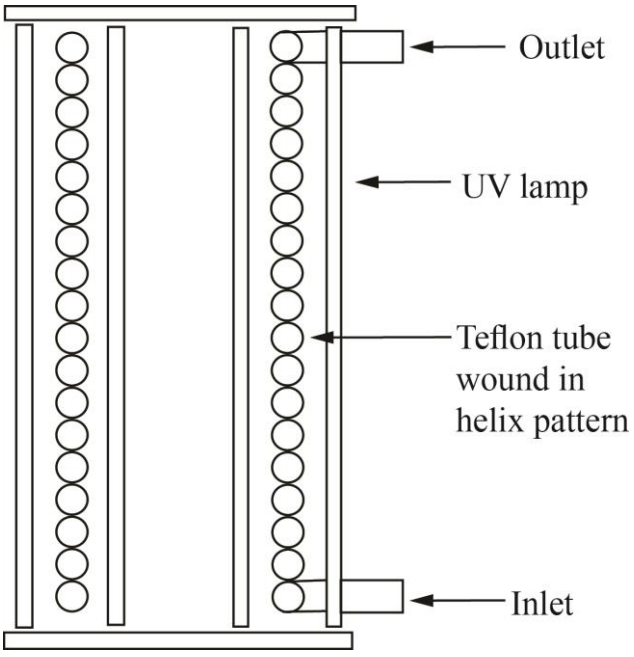

Figure 2.6. Dean flow UV reactor

(Source: Koutchma, 2008)

2.3.2.5. Centrifuged UV Reactors

There is another type of UV reactor designed for the maintenance of a thin film flow by applying a centrifugal force. Using a centrifugal UV reactors, UV treatment of grapefruit juice or serum plasma is studied (Geveke and Torres, 2012; Ijici et al, 1964). Currently, the pharmaceutical industry uses centrifugal UV irradiators to inactivate viruses in liquids, such as serum plasma. Figure 2.7 represents an example for centrifugal UV reactor (Geveke and Torres, 2012).

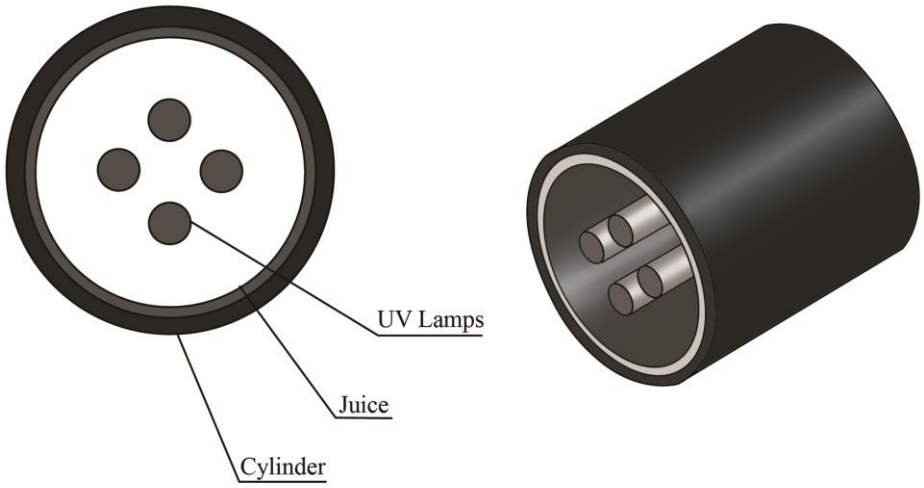

Figure 2.7. Centrifuged UV Reactor
(Source: Geveke and Torres, 2012)

In this type of reactor, UV lamps are generally fixed at the center of flow volume. In order to prevent fluid contact to lamp surface, lamps are covered and sealed by quartz sleeves. Air gap is used to remove excessive heat produced by UV lamps. When the fluid is passed throughout the reactor and around the lamps, outer cylinder rotates at a constant angular speed and inclination at a certain angle produces thin film and maintain homogenity of fluid for efficient irradiation.

2.4. Determination of UV Dose

In the scientific literature, there are many studies about the UV treatment of clear liquid foods. Nevertheless, comparison of studies can not be made effectively due to the

lack of direct method of measuring or calculating UV doses in continuous flow UV reactors, especially when the UV systems have complex geometries and if opaque solutions are treated (Koutchma et al, 2004, 2006, 2009). Additionally, UV dose measurement can be limited by the optical properties such as UV absorbance coefficient or processing and design parameters like physicochemical and optical properties of irradiated food, type of UV light source, flow regime, type of UV equipment or sensitivity of various organisms to UV light (Jacob and Dranoff, 1970; Petrasek et al, 1980). UV intensity is necessary to be measured to calculate UV dose in the UV reactor systems. It is difficult to measure UV dose throughout the UV reactor since UV intensity can not be measured directly inside the reactor. UV radiometer can measure direct incident intensity at a surface in bench top UV systems. But it is inappropriate for annular or tubular flow geometries for estimation of 3-D intensity (Jacob and Dranoff, 1970; Petrasek et al, 1980). UV sensors have the ability to measure incident intensity only at the surface (Huff et al, 1965).

Nonetheless UV dose measurements are also difficult for the treatment of two phase food materials such as apple cider, pulp orange juice. containing solid and liquid parts. In this case, solid particles scatter the UV light and prevent the UV light to reach microorganisms found as freely dispersed in liquid medium or attached the solid particles. As a result of this, UV intensity measurement needs determination of particle positioning and residence time, simultaneously (Johnson and Qualls, 1981). Under these limitations, several methods have been developed to determine UV dose and intensity distribution in the flow systems. These are classified as biodosimetry method, chemical actinometry method and a method based on computational fluid dynamics (CFD).

2.4.1. Biodosimetry Method

Biodosimetry (i.e., bioassay) method is widely used for UV intensity measurement to calculate dose delivered both in static bench top systems and continuous flow UV systems (Koutchma, 2009; Koutchma et al, 2006, 2009). Biodosimetry is also determined as the biological method in which the inoculated liquid food product is passed throughout the UV reactor and exposed to UV light at a certain UV dose. Firstly, in this method, a single or multiple target microorganisms is inoculated to a known amount of liquid food. Then liquid food is exposured to UV light by means of a bench top collimated beam apparatus (static system) or a continuous flow UV reactor. Inactivation rate of

microorganisms by UV treatment is defined as the logarithmic ratio of the number of survival microorganisms (N) in the irradiated sample to the initial number of microorganism (N_0) in untreated sample. Lastly, the UV dose-response curve for a target microorganism inoculated in a liquid food is constructed by plotting UV dose and inactivation rate (log reduction) obtained by means of a static system is plotted. For this purpose, inactivation data is collected at certain UV doses estimated at each time interval. UV dose is calculated by using Beer Lambert's law described in Eqns 2.1 and 2.2.

In order to estimate the UV dose delivered in the continuous flow UV reactor, the same liquid food inoculated with the same type of a target microorganism is passed through the continuous flow UV reactor and inactivation rate is recorded. Then UV dose is marked on the UV dose-response curve by matching the recorded inactivation rate. This delivered dose level is named as reduction equivalent dose. It might be possible to have higher UV dose for the collimated beam aparatus, comparing with continuous flow UV reactors, possibly due to the volumetric difference of irradiated fluid food (Linden and Darby, 1997, Koutchma et al, 2009). Biodosimetry process can be summarized in Figure 2.8.

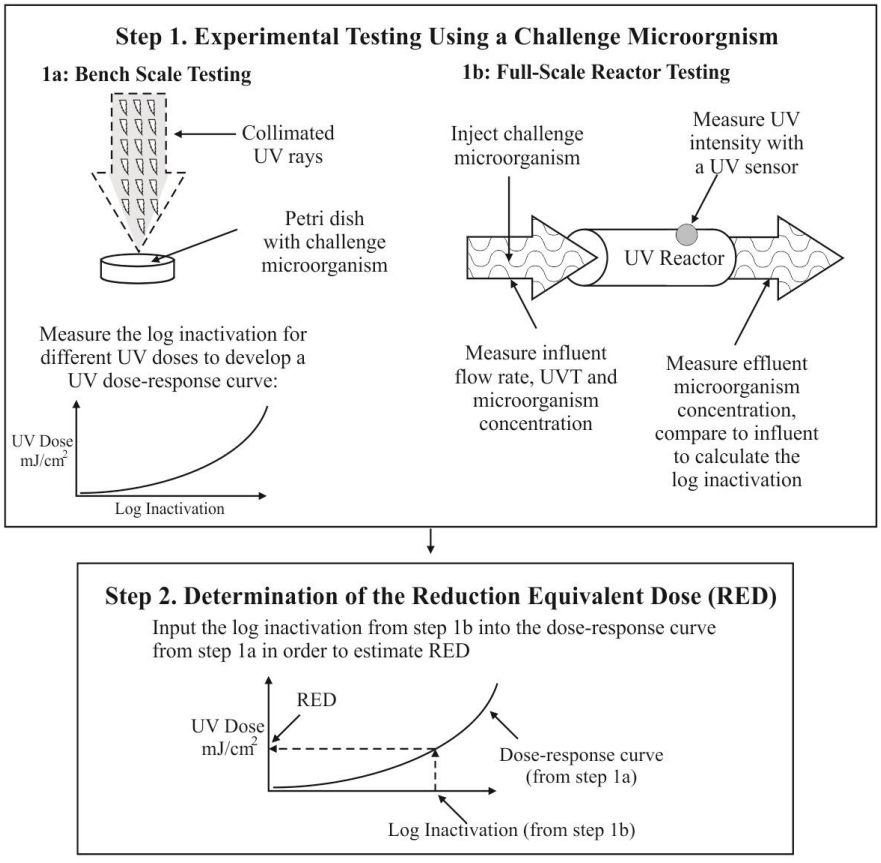

Figure 2.8. Overall biodosimetry process

Determination of dose delivered in a continuous flow UV reactor can be also estimated using modified biodosimetry method (Koutchma et al, 2004, 2007, 2009). Generally, *E.coli* K-12 is used as the target microorganism for biodosimetry estimation due to being surrogate of pathogenic *E.coli* O157:H7 for fruit juice products (Koutchma et al, 2004, 2007; Koutchma et al, 2009; Murakami et al, 2004; Pala and Toklucu, 2013). In this method, a target microorganism, e.g., *E.coli* K-12, is introduced as a pulse injection from the inlet of the UV reactor. Then, bacterial concentration is measured at the outlet. Injection of bacterial suspension is repeated twice with UV lamps on and off. In first case, residence time distribution of unirradiated bacteria is determined when UV lamps are off. The distribution curve of unirradiated bacteria concentration directly relates with residence time distribution, whereas the distribution curve of survival bacteria after UV irradiation gives information about both residence time and UV irradiation distribution. The application of this method is useful for comparison of the reactor performance as well as the process efficiency.

2.4.1.1. Modeling of UV Inactivation Kinetics

In order to study the inactivation kinetics of a UV dose response curve, linear and non-linear inactivation kinetic models can be used. In non-linear inactivation curve, when there is a resistivity to inactivation of target microorganism at the beginning of UV disinfection, this behavior is represented as “shoulder” effect (Benabbou et al, 2007; Bermudez-Aguirre et al, 2009; Huang, 2009; Marugán et al, 2008). If the inactivation rate slows down at the end of inactivation process, this part of inactivation curve is named as “tailing” (Bialka et al, 2008; Buzrul and Alpas, 2007; Fernández et al, 2007; Huang, 2009; Marugán et al, 2008, Van Boekel, 2002). Tailing of inactivation curve occurs by the shadowing effect of high concentration of non-microbial solid particles or improper mixing of liquid food (Marugán et al, 2008). Another reason of tailing effect might be the increase in resistant and survival rate of microbial population in disinfected liquid food. Also agglomeration of death population is likely to prevent UV penetration to living cells due to improper mixing. Instead of Log-Linear model, these non-linear behaviors of microbial inactivation are carried out using empirical models.

2.4.1.1.1. Log-Linear Model

Log-Linear model is widely accepted and used to describe the microbial inactivation resulted from application of both thermal and non-thermal processes. This model assumes that death of microorganisms follows the rule of first order kinetics. The model is given in the following equation (Marugán et al, 2008; Van Boekel, 2002):

$$\log_{10}\left(\frac{N}{N_0}\right) = -kt \qquad (2.3)$$

where t is treatment time (min) and k is the inactivation rate constant (min^{-1}). The inactivation rate of target microorganism in bench top system is determined and the dose, which is needed for decimal reduction (D_{10}) rate is estimated from inactivation curve (dose vs. logarithmic inactivation). If the inactivation rate is linear, this decimal reduction rate is used in determination of the delivered germicidal dose for target microorganism in continuous flow UV reactor. Classical D value is calculated from the reciprocal of the first order rate constant (min/Log CFU). Eqn. 2.3 is also known as Chick-Watson linear equation (Marugán et al, 2008).

2.4.1.1.2. Weibull Model

In some cases, inactivation efficiency decreases by the effect of multiple hit. In this phenomenon, multiple UV contacts on a single cell or single UV light affects on a group of cells. Thus, less resistant cells are eliminated first, then more resistant cells are left to form a tail in survival curve (Bialka et al, 2008; Buzrul and Alpas, 2007; Fernández et al, 2007; Gómez et al, 2005; Van Boekel, 2002). Weibull distribution is defined as a simple kinetic model for description of microbial inactivation by thermal and non-thermal treatment methods. Weibull model usually describes sigmoid curves and exhibits concavity or convexity behaviors through downwards or upwards as a function of inactivation time or UV dose (Albert and Mafart, 2005; Stone et al, 2009). It is described as the following correlation (Bermudez-Aguirre et al, 2009; Bialka et al, 2008; Buzrul and Alpas, 2007; Chen, 2007; Fernández et al, 2007; Gómez et al, 2005; Huang, 2009; Van Boekel, 2002),

$$\log_{10}\left(\frac{N}{N_0}\right) = -\frac{1}{2.303}\left(\frac{t}{\alpha}\right)^{\beta} \tag{2.4}$$

where α is scale parameter and β represents shape parameter (or concavity index). When β is equal to 1, the inactivation curve appears first order linearly oriented. Upward concavity of the inactivation curve indicates stress adaptation of target microorganism, survived after UV exposure, in the case of β smaller than 1. Downward concavity shows accumulated damaging rates of UV in the cells, when β is greater than 1. Figure 2.9 represents the tailing and shouldering effects of the scale parameter.

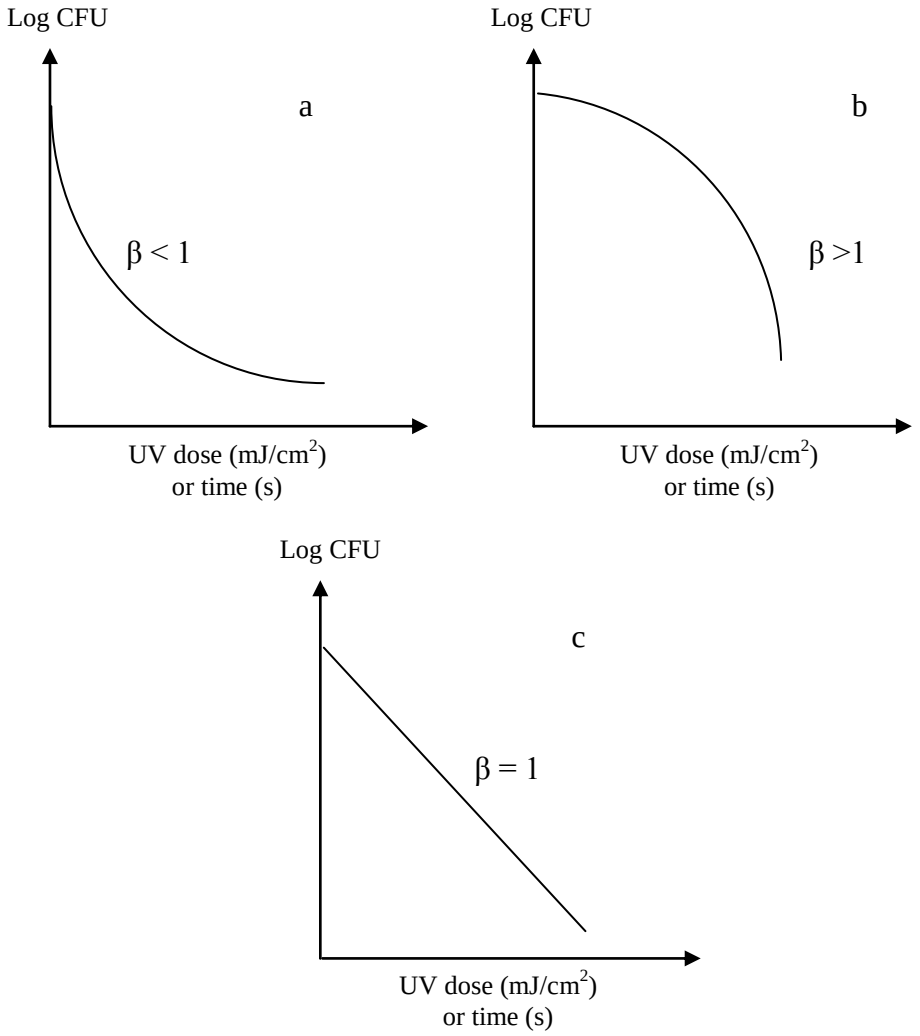

Figure 2.9. Microbial inactivation curves based on Weibull model after UV disinfection (a) Concavity (tailing) (b) Convexity (shoulding) (c) Linearity

The reliable time (t_R) is the life time indicating 90% reduction of the number of microbial cells (Van Boekel, 2002). It is similar to D value (the time necessary to reduce the number of microorganisms by a factor "10" but it shows high dependency on β. t_R for UV inactivation is calculated using Eqn. 2.5 (Bialka et al, 2008; Van Boekel, 2002):

$$t_R = \alpha \left(2.303\right)^{\frac{1}{\beta}} \tag{2.5}$$

2.4.1.1.3. Modified Chick-Watson Model

Chick-Watson equation is an empirical disinfection model considering the inactivation rate of a target microorganism changing as an exponential function of the disinfectant agent concentration (Chick, 1908; Watson, 1908). Integrated as a function of time, model can be represented as,

$$\left(\frac{N}{N_0}\right) = \exp\left(-kC^n\, t\right) \tag{2.6}$$

where k represents the Chick-Watson coefficient of specific lethality (min^{-1}), C is the concentration of disinfectant (mg/L), n is the dilution coefficient and t is the disinfection time (min). At low concentration of microbial population exposed to a long treatment period, the rate of inactivation stays constant until the end of inactivation process (Huang, 2009; Marugán et al, 2008). In order to describe the outward convexty or inward concavity in the inactivation curve, Chick-Watson model could be modified by introducing two parameters in the Eqn.2.6 (Cho et al, 2003; Marugán et al, 2008),

$$\log \frac{\mathrm{N}}{\mathrm{N}_0} = -\mathrm{k}_1\left[1 - \exp(-\mathrm{k}_2 \mathrm{t})\right] \tag{2.7}$$

where k_1 is the inactivation rate constant (min^{-1}) for the log-linear inactivation part of the curve, and k_2 is the first order UV decay constant (min^{-1}), representing the tailing effect of decelerated inactivation (Figure 2.10).

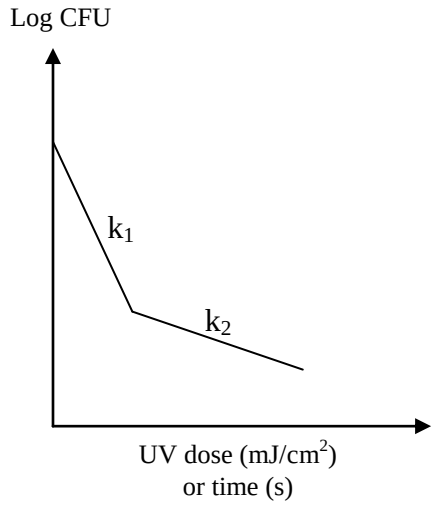

Figure 2.10. Representation of Modified Chick-Watson model for inactivation and first order UV decay constants

2.4.1.1.4. Hom Model

Hom model incorporates the parameter "h". The expresion is,

$$\log\left(\frac{N}{N_0}\right) = -k't^h \tag{2.8}$$

where k' is the inactivation rate constant of Hom model (min^{-1}) and "h" represents the UV penetration rate constant that describes the tailing or shoulder effect of inactivation rate. When h=1, this equation simplifies to Log-Linear equation. For the case h < 1 the equation permits the fitting of the tailing (inward concavity) part of the inactivation curve, for h > 1, the shoulder (outward convexity) part is predicted (Haas and Joffe, 1994; Lee and Nam, 2002; Marugán et al, 2008). Small k` value (inactivation rate constant) indicates that the microorganism shows larger resistivity to treatment (Figure 2.11).

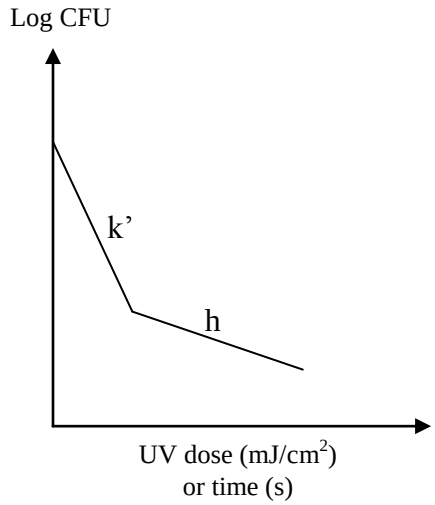

Figure 2.11. Representation of Hom model for inactivation and penetration rate constants

2.4.2. Chemical Actinometry Method

Actinometry is known as determination of the photon flux for a system of specific geometry (Kuhn et al, 1989, 2004; Rahn, 1997; Rahn et al, 2002). Actinometer is determined as the material that is used in the UV and visible spectral range for determination of UV dose. In this method, a reference substance undergoes to a photochemical reaction, of which quantum yield is known or can be calculated (Rahn, 1997; Rahn et al, 2003). Chemical actinometers can be calibrated against a physical device, other type of actinometers or by calorimetric methods (Kuhn et al, 1989; Liu et al, 2004; Rahn, 1997; Rahn et al, 2002, 2006). Most common chemical actinoneters are ferrioxalate or iodide-iodate solutions (Kuhn et al, 1989; Kuhn et al, 2004; Rahn et al, 1999; Rahn et al, 2003 and Bohrerova et al, 2005, 2008).

The most preferred chemical actinometers are potassium ferrioxalate ($K_3Fe(C_2O_4)_3$) and potassium iodide (KI) solutions. In the actinometry method where potassium ferrioxalate is used, iron, having 3^+ of oxidation state, is converted to ferrioxalate complex by photoreduction. Then decomposition occurs to form $Fe(C_2O_4)_2^{2-}$ and CO_2 by reducing the iron from 3+ to 2+ (Goldstein and Rabani, 2008; Hachard and Parker, 1956; Kuhn et al, 2004; Parker, 1953; Seliger, 1964). This method is applicable at 510 nm of wavelength for absorbance measurement of Fe(I1)-I.lo-phenanthroline complex in buffered acidic solution.

Nonetheless, the iodide/iodate chemical actinometry method, is applicable at 254 nm. Potassium iodide is dissolved in ultrapure water for a transition to a charge transfer. The charge transfer state then relaxes to a caged complex (I, e^-):

$$I^- + H_2O + hv \rightarrow I^-H_2O$$
$$I^-H_2O \rightarrow (I, e^-) + H_2O$$

A reversible reaction between the iodine atom and the electron produces free iodide. The breakdown of the caged complex can be formed when migration of the electron into the bulk solution is free to react as an aqueous electron:

$$(I, e^-) \rightarrow I^-$$
$$(I, e^-) \leftrightarrow I + e_{aq}^-$$

In the absence of an added electron scavenger, the bulk electrons can recombine with iodine atoms to form iodide. An equivalent number of iodine atoms in the bulk solution can then react with iodide to produce triiodide as follows:

$$I + I^- \rightarrow I_2^-$$
$$2I_2^- \rightarrow I_3^- + I^-$$

In spite of these chemical actinometers, of which are directly used by dissolution of water, there is no study mentioned about the use of these UV sensitive chemicals by dissolution of high acid food products, such as fruit juices. Phenols and other suspended materials can bound to chemical actinometer when dissolving in fruit juices. Then high change in color and absorptivity can be observed and makes impossible to measure absorptivity. As a result of this phenomena, using aqueous solutions of chemical actinometers may not be practical for determination of UV intensity in fruit juice.

2.4.3. Computational Fluid Dynamics (CFD)

Computational fluid dynamics (CFD) is the numerical solution method using fluid dynamics principles to predict the flow field of fluid in geometrical systems (Bolton and

Cotton, 2008; Versteeg and Malalasekera, 1995). It is applied to model a variety of flow phenomena, as well as to define physical, thermal and structural loads on bodies immersed in fluids. The aim of the application of computational fuid dynamics (CFD) is to simulate the fluid flow throughout a specified geometry (Versteeg and Malalasekera, 1995). The simulation of the flow field is governed by the equation of continuity, momentum, energy and mass transfer equations. Simultaenous solution of these equations and non linearity does not allow an analytic solution. Therefore, the numerical solution of the partial differential equations are used to define the distribution of one parameter (Versteeg and Malalasekera, 1995).

CFD simulation is composed of three main steps including pre-processing of the domain processing of the domain and post-processing of solutions. In the **pre processing step**, CFD problem is defined based on the physical problem. The domain is created based on the physical geometry. The boundaries of physical geometry such as domain inlet, outlet and boundary areas of solids are determined. Grid (mesh) structure is constructed. In the **processing** step, all of the governing equations is converted into algebraic form and solved by using direct or iterative methods at each grid elements. According to CFD solver and problem, solution techniques can be different but in contrast physical conditions are the same and well defined. The last step, **post processing** helps to analyze results of numerical solutions by representing them in both numerical and graphical form. Post processing can either be represented as numerical data or graphical and animated objects of fluid flow or distribution of properties (heat, mass and momentum). The distribution of the property is visualized by contour plots, streamlines, vectors or particle tracks throughout the domain.

Mathematical modeling by an appropriate CFD solver has been a fundamental part of UV processing and design of UV treatment systems to determine UV dose distribution. There are several reasons for application of mathematical modeling for the distribution of UV dose (Sozzi and Taghipour, 2006). Estimation of UV dose distribution by mathematical modeling helps the detection of points which recieve the less UV light in the designed UV system operating at a certain flow rate. UV light emission of continuous flow UV treatment systems depends on the size and geometry of UV tube, in addition to residence time distribution (RTD) of irradiated food (Sozzi and Taghipour, 2006; Koutchma, 2009; Koutchma et al, 2009).

To estimate UV intensity and RTD in continuous flow UV systems, an appropriate CFD software is needed. For design of a UV reactor by CFD, it is also essential to consider

the physical and optical properties of fluid food to calculate the optimum dimensions and geometry for high inactivation efficiency. The fluid foods may consist of either liquid phase (clarified fruit juices) individually or liquid-solid phase (pulp fruit juices or apple cider). For two phase liquid systems, particle modeling such as disperse particle model (DPM) is needed to determine the velocity and residence time distributions of solid particles. As a result, the quantity of absorbed UV energy can be computed. Nonetheless, suspended particles prevent the UV light passage by scattering and blocking (Koutchma, 2009; Koutchma et al, 2004; Unluturk et al, 2004). Hence, modeling of particles is used to define the UV intensity and residence time distribution of both suspended particles and microbial population that is either in free motion in the liquid phase or attached on the suspended particles (Bolton and Cotton, 2008; Christensen and Linden, 2001).

Computational fluid dynamics is a method of mathematical modeling that is used to operate the laws of fluid dynamics to predict the actual position of the small particles (i.e., microorganism) in irradiated fluid when it passes through a UV reactor (Bolton and Cotton, 2008; Koutchma et al, 2009). In order to estimate the irradiation effciency of a UV reactor, the CFD solver is integrated with an UV irradiance distribution model. After determinaton of flow domain and grid structure of UV reactor, the domain is integrated to CFD solver to analyze the flow using finite volume element method and iterative solution procedure. The CFD solver allows to inject single or group of microbial particles, randomly from the inlet of the reactor stream having an initial velocity and flow rate. During the determination of the path of particle(s) throughout the reactor, the UV dose rate is computed simultaneously from the irradiance distribution of particle(s) at each volume element that is multiplied by the residence time. Then, the CFD program integrates the UV dose for all the volume elements to obtain total UV dose for particle(s). The result is given as UV dose distribution in the flow volume. In the modeling of UV dose estimated by CFD, the calculated irradiance can be averaged over all the volume elements in the reactor. As a result, the volume averaged irradiance is estimated along with the residence time. (Bolton and Cotton, 2008; Koutchma, 2009).

CHAPTER 3

DETERMINATION OF UV DOSE BY BIODOSIMETRIC METHOD

3.1. Introduction

Fruit juices have a fundamental marketing in the worldwide industrial food. Most of fruit juice products have pH level less than 4.5. Grape juice is used in traditional and industrial production of red or white wine (Fredericks et al, 2011) or vinegar (Antonelli et al, 2004; Dávalos et al, 2005). The inhibition of low density lipoprotein oxidation that causes to lower the cholesterol in human blood might be maintained by antioxidant effect of grape juice (Frankel et al, 1998). Moreover, grape juice subserves platelet aggregation due to eicosanoid synthesis (Folts et al, 1997; Keevil et al, 2000). As a nutritional source, grape juice supplies energy, carbohydrate and Vitamin B-C for human body. But in contrast, these nutritive factors enable growing of spoilage microorganisms, such as yeasts and lactic acid bacteria (Garde-Cerdán et al, 2007; Marsellés-Fontanet et al, 2009).

The aim of the short-wave UV-C light treatement of fruit juices is to decrease the microbial population in addition to extend their shelf life (Demirci and Panico, 2008). As mentioned in Chapter 2, UV-C light affects DNA of microorganisms by penetration through the cell membranes and photoproduct accumulation. Transcription and replication of DNA stops and cell lysis occurs by inhibition (Bolton & Linden, 2003; Guerrero-Beltrán and Barbosa-Cánovas, 2005, 2006; Koutchma, 2009; Quek and Hu, 2008).

The objective of this study was to construct UV dose response curves for the freshly squeezed opaque grape juice (FSOGJ) and pasteurized clear grape juice (PCGJ) inoculated with different target microorganisms e.g., spoilage microorganisms (yeast and mold, and lactic acid bacteria), *S.cerevisiae* and *E.coli* K-12 by means of a bench top collimated beam apparatus (static system). The inactivation kinetics of microorganisms were studied by applying different mathematical models including Weibull, Log-Linear, Hom and modified Chick-Watson models. Additioanlly, the efficiency of UV-C irradiation as a non-thermal pasteurization process for freshly squeezed opaque and pasteurized clear grape juices were investigated. For this purpose, fermented and spoiled grape juice samples

and inoculated pasteurized clear grape juice samples were exposed to a UV-C irradiation of incident intensity level of 0.88 mW/cm^2 with sample depth of 0.153 cm for 0, 5, 10, 15, 20, 25, 30, 35 and 40 min in bench top collimated beam apparatus.

3.2. Experimental Study

3.2.1. Materials

Freshly squeezed opaque grape juice (FSOGJ) was obtained from Sultana type Turkish white grapes (*V.vinifera* spp. seedless) purchased from a market place in Izmir, Turkey. A household table top fruit juice extractor (Arçelik, Robolio, İstanbul) was used to mash the grapes without applying a washing step in order to supply an initial microbial load for spoilage of the juice. After the pressing step, white grape juice was strained twice by means of cheese cloths. In order to protect the color of juice during the long preperation step, L-ascorbic acid (Merck, Germany) in the amount of 600 mg/kg, was added as an antioxidant agent. Strained white grape juice was placed in an orbital shaker (Thermo Electron Corp., Ohio, United States) and mixed by applying 100 RPM agitation speed at 4 °C for 2-3 hours in order to allow precipitation of potassium bitartrate particles. Following a straining step and removal of bitartarates, the juice was packed in a plastic bottle and stored at the freezer (-18 °C) until it was used. Commercial pasteurized clear white grape juice (PCGJ), produced from seedless Sultana type traditional Turkish grapes, was purchased from a local market (Kavaklıdere, Ankara). Pasteurized juice was selected since it does not contain significant level of background flora. Juice samples in the size of 200 mL bottles were stored at room temperature (20 ºC) until it was used.

3.2.2. Target Microorganism and Cultivation

S.cerevisiae was selected because yeasts were known to be more resistant to UVC irradiation than pathogenic microorganisms in liquid food products. Another means, when yeasts are inactivated properly by exposing to UV light, pathonegic microorganisms are already assumed to be eliminated in the medium (Char et al, 2010; Hijnen et al, 2006; Ukuku and Geveke, 2010; Unluturk et al, 2008, 2010). It was also difficult to ferment

PCGJ to increase natural flora, instead *S.cerevisiae* was chosen for inoculation of PCGJ samples in the first study.

S.cerevisiae (NRRL Y 139) strain was kindly obtained from Dr. Ayse Handan Baysal at the Department of Food Engineering in Izmir Institute of Technology (Turkey). *S.cerevisiae* (NRRL Y 139) in plastic cryovials containing 20% of glycerol was stored at -80 ºC. "Peptone-Yeast Extract-Malt Extract" (PYM) Broth (10 g glycose, 5 g peptone, 3 g yeast extract, 3 g malt extract per 1 L of distilled water, Merck, Germany) was prepared for cultivation of *S.cerevisiae* strain. Acidity of broth was adjusted to pH 4.5. Enrichment of subculture was prepared by inoculation of 100 µl of *S.cerevisiae* from the stock culture into 100 mL of PYM broth. Then incubation was carried out for 24 hours by shaking at 225 RPM in orbital shaker (Thermo Electron Corp., Germany) at 30 ºC. In order to determine the number of *S.cerevisiae,* the samples were collected aseptically at every 2 hours by surface plating on Potato Dextrose Agar (PDA, Difco Corp., United States). The samples were also used for optical density measurement in UV-visible spectrophotometer (Carry 100, Varian Inc., United States) set at 600 nm of wavelength. It was observed that this strain completed the logarithmic phase at a concentration of ca. 8 Log CFU/mL after 20 hours incubation reaching to an optical density of 2.25. At stationary phase, yeast cells were centrifuged at 3000 RPM for 15 minutes at 4 ºC (Rotina 380R, Hettich Centrifuge, UK). Cells were rinsed with 0.85% sodium chloride (NaCl) solution twice. After the final centrifugation, the cell precipitate was harvested and inoculated into 500 mL of PCGJ. Microbial population level was 5-6 Log CFU/mL. Determination of microbial reduction level after each UV cycle was provided by serial dilutions using Phosphate Buffered Peptone Solution (Merck, Germany). The samples were inoculated after serial dilution in Potato Dextrose Agar (PDA, Difco Corp, United States) and incubated at 30 ºC for 72 hours.

100 mL of FSOGJ was fermented (or spoiled) by shaking at 100 RPM and incubating at 30 ºC for 16-24 hours. After fermentation, the microscopic examination revealed that the majority of spoilage microorganisms composed of mostly yeasts and lactic acid bacteria. During fermentation, sampling was carried out at every 3-4 hours to determine the stationary phase (approximately 16 h). In order to count yeasts and lactic acid bacteria in fermented juice, 50 µL of the sample was inoculated onto Tryptic Soy Agar (TSA, Difco Corp, United States), Potato Dextrose Agar (PDA, Difco Corp, United States) acidified with 10% tartaric acid by spread plating technique and De Man Rogosa-Sharp Agar (MRS, Merck, Germany) by single layer pour plate technique. TSA plates

were incubated at 37 ºC for overnight to determine total aerobic count. Yeasts were counted on PDA plates after incubation at 25 ºC for 2 days. Lactic acid bacteria inoculated in MRS plates were counted after incubation at 30 ºC for 2 days.

E.coli K-12 (ATCC 25253), a non pathogenic surrogate of *E.coli* O157:H7, was also used as target microorganism. Since the pH of PCGJ and FSOGJ was less than 3.6 and 3.94, *E.coli* K-12 (ATCC 25253) strain was needed to be first adapted to these pH levels by using malic and tartaric acid applied within several steps (Koutchma et al, 2007; Pala and Toklucu, 2013). For this purpose, malic and tartaric acid were added to 100 ml of TSB gradually and pH was adjusted at each time. *E.coli* K-12 (ATCC 25253) starting culture was inoculated to 100 ml of Tryptone soy broth (TSB, Merck, Germany) with pH level of 7.20. Culture was enriched at 37 ºC for overnight. One milliliter of this culture was incubated in TSB adjusted to pH 6 at 37 ºC for 18-24 h. 1 mL of culture, adapted to pH 6 culture was inoculated to TSB which was adjusted to pH 5.5 and then incubated for 18 h at 37 ºC. Similarly, 1 ml of culture adapted to pH 5.5 was inoculated to TSB which was adjusted to 5.0 pH. This procedure was repeated for TSB adjusted to pH 4.5 and pH 4.0. Finally, Enriched TSB culture, adopted to pH 4.0 was inoculated to TSB of which pH is 3.6. After adaptation of *E.coli* K-12 to pH 3.6, a single colony was transferred to 100 ml of TSB supplemented with 0.75% (w/v) glucose (Merck, Germany). and then left for incubation at 37 ºC for overnight. Enriched TSB adjusted to pH 4 was used to inoculate FSOGJ. 100 mL of enriched TSB broth was centrifuged at 750 RPM for 5 min to obtain a yield of concentration about 6-7 Log CFU/mL in 500 ml of grape juice samples. Enumeration of *E.coli* K-12 (ATCC 25253) was determined on Tryptic soy agar (Merck, Germany) using appropriate dilutions with peptone water using a phosphate buffer (Merck, Germany) at 37 ºC for 18 h.

Before biodosimetry study, the acid adapted culture prepared in TSB having pH adjusted to 4.0 and 3.6 was tested by inoculating into grape juice products (Pala and Toklucu, 2013). In order to determine the possible inactivation by the effect of high acidic environment of grape juice, both acid adapted TSB broth was centrifuged at 3000 RPM for 5 min at 4 ºC and supernatant was separated. Cells were inoculated to 100 ml of FSOGJ and PCGJ with initial concentration of 10^{7-8} CFU/mL. Inoculated grape juices were then incubated at 37 ºC for 24 h and microbal count was done after 2, 4, 6, 7, 10 and 24 hours by tryptone soy agar (TSA, Merck, Germany).

In order to eliminate total microbial backflora, FSOGJ was pasteurized by thermal treatment before inoculation of *E.coli* K-12. For this aim, 100 ml of FSOGJ was heated in

a water bath from 25 °C to 72 °C, of which is defined as optimum pasteurization temperature for grape juice (Sanchez-Moreno et al, 2004; Timmermans et al, 2011). Temperature was controlled by a thermocouple, placed into the center of sample. Moreover, grape juice sample was shaked continuously to maintain homogeneous temperature distribution during heating. After 10 minutes, center of sample was reached to 72 °C. Then sample was kept at 72 °C for 10-20 seconds for pasteurization. Finally grape juice sample was immediately placed into icebath for cooling.

3.2.3. UV Dose Response Curves

In order to construct a UV dose response curve of microorganisms, UV biodosimetry experiment was conducted by using collimated beam apparatus described in Bolton, (2003). Grape juice samples were exposured to UV by using closed bench top ultraviolet system, shown in Figure 3.1. Bench top system consists of two identical low pressure mercury vapor UV lamp at 254 nm wavelength (UVP XX-15, UVP Inc., CA, USA), a platform on which petri dish and a vortex mixer was placed for UV exposure. The UV intensity level and the distance is controlled by raising or lowering the tray system. A hole is placed on top of the system with dimensions equal to one of a standard petri dish diameter. A shutter is used to block UV light before measurement. Ultraviolet lamps were switched on about 30 minutes before the measurement to provide complete activation.

A cover was closed in front of the system during UV experiment to prevent direct contact of UV light with human skin. The whole system was constructed by cardboard with a flatblack paint in order to minimize the loss of light. Samples were placed in 50 mm diameter Petri dishes located directly under the collimated UV beam and stirred continuously during the irradiation with a vortex mixer (IKA, Yellowline TTS 2, IKA® Werke GmbH & Co. KG, Germany) set at dial #5. The UV intensity at the surface of the sample (incident intensity (I_o) or irradiance at the surface) was measured using a radiometer with UVX-25 sensor (UVX, UVP Inc., CA, USA). The radiometer was placed at a similar distance from the UV lamp as the grape juice samples. The UV lamp was switched on for about 30 min prior to UV treatment of grape juice samples in order to minimize fluctuations in intensity.

3 ml of fermented FSOGJ mixture was poured into sterile plastic Petri dish. By this way, 0.154 cm of sample depth was provided. Moreover, the entire sample totally covered

the Petri surface without any empty space (Figure 3.1). Prior to usage, the collimated beam apparatus was cleaned and sanitized. For the UV inactivation treatments, inoculated plates were subjected to different doses of UV-C light. The average UV intensity in the stirred sample (I_{ave}) was calculated by an integration of Beer-Lambert law as in Eqn 2.1 in Chapter 2. I_0 was measured at as 0.88 mW/cm^2 at the position of 1st tray (36 cm close to lamp surface). I_{ave} was calculated as 0.34 mW/cm^{2}for FSOGJ (A_{254}=15.317 cm^{-1}) and 0.66 mW/cm^2 for PCGJ (A_{254}=3.895 cm^{-1}). UV dose was calculated from these irradiance values and exposure times ranging from 0 to 40 minutes and applying Eqn 2.2 in Chapter 2.

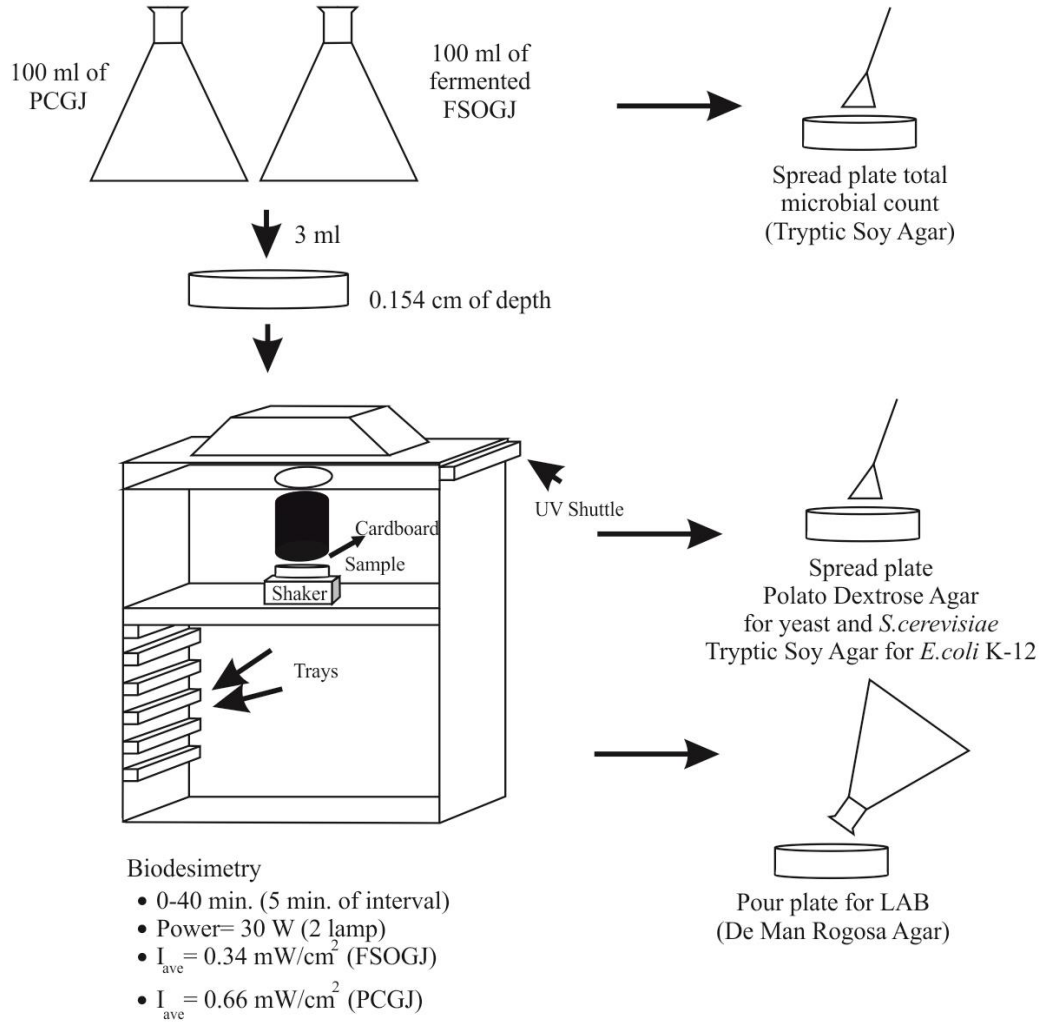

Figure 3.1. Biodosimetric study with grape juice samples in closed bench top collimated beam apparatus

3.2.4. Modeling of UV-C Inactivation Kinetics

Data from bench top collimated beam apparatus were used for inactivation kinetic models, represented in Chapter 2, Section 2.4.1. Duplicate experiments were carried out. Inactivation and model parameter results were expressed as average ± standard deviation. The parameters in the Weibull distribution, Log-Linear, Hom equation and modified Chick Watson equation were estimated by a program written in MATLAB® (MATLAB® 7.1, Mathworks Inc., Natic MA, USA) to find the best fit. In order to determine the suitability of fitted functions, the root mean squared error (RMSE) was computed using the calculated and experimentally determined logarithmic reductions by the following correlation:

$$RMSE = \sqrt{\frac{1}{n}\sum\left[\left(\log\frac{N}{N_0}\right)_{cal} - \left(\log\frac{N}{N_0}\right)_{\exp}\right]^2} \qquad (3.1)$$

The analysis of Variance (ANOVA, p=0.05) was performed by using commercial spread sheet (Microsoft Excel, Redmond, WA, USA).

3.3. Results and Discussion

After acid adaptation of *E.coli* K-12 (ATCC 25253), 10^8 CFU/ml of population was enumerated at pH 3.5-4.0 (Figure 3.2a). To determine the resistance of *E.coli* K-12 to acid adaptation, culture was inoculated to both grape juices and enumerated during 24 hours. It was seen that, 8 Log CFU/ml of initial load was decreased to 7 Log CFU/ml after 24 hours in PCGJ. Initial number of population did not change after 2 hours. Besides, microbial population in FSOGJ (pH=3.94) increased to 9 Log CFU/ml after 24 hours. Slight increase was seen in microbial load after 2 hours (Figure 3.2b). It could be commented that, no significant population decrease after 2-4 hours was noticed due to pH effect of these juice products. Unlikely Pala and Toklucu et al (2012). found that complete inactivation of *E.coli* K-12 after 10 h of incubation due to the effect of low pH of original fruit juice.

Before fermentation, total microbial load of pasteurized FSOGJ was examined by spread plating on TSA. No initial microbial load was found. Then, FSOGJ samples inoculated with acid adapted *E coli* K-12 were treated with UV in bench top collimated

beam apparatus. UV treatment was carried out for FSOGJ by applying UV doses between 0-0.816 J/cm^2 (0-40 min) at 0.34 mW/cm^2 of average UV intensity. On the other hand UV dose range of PCGJ was 0-1.588 J/cm^2 at 0.66 mW/cm^2 of average UV intensity.

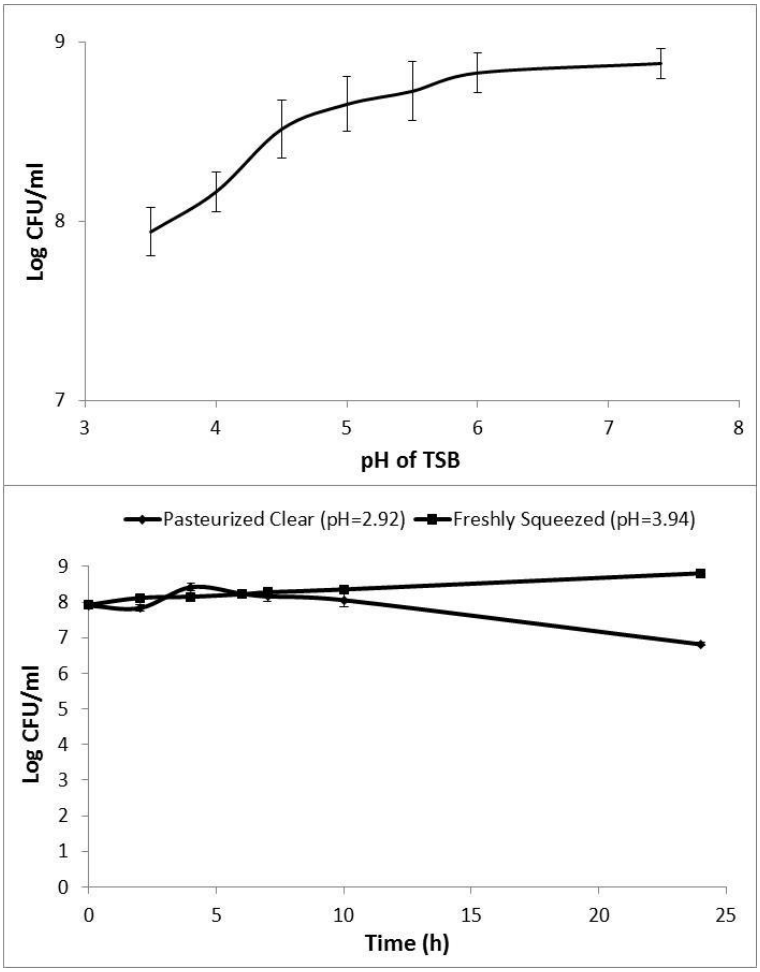

Figure 3.2. (a) Acid adapted *E.coli* K-12 (ATCC 25253) with respect to pH (b) Resistance of acid adapted *E.coli* K-12 (ATCC 25253) in grape juices

Sample was collected at every 5 min of UV treatment (0, 5, 10, 15, 20, 25, 30, 35 and 40 min of sampling). For yeast, 3.539±0.123 Log CFU/ml reduction was achieved in fermented FSOGJ. On the other hand, inactivation of LAB was 5.501±0.042 Log CFU/ml after application of 816 mJ/cm^2 and 40 min UV exposure. (Figure 3.3). Higher inactivation rate was seen for *E.coli* K-12 (6.910±0.090 Log CFU/ml) inoculated in pasteurized FSOGJ at the same UV dose. On the other hand, inactivation level of *E.coli* K-12 was the highest (7.426±0.063 Log CFU/ml) in PCGJ when 1588 mJ/cm^2 UV dose applied. The inactivation of *S.cerevisiae* was 6.387±0.046 Log CFU/ml at the same UV dose. Murakami et al, (2006) inactivated *E-coli* K-12 in apple juice/cider using bench top collimated beam

apparatus. They applied 0-100 mJ/cm^2 of UV dose and reached 3.6 Log CFU/ml inactivation rate. The results obtained in our study were much higher than those of Murakami et al (2006). This is because of the differences in UV dose levels applied in two studies.

It was seen that all of the target microorganisms inoculated in pasteurzed/fermented FSOGJ and PCGJ showed tailing effect after 10 min. These results also showed that low microbial inactivation rate of yeast was due to heterogenic distribution of microbial population during UV-C treatment (Bialka et al, 2008; Unluturk et al, 2008; Unluturk et al, 2010). There might be several reasons for having lower inactivation for yeast compared to that of LAB and *E coli* K-12. In comparison of bacteria, cell wall of yeasts are thicker that could slow down the inactivation mechanisms (Ortuño et al, 2012). Besides, large yeast cells might not be in good contact with UV light due to having extra emission source such as solid particles and precipitates in the flow medium (Ortuño et al, 2012). Another reason of obtaining less inactivation rate might be due to the low pH level of fruit juice, which allow the growth of spoilage yeasts. In fruit juices, spoilage yeasts can adopt low pH in the presence of high concentration of salt or sugar (Battey et al, 2002; Ochoa-Velasco and Guerrero-Beltrán, 2012; Piper et al, 2001; Wareing and Davenport, 2007). Hence, the inactivation rate of yeast in FSOGJ was less than that of bacteria.

The microbial inactivation curves obtained from the application of UV-C irradiation of opaque grape juice samples exhibited tailing behavior (Figure 3.3). The shoulder effect on the inactivation of LAB and *E.coli* K-12 was negligible. The tailing might be due to the suspended solid particles in the medium or/ and cell aggregation caused by improper mixing. This behavior results in non-homogeneous irradiation and nonlinear inactivation kinetics (Unluturk et al, 2008, 2010). Thus, modeling of inactivation kinetics was carried out by non-Log-Linear models including Weibull, Hom and modified Chick Watson models, instead of Log Linear model. Reliable time (t_R in min.) was also estimated by using Weibull model parameters. It was found that kinetic parameters of Chick Watson model were much higher than that of Hom and Weibull models. Unluturk et al, (2010) also reported that the kinetic parameters (k1 and k2) of the modified Chick Watson model were higher than Log-Linear and Hom models. k_1 value (min^{-1}) was estimated as 2.473±0.829 for spoilage yeast in FSOGJ (Table 3.1). But in contrast, k_1 value of LAB was noticed higher (4.816±0.869) than that of yeast. This was explained as two-fold higher inactivation rate for LAB compared to spoilage yeast when exposed to UV treatment (Figure 3.2). Highest k_1 was seen as 6.220±0.889 for *E.coli* K-12, which shows

less resistivity to UV light than that of yeast and LAB in FSOGJ. k_1 value (min^{-1}) was 6.603±1.095 for *E.coli* K-12 inoculated in PCGJ. Nonetheless, k_1 was determined as 4.900±1.411 min^{-1} for *S.cerevisiae* in PCGJ.

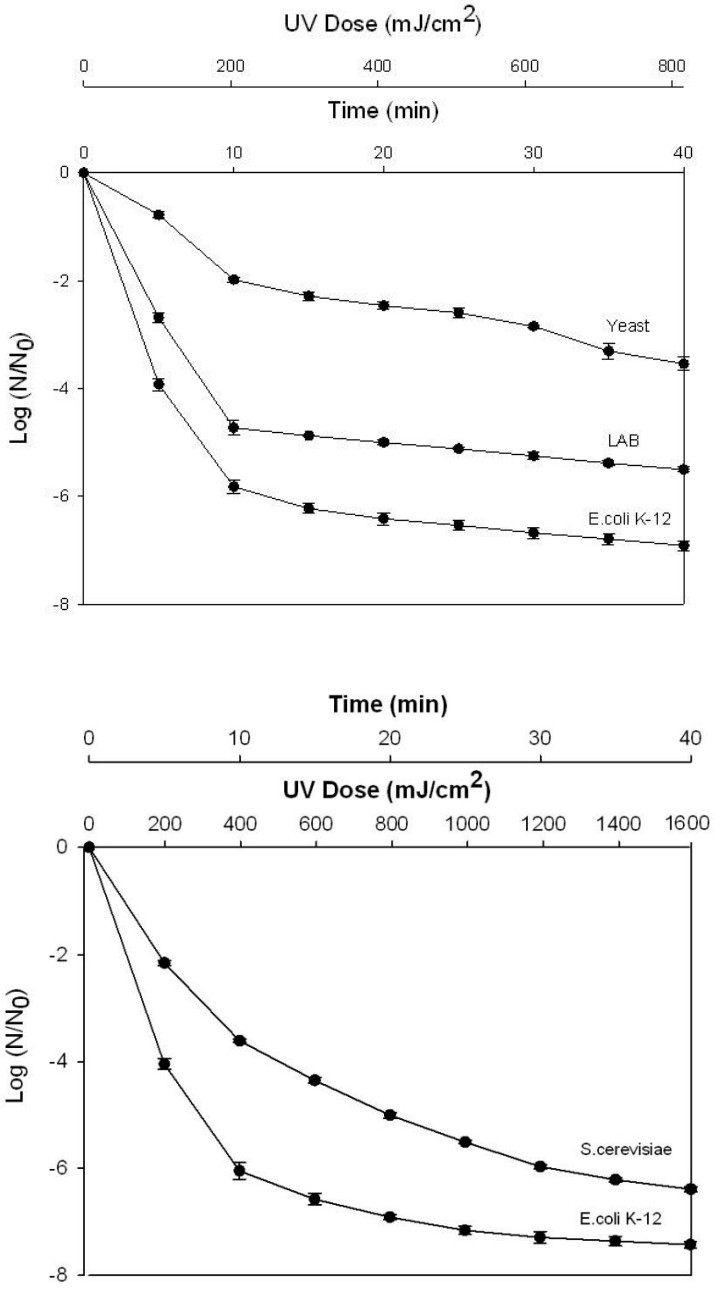

Figure 3.3. UV dose response curves of (a) Yeast, LAB and *E.coli* K-12 in FSOGJ (b) *S.cerevisiae* and *E.coli* K-12 in PCGJ

Table 3.1. Modified Chick-Watson Model Parameters for Target Microorganisms

Type of Grape Juice	Microorganism	k_1 (min^{-1})	k_2 (min^{-1})
FSOGJ	Yeast	2.473±0.829	0.611±0.459
	LAB	4.816±0.869	0.660±0.540
	E.coli K-12	6.220±0.889	0.661±0.544
PCGJ	*S.cerevisiae*	4.900±1.411	0.607±0.460
	E.coli K-12	6.603±1.095	0.633±0.503

The resistance of inactivated microorganism was determined by the comparison of the kinetic constant (k′) in Hom model. The parameter h in the Hom model was calculated less than 1 for all the flow conditions and fluid cases. Results were represented in Table 3.2. As commented for the results in modified Chick Watson model, UV light resistivity of yeast population in FSOGJ was found to be higher. Moreover, LAB was less resistance than yeast in UV irradiated FSOGJ. As mentioned for Modified Chick-Watson model, *E.coli* K-12 had highest k′ for both grape juice samples defined as the least resistance to UV-C than that of yeast and LAB. These results were also supported by Gabriel (2012). In that study, *E.coli* O157:H7 and spoilage yeast strains were inactivated in clear pasteurized apple juice by UV-C light. Although, 2.5 min of exposure time is required for 1 Log CFU/mL reduction in *E.coli* O157:H7, 8.0 min was necessary for yeast at the same UV intensity. It was claimed that high amount of UV-C light was absorbed by yeast, reducing UV-C treatment efficiency (Gabriel, 2012).

Table 3.2. Hom Model Parameters for Target Microorganisms

Type of Grape Juice	Microorganism	k' (min^{-1})	h
FSOGJ	Yeast	0.156±0.037	0.934±0.073
	LAB	0.311±0.140	0.961±0.045
	E.coli K-12	0.386±0.206	0.982±0.011
PCGJ	*S.cerevisiae*	0.300±0.081	0.952±0.047
	E.coli K-12	0.360±0.180	0.998±0.004

Results of Weibull model were listed in Table 3.3. This results indicated that remaining cells are less probable to be terminated since an increase in resistivity occurs when exposed to UV-C light at longer treatment times (Van Boekel, 2002). But in contrast, shape parameter was greater than 1 for each strain. The scale parameter α is known as the measure of the organism resistance to treatment. The highest α (1.045±0.061) was estimated for *E.coli* K-12. Besides, α was estimated as higher for LAB (1.025±0.021 min)

than yeast (1.009±0.016 min). Unluturk et al, (2010) found that the scale parameter of *E.coli* K-12 was higher than *L. innocua*. They also defined lower reduction for *E.coli* K-12, depending on the α. In order to withdraw a definite conclusion, reliable time (t_R) values were compared (Table 3.4). Reliable time value of yeast was two-fold higher (4.991±2.255 min) than that of LAB (2.561±0.356 min). Lower reliable time (2.502±0.375) was seen for *E.coli* K-12 in FSOGJ samples which is indicating the highest sensitivity to UV than yeast and LAB. Large standard deviation of t_R for yeast might be explained with the high turbid structure of FSOGJ causing a competitive environment for yeast population during UV-C exposure. Nonetheless, it was found that the values for kinetic parameter h determined by Hom model were smaller than those of β estimated by Weibull model. This is because, some of the data were not used for the estimation of Weibull model parameters. Other than the shape parameter and the concavity index, the reliable time (t_R) was checked, while applying the Weibull Model. Since the standard deviations of some of the inactivation data are quite large, in order to get meaningful and logical t_R values, some of these outlier data were not included in the calculations while testing the performance of the Weibull model. Therefore, Hom model parameter (h) and shape parameter of Weibull model (β) might not be comparable. Besides, the increase in standard deviation levels was due to the experimental problems caused by using of FSOGJ samples having high UV light absorptivity and in-homogeneity structure, fluctuation in UV light during inactivation and shadowing effect of suspended particles. The models were compared based on RMSE and R^2, and shown in Table 3.4. Although, modified Chick Watson model resulted in a very good fit of the experimental data for each microbial populations with the correlation coefficient (R^2) higher than 0.996, Hom model estimated more reliable parameters based on lower RMSE values.

Table 3.3. Weibull Model Parameters for Target Microorganisms

Type of Grape Juice	Microorganism	α_{ave} (min)	β_{ave}	t_{Rave} (min)
FSOGJ	Yeast	1.009±0.016	0.559±0.085	4.991±2.255
	LAB	1.025±0.021	0.858±0.166	2.561±0.356
	E.coli K-12	1.045±0.061	0.990±0.173	2.502±0.375
PCGJ	*S.cerevisiae*	1.005±0.026	0.833±0.086	2.830±0.308
	E.coli K-12	1.005±0.051	0.981±0.200	2.573±0.441

Table 3.4. Goodness of Fit Parameters for Models

Type of Grape Juice	M.orgn.	Model	RMSE	R^2
FSOGJ	Yeast	Weibull	0.0003	0.996
		Chick Watson	0.0003	0.998
		Hom	0.0003	0.999
	LAB	Weibull	0.0007	0.994
		Chick Watson	0.0008	0.997
		Hom	0.0003	0.999
	E.coli K-12	Weibull	0.0431	0.992
		Chick Watson	0.3577	0.986
		Hom	0.0553	0.991
PCGJ	*S.cerevisiae*	Weibull	0.0002	0.997
		Chick Watson	0.0002	0.996
		Hom	0.0001	0.999
	E.coli K-12	Weibull	0.0001	0.998
		Chick Watson	0.0002	0.995
		Hom	0.0006	0.991

3.4. Conclusions

Biodosimetric method was applied to construct UV dose response curves for FSOGJ and PCGJ inoculated with different target microorganisms including spoilage yeast and LAB, *E coli* K-12 and *S.cerevisiae*. For this aim, a bench top collimated beam aparatus was utuilized. Samples were treated by UV-C light for 0-40 min at a certain UV intensity levels (0.34 and 0.66 mW/cm^2) and doses (0-816 and 0-1588 mJ/cm^2). The number of *E.coli* K-12 suspended in FSOGJ and PCGJ was reduced by 6.910±0.090 Log CFU/ml and 7.426±0.063 Log CFU/ml, respectively under studied conditions. It was also observed that inactivation rate of LAB (5.501±0.042 Log CFU/ml) was higher than that of spoilage yeast (3.539±0.123 Log CFU/ml) suspended in FSOGJ. Non-linear inactivation models (Modified Chick Watson, Hom and Weibull model) were applied to examine the inactivation kinetics of dose response curves. These three models agreed that the spoilage yeast was the most resistant and *E.coli* K-12 is the most sensitive microorganisms to UV-C irradiation under studied conditions. The inactivation kinetics of spoilage microorganisms and *S.cerevisiae* were best described by Hom model with the smallest root mean squared error (RMSE) ($R^2 \geq 0.99$). On the other hand, the inactivation kinetics of *E.coli* K-12 was well correlated by using Weibull model. Consequently, UV dose response curves constructed by means of the biodosimetric method and described by Hom and Weibull models will be used for determination of the UV dose delivered in a continuous flow UV reactor. More details about this issue will be given in Chapter 7.

CHAPTER 4

DETERMINATION OF UV DOSE AND UV INTENSITY BY CHEMICAL ACTINOMETRY METHOD

4.1. Introduction

The problem in positioning of a UV sensors limits the determination of UV intensity in continuous flow UV reactor. Moreover, signal saturation from the high-intensity and short pulsing time of UV light source complicates the measurement of UV intensity and dose (Bohrerova et al, 2008). Chemical actinometry can be described as the photochemical method to be used for measurement of the UV intensity of a light source. Chemicals, which are sensitive to UV light at definite wavelengths are exposured to UV light and photochemical changes (color or absorptivity change) are mesured both spectrophotometrically or colorimetrically (Kuhn et al, 1989; Liu et al, 2004; Rahn, 1997, Rahn et al, 2002, 2006). The relation between absorbed photons by chemical and photochemical conversion changes are used for the determination of UV intensity level of the UV system. The chemical actinometric method can be used for both bench top collimated beam apparatus and thin-film continuous flow UV reactor. The first objective of this study was to compare the UV intensity measured by using a chemical actinometric method with the one recorded by a radiometer in bench top collimated beam apparatus. The second study was to determine UV intensity in a continuous flow UV reactor by means of triiodide (I_3) formation from the potassium iodide (KI) solution reacting under UV exposure.

4.2. Experimental Study

4.2.1. Materials

Iodide iodate solution was used as a chemical actinometer to measure UV intensity of the bench top collimated beam apparatus and a continuous flow UV reactor. For this

aim, 0.6 M of potassium iodide (KI, Merck, Germany), 0.1 M of potassium iodate (KIO_3, Merck, Germany) and 0.01 M of borax ($Na_2B_4O_7.10H_2O$, Merck, Germany) were mixed and stored at refrigerated temperature prior to use.

4.2.2. Methods

4.2.2.1. Preparation of Actinometry Solution

Preparation of chemical actinometer was performed according to the method described in Rahn, (1997) by following two procedures: In the frst procedure, 9.96 g of potassium iodide (0.6 M of KI, Merck, Germany) was mixed with 2.14 g of potassium iodate (0.1 M of KIO_3, Merck, Germany) and 0.381 g of Borax (0.01 M of $Na_2B_4O_7.10H_2O$, Merck, Germany) to have 100 ml reaction mixture. This solution is used in the bench top collimated beam apparatus in order to measure UV intensity. In the second one, 49.8 g of potassium iodide was mixed with 10.7 g of potassium iodate and 1.905 g of borax to prepare 500 ml of samples for UV intensity measurement in the continuous flow UV reactor constructed in the Department of Food Engineering, IZTECH, Izmir, Turkey. Sterile ultrapure water was used to prepare reaction mixture. Materials used to prepare actinometer solution were reagent grade and used without further purification. Actinometry solution is very sensitive to thermal oxidation which may result in increase in the triiodide concentration. Consequently, iodide/iodate solution was prepared daily without any direct daylight contact to prevent primary reaction of the mixture (Kuhn et al, 1989, Rahn, 1997, Rahn et al, 2003, 2006).

4.2.2.2. UV Intensity Measurement in Bench Top Collimated Beam Apparatus

Bench top collimated beam apparatus was defined briefly in Section 3.2.2.3. Actinometrical solution was irradiated using two low mercury UV lamps, emitting light at 254 nm (15 W, UVX, UVP Inc., CA, USA). 6 ml of iodide/iodate solution was poured into sterile plastic Petri dish having 6 cm diameter. By this way, not only 0.3 cm of sample depth was provided, but also the entire sample covered the Petri surface homogeneously.

The UV intensity at the surface of the sample (I_o) was measured using a radiometer equipped with UVX-25 sensor (UVX, UVP Inc., CA, USA). UV lamps were switched on for about 30 min prior to actinometrical study to minimize the fluctuations in the UV intensity. The sample was exposured to UV light for 32 min. For every 4 min interval, different samples were used for exposure. Spectrophotometrical data was collected and used for estimation of the UV dose by following the step by step procedure summarized in the section of 4.2.2.3. In that case, measurement of bench top radiometer was applied under the same UV light distance to compare actinometrical measurements.

4.2.2.3. UV Intensity Measurement in Continuous Flow UV Reactor

The schematic diagram of completed S-shaped UV disinfection system was shown in Figure 4.1. UV system was composed of a S-shaped annular UV tube, made from quartz glass and equipped with a cylindrical reflector (Afe Olgunlar Inc., Turkey) and seven 254 nm low mercury UV lamps (UVX Inc., England). One of the UV lamps was placed in the middle of the system, whereas remaining 6 UV lamps were installed around the outer cylinder of UV tube at an equivalent distance (Figure 4.1). Heat accumulation caused by UV lamps was removed from the reactor by an air pump compressor (KNF Inc., Germany). The glass sample tank with cooling unit (Guven Cam, Turkey) was integrated with the UV reactor to control the temperature of irradiated liquid. All the measurements were done at room temperature. Transferring of reaction mixture was carried out by silicone piping. Sampling was done by using glass sample taps. A peristaltic pump (Watson Marlow Inc., England) was used to transfer the fluid from the tank to the system and vice versa. Properties of S-shaped continous flow UV reactor was summarized in Table 4.1. The residence time of liquid to complete one passage from the UV system was determined as 244 seconds at 0.90 mL/s of flow rate.

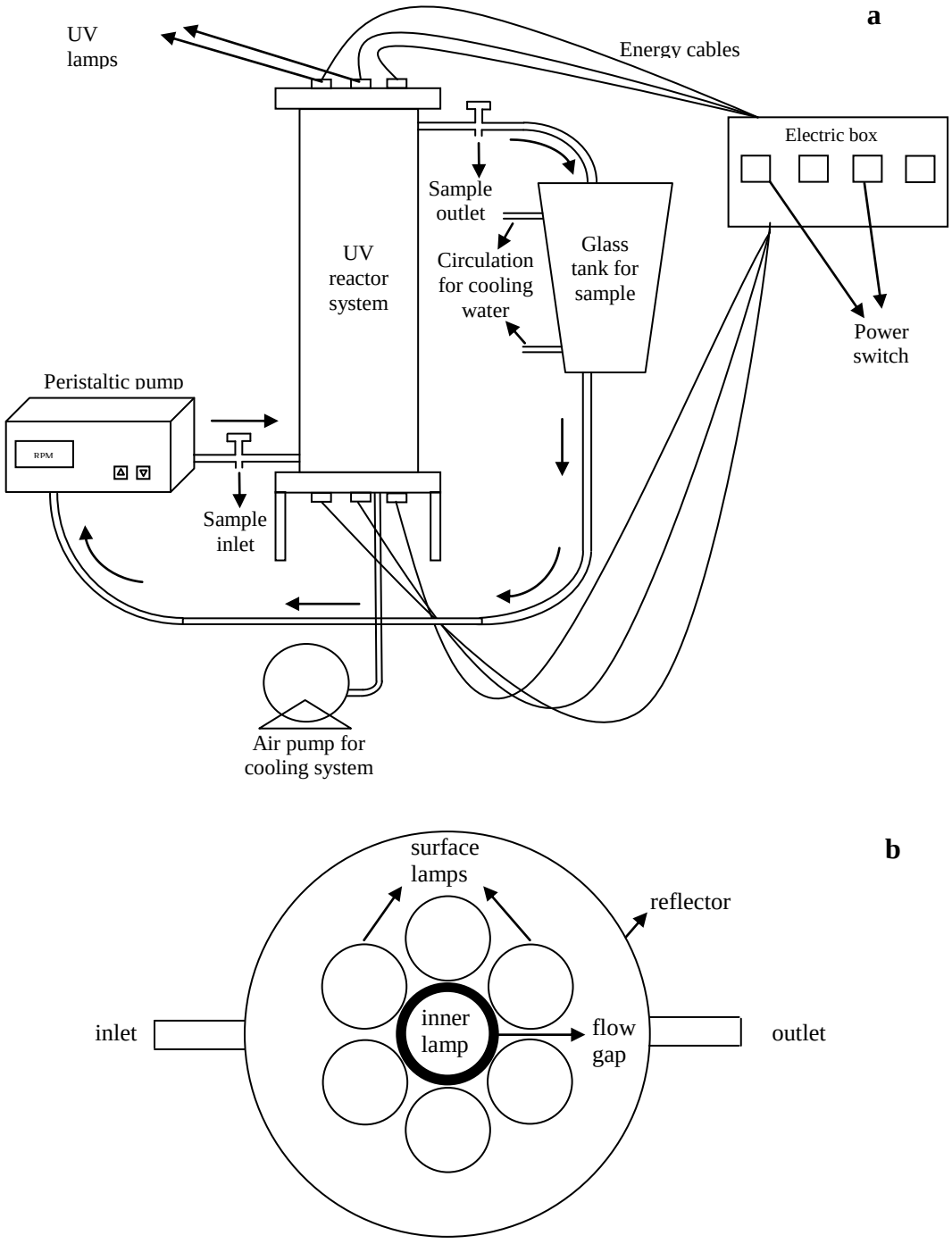

Figure 4.1. (a) Schematic view of continuous flow S-shaped UV system with flow direction (b) Lamp configuration (top-view)

Table 4.1. Geometric Properties of S-shaped UV Reactor

Tube Material	Quartz glass
Glass Thickness (m)	0.002
$D_{out\ cylinder}$ (m)	0.04
$D_{in\ cylinder}$ (m)	0.03
$D_{flow\ inlet}$ (m)	0.004
H_{tube} (m)	0.4
Flow Gap (m)	0.005
A_{flux} (m^2)	5.498×10^{-4}
V_{flux} (m^3)	2.199×10^{-4}
A_{inlet} (m^2)	1.26×10^{-4}
Lamp Properties	254 nm, low mercury
# of UV Lamp	7
Total Power (W)	105
Q_{inlet} (ml/s)	0.90
Residence time (s/cycle)	244
Re_{inlet}	36.38

500 ml of iodide/iodate solution was UV irradiated in the continuous flow UV reactor by recycling 8 times. Two different studies were carried out: First study was applied by switching central lamp on and keeping 6 of the surface lamps off. By this way, UV intensity of single lamp was measured in UV reactor. Second study was done by switching the 6 lamps on and switching central lamp off. UV intensity was measured for the case when 6 lamps were on in the reactor. As a result of these two studies, UV intensity measurements by using single and multiple lamps were evaluated. After each cycle, the irradiated solution was collected through the sterile glass tubes and kept under refrigerated conditions in dark prior to spectrometric analysis. During UV irradiation, sample was collected from each cycle at exit of the UV system and its absorbance was immediately recorded using a UV-visible spectrophotometer (Carry 100, Varian Inc., CA, United States) set at a wavelength of 300 and 352 nm. Since absorptivity of the original triiodide solution was not appropriate for optical density measurement, all the samples were diluted 1:100 by dilution factor of 100. UV intensity rate was estimated as described in Rahn (1999) and Rahn et al, (2003, 2006). First, optical density of the original KI solution was measured before UV application at 300 and 352 nm. Then, the initial amount of iodide concentration was calculated by using the following formula:

$$[c_{iodide}](M) = \left.\frac{OD}{1.061 * l}\right|_{@300\,nm} \tag{4.1}$$

where ε referred to the extinction coefficient and is equal to 1.061 $(M*cm)^{-1}$ and *l* was the path length which is equal for 1 cm (the width of the quartz cuvette used in spectrophotometer). The rate of a photochemical reaction was described as the quantum yield, defined as the ratio of number of absorbed molecules to the number of photons absorbed per unit time. Quantum yield was determined by a temperature (T) dependent expression (Rahn et al, 1997) shown as in Eqn 4.2:

$$\Phi = 0.75[1 + 0.02(T - 20.7)][1 + 0.23(c_{iodide} - 0.577)] \tag{4.2}$$

For determination of triiodide concentration after photocatalytic reaction, the following equation was used (Rahn et al, 1997, 2003):

$$[c_{triiodide}](M) = \left. \frac{OD}{26400 \frac{1}{M\ cm} * l} \right|_{@352\,nm} \tag{4.3}$$

where 26400 $(M\ cm)^{-1}$ is molar extinction coefficient of triiodide formed for a 1 cm pathlength cell. Total number of moles of triiodide formed was found by the following equation:

$$n_{triiodide} = c_{triiodide} * V_{sample} \tag{4.4}$$

The moles of product were divided by the quantum yield to maintain the number of einsteins of photons absorbed by the sample:

$$E\left(\frac{einsteins}{L}\right) = \frac{\Delta OD_{352\,nm} * V_{sample}}{26400 * \Phi} \tag{4.5}$$

Assuming that all photons absorbed at 254 nm of wavelength, the total energy absorbed by the sample (incident joules) can be represented as the following:

$$Incident\ joules = \frac{4.72*10^5\ J}{Einstein\ photons} * E\left(\frac{Einstein}{L}\right) \tag{4.6}$$

Rate of UV exposures (UV fluence) was then calculated as:

$$UV\ fluence\ (W) = \frac{incident\ joules}{UV\ time(s)} \tag{4.7}$$

Finally, UV intensity was estimated by the following correlation:

$$UV\ Intensity\ (W/cm^2) = \frac{incident\ joules}{area*UV\ time(s)} = \frac{UV\ fluence}{area} \tag{4.8}$$

4.3. Results and Discussion

In the literature, limited number of study is present considering the use of iodide/iodate solution as an actinometrical method for determination of UV intensity and dose in a continuous flow UV reactor. All the actinometric studies were carried out under static conditions, using bench top collimated beam apparatus (Bohrerova et al, 2008; Goldstein and Rabani, 2008; Rahn, 1999, Rahn et al, 2003, 2006, 2010). Consequently, UV intensity from actinometry method might be compared to that of instrumental (radiometer) results. The estimated UV intensity from the actinometric method and intensity values measured by a radiometer are represented in Table 4.2. UV intensity computed from actinometry data was expected to be comparable to that of radiometer reading. Due to the effect of high absorptivity of photoreactive medium, UV intensity was decreased as time passed. On the other hand, radiometer measurement did not show significant change with respect to time. According to results in Table 4.2, UV intensity was comparable between 4-8 min of UV exposure. By interpolation, UV intensity was determined as 1.790 mW/cm^2, which is close to the radiometer reading (1.792 mW/cm^2) at 6.28 minutes of UV exposure (Figure 4.2a). The amount of triiodide formation is depicted in Figure 4.2b. Actinometrical measurement in the bench top collimated beam apparatus was resulted in a linear reaction rate for the formation of triiodide from iodide/iodate at the

end of 15-18 min. Nonetheless, triiodide formation was maximum between 20-30 min interval of UV exposure due to the absence of reactant iodide/iodate.

Table 4.2. Chemical Actinometry Data for Bench Top Collimated Beam Apparatus

Time (min)	**UV Dose (J/cm^2)**	**UV Intensity (mW/cm^2)**	**UV Intensity from radiometer (mW/cm^2)**	**E (10^{-10}einstein/s) from actinometry**	**E (10^{-10}einstein/s) from radiometry**
4	0.601	2.504	1.795	1463.74	1049.271
6.28	**0.958**	**1.790**	**1.792**	**1046.39**	**1047.52**
8	1.202	1.252	1.79	731.870	1046.348
12	1.803	0.835	1.786	487.913	1044.01
16	2.404	0.626	1.781	365.935	1041.087
20	3.005	0.501	1.774	292.748	1036.995
24	3.606	0.417	1.768	243.957	1033.488
28	4.207	0.358	1.762	209.106	1029.981
32	4.808	0.313	1.757	182.968	1027.058

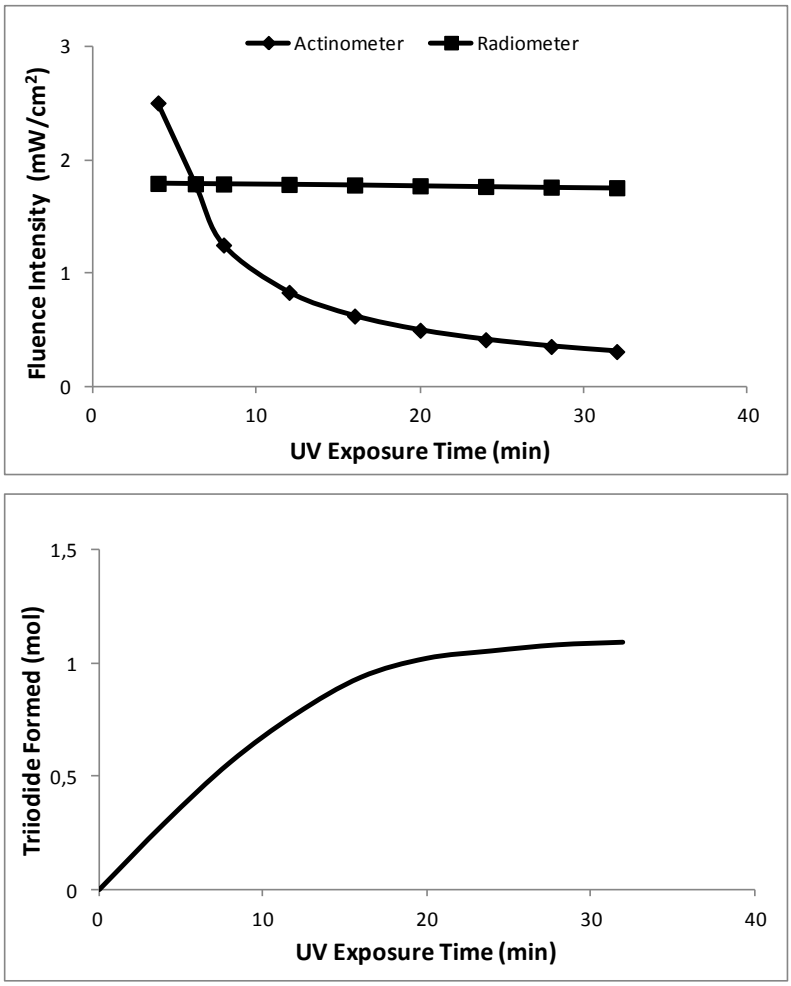

Figure 4.2. Chemical actinometry results in bench top collimated beam (a) UV intensity vs. UV exposure time (b) Triiodide formation vs. time

Similarly, Rahn et al, (1997) UV irradiated 5 ml of iodide/iodate solution by a 254 nm of low mercury UV lamp in an open beaker for 5 min. It was found that 5 min of exposure was adequate to measure UV intensity by using both radiometry (0.114 mW/cm^2) and actinometry (0.141 mW/cm^2) methods. Additionally, Bohrerova et al, (2008) determined the comparable results for both methods. UV irradiation was applied to 10 ml of iodide/iodate solution by low and medium pressured mercury UV lamps for 2-20 seconds. Both methods gave similar UV intensity results (0.25 mW/cm^2). Table 4.3 summarizes the chemical actinometric data for continuous flow UV reactor in the case of center lamp was on. Average UV intensity was 0.01 W/cm^2 (Figure 4.3a). As the chemical reaction of iodide/iodate actinometer continued, triiodide formation was resulted in dark orange-brownish color and UV intensity was decreased as the absorptivity of the medium was increased. At the end of 8^{th} cycle, total UV dose level of reaction medium was estimated as 88.754 J/cm^2, as the summation of UV intensity of 8 cycles.

Unlike the bench top collimated beam apparatus, triiodide production in continuous flow UV reactor after 33 min of UV exposure did not stop due to the presence of unreacted iodide/iodate (Figure 4.3b). As shown in figure 4.2b, no reactive iodide/iodate was present in 6 ml of actinometric sample, indicating the end of triiodide formation. But in contrast, reaction was not ended in 219.9 ml of UV reaction medium, even after 32 min of UV exposure (Figure 4.3b).

Table 4.3. Chemical Actinometry Data for Continuous Flow UV Reactor (Center Lamp on)

Center Lamp On (Area of irradiated sample = 377 cm^2)					
Cycle	**Time (min)**	**Incident Joules**	**Incident Rate (W)**	**UV Dose (J/cm^2)**	**UV Intensity (W/cm^2)**
C_{1out}	4	830.706	3.404	2.203	0.0090
	6.28	1290.752	3.426	3.424	**0.0091**
C_{2out}	8	1769.659	3.626	4.694	0.0096
C_{3out}	12	2648.748	3.618	7.026	0.0096
C_{4out}	16	4014.124	4.112	10.648	0.0109
C_{5out}	20	4987.519	4.088	13.229	0.0108
C_{6out}	24	5762.462	3.936	15.285	0.0104
C_{7out}	28	6423.419	3.761	17.038	0.0100
C_{8out}	33	7022.872	3.598	18.628	0.0095
				Ave	**0.0100±0.0006**

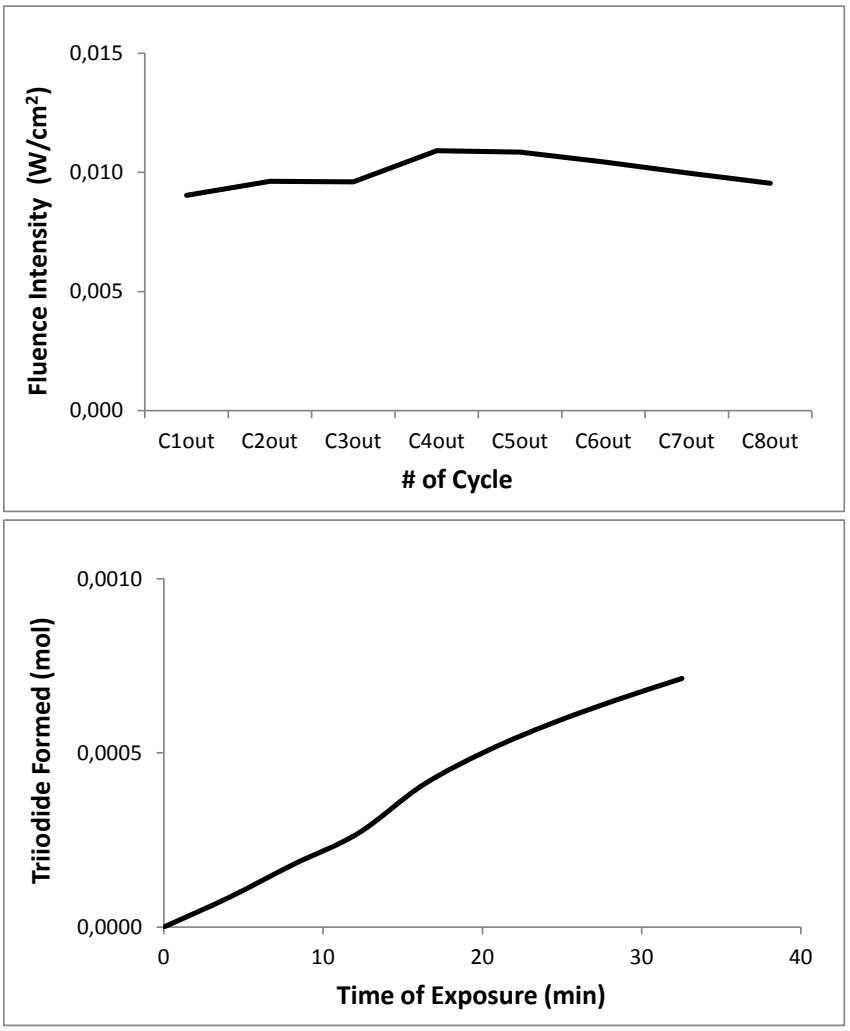

Figure 4.3. Chemical actinometry results in continuous flow UV reactor when center lamp on; (a) UV intensity vs. UV exposure time. (b) Triiodide formed vs. time

UV intensity, in the case of surface lamps were on, was represented graphically in Figure 4.4a and Table 4.4. At the end of 2nd cycle, UV intensity level increased from 0.0396 W/cm^2 to 0.0605 W/cm^2 due to rapid formation of triiodide by UV light. At the end of 8th cycle, average UV intensity was estimated as 0.0544 W/cm^2 of which was nearly 6-fold of UV intensity obtatined when the single lamp was on (0.009 W/cm^2). Figure 4.4b shows the triiodide formation during the photoreaction under UV light exposure. As in the first case, the amount of UV dose, applied on the reaction medium from cycle-1 to cycle-8 was determined as directly proportional to production of triiodide during reaction. Between 7th and 8th cycles, it was seen that tiriiodide formation was nearly stopped, as shown in Figure 4.4b.

Table 4.4. Chemical Actinometry Data of Continuous Flow UV Reactor (Surface Lamps on)

Surface Lamps On (Area of irradiated sample = 502.65 cm^2)					
Cycle	**Time (min)**	**Incident Joules**	**Incident Rate (W)**	**UV Dose (J/cm^2)**	**UV Intensity (W/cm^2)**
C_{1out}	4	4858.419	19.911	9.665	0.0396
	6.28	6948.562	25.607	19.195	**0.0509**
C_{2out}	8	14833.990	30.397	29.511	0.0605
C_{3out}	12	22409.099	30.613	44.581	0.0609
C_{4out}	16	28625.863	29.330	56.949	0.0583
C_{5out}	20	35094.173	28.766	69.817	0.0572
C_{6out}	24	40743.163	27.830	81.056	0.0554
C_{7out}	28	46266.381	27.088	92.044	0.0539
C_{8out}	33	48810.582	25.005	97.105	0.0497
				Ave	**0.0544±0.006**

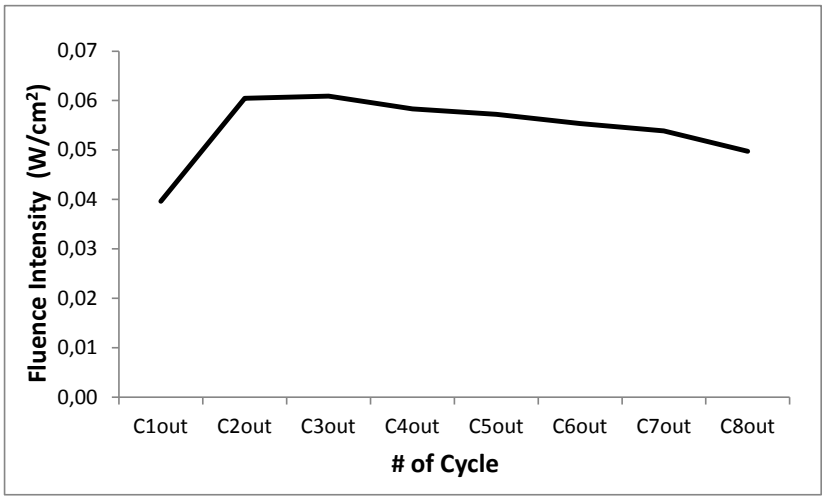

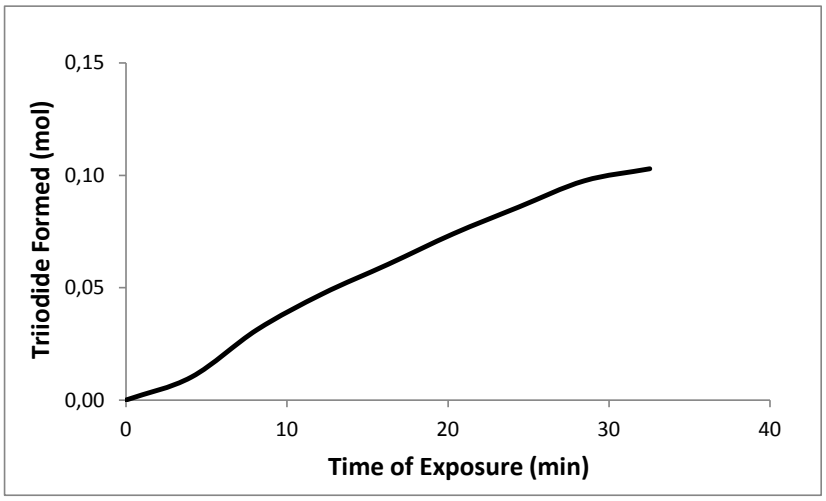

Figure 4.4. Chemical actinometry results in continuous flow UV reactor when surface lamps on; (a) UV intensity vs. UV exposure time (b) Triiodide formed vs. time

In order to find average UV intensity in the case of grape juice that was passed through the UV sisytem, UV intensity values estimated from actinometric method was used. Average UV intensity was calculated by using Beer-Lambert Law, shown in eqn 2.1 in Chapter 2. For this aim, absorbance coefficient of FSOGJ, measured in section 3, was used (23.92±0.96 cm^{-1}). Depth of fluid was described as 5 mm in Table 4.1. (Section 4.2.2.3). It was noticed that UV intensity distribution was decreased exponentially from both sides of UV tube (Figuse 4.5). The UV penetration length was 1 mm when the bench top collimated beam apparatus was used (Fig. 4.5a). The penetration lenght was also the same in the case of UV light source placed at the center (Fig. 4.5b). It means UV light emitted from the single lamp located at the center of UV reactor was reduced after the radial distance was higher than 1 mm and levelled off throughout the flow gap (Figure 4.5b). Nevertheless, the penetration lenght of UV light, emitted when the six of the surface lamps were on, was much more higher than that of the single UV lamp was on. When six lamps located around the flow gap were working simultaneously, the UV penetration length was calculated as 2.5 mm and decreased gradualllly after this point but did not level off in the flow gap (Figure 4.5b).

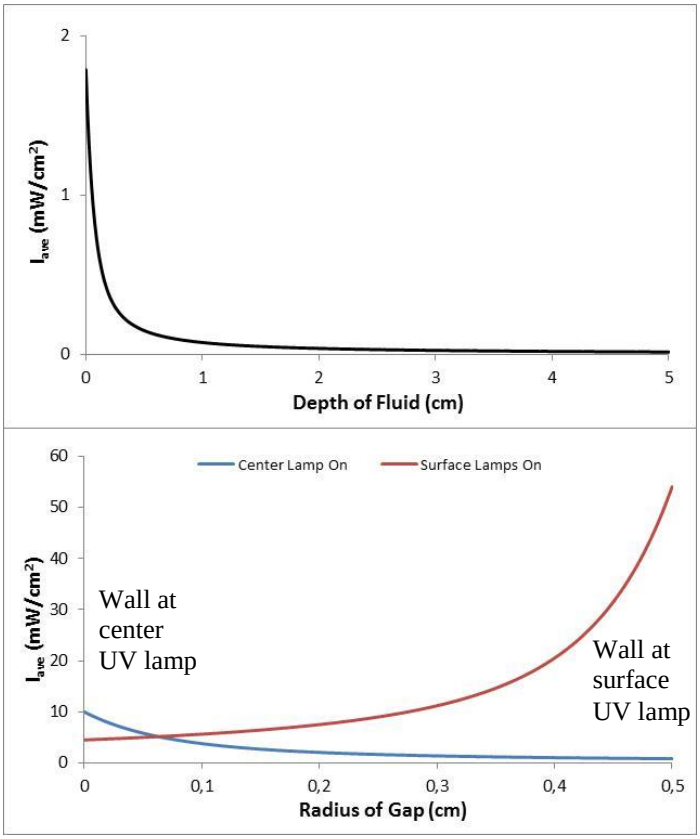

Figure 4.5. UV intensity distribution of UV irradiated FSOGJ by Beer Lambert Law for (a) Bench top collimated beam apparatus (b) Continuous flow UV reactor

Average UV intensity was calculated as 2.33±1.91 mW/cm^2 when center lamp was on and 13.05±10.69 mW/cm^2 when surface lamps were on. The residence time of one passage of grape juice samples was estimated as 244 seconds at 0.90 mL/s of flow rate. UV dose were estimated by multiplying the UV intensity from actinometry method, mentioned in eqn 2.2 (Chapter 2). It was found that 0.57 J/cm^2 of UV dose was delivered in the UV system when the center lamp was working. Nonetheless, UV dose was computed as 3.18 J/cm^2 when 6 surface lamps were on. The UV dose in the case of surface lamps on was approximately 6 times higher than the case when single lamp was on.

4.4. Conclusions

UV dose and intensity in the thin film UV reactor was measured by using an actinometric method. For this aim, iodide/iodate solution was used as a chemical actinometer. Iodometric method was successfully applied in bench top collimated beam apparatus and continuous flow UV reactor to estimate UV intensity in both cases. It was found that UV intensity measurements obtained from actinometric method (1.790 mW/cm^2) and radiometer (1.792 mW/cm^2) were comparable when 6.3 minutes of UV exposure time was reached. Another means that, 6.28 minutes of reaction time showing an overlap with the data of radiometric measurements was enough for determination of UV intensity when actinometric method was used. Measurement of UV intensity value based on the 6.28 minutes reaction time was used to determine the average UV intensity for the case when grape juice was passed through the continuous flow UV reactor. When center lamp was on, UV intensity was estimated as 9.1 mW/cm^2 after 6.28 minutes of UV exposure. Moreover UV intensity was calculated as 50.9 mW/cm^2 in case of surface lamps on. It can be commented that iodometric method for chemical actinometry is dependent upon the sample volume, irradiation area and initial concentration of iodide/iodate solution.

CHAPTER 5

COMPUTATIONAL FLUID DYNAMICS (CFD)

5.1. Introduction

In order to solve fluid dynamics problems, both experimental and simulational studies are needed (Norton et al, 2006; Scott and Richardson, 1997; Wang and Sun, 2003). Experimental work is known as the quantitative description of the flow phenomena using measurements for one quantity at a a limited number of points and time instants for a laboratory-scale model. In experimental work, a limited number of problems and operating conditions are possible for solution. Moreover, it is essential to collect experimental data for error sources including measurement errors and flow disturbances by means of different probes (Mills, 1998, 1999; Le et al, 1997; Scott, 1996). The simulation of an experimental part is used for describing the actual flow in a domain of any problem having realistic operating conditions. Additionally, the simulation of an experimental section predicts the flow phenomena for all desired quantities with high resolution in space and time (Schaldach et al, 2000; Versteeg and Malalasekera, 1995).

Computational fluid dynamics (CFD) is a numerical solution method to solve the governing equations of fluid flow throughout a flow geometry (Collins and Ciofalo, 1991; Dhanasekharan et al, 2004; Friis and Jensen, 2002; Norton and Sun, 2002; Quarini, 1995; Shang, 2004; Wang and Sun, 2003). Computational fluid dynamics (CFD) is described as a branch of fluid mechanics that uses numerical methods and algorithms to solve and analyze problems that involve flows. The main aspect of CFD application is the successiveness of the solution of numerical simulation. Another means that the numerical results is required to be comparable to experimental data. The simulations can ability to predict a highly complex phenomena that can not be possible to establish in the laboratory conditions (Sethian, 1993). As a summary, CFD provides a perspective for the difficult, complex flow phenomena or unfeasible flow patterns which can not be experimentally studied. CFD has been developed and received attention in worldwide due to the advent of the powerful computational technology. Since 1960s, CFD application in industry and science has been increasingly used for fluid dynamics (Le et al, 1997; Schaldach et al,

2000). CFD analysis has been operated to analyse the flow and performance of industrial instruments, such as baking ovens (Mills, 1998, 1999), refrigerated display cabinets (Cortella et al, 1998, 2001), stirred tanks (Sahu et al, 1999), spray dryers (Kieviet et al, 1997), and heat exchangers (Kumar, 1995). CFD software programs have standard numerical iteration tools for prediction of fluid flow and transport phenomena of heat, mass (diffusion, dissolution, pipe transfer), phase change (freezing, melting, boiling, chilling), chemical reaction (combustion, decomposition, oxidation, reduction), and momentum transport (impeller, pistons, fans).

CFD has been an effective iteration tool for non-analytical solutions of the complex problems. It has been applied for many food applications (Scott, 1996; Xia and Sun, 2004). CFD has been accepted as a feasible method for solution of complex problems and design of equipments and processes (Burfoot et al, 1999; Scott and Richardson, 1997).

CFD was first applied for the aim of predicting fluid motion by using appropriate numerical techniques of which was applicable for all types of fluids in different industries (Courant et al, 1928; Richardson, 1910). In industrial and non-industrial (educational) area, But the numerical simulation of CFD results are required to be validated by accurate experimental data. The numerical simulations allow to study some of the experimental cases in which a complex phenomena can not be isolated in the laboratory conditions (Sethian, 1993). CFD technology has been developed in 1960s to deal problems in manufacturing aircraft and jet engine. Recently, CFD application is widely used in the design of equipments such as ovens, heat exchangers, refrigerated display cabinets, spray dryers furnace and other equipments (Versteeg and Malalasekera, 1995; Norton et al, 2007). CFD programs are considered as standard numerical tools which predict fluid dynamic behaviour, heat and mass transfer phenomena (diffusion, convection or chemical reaction) in multiphase systems, and mechanical energy input (reactor or bioreactor impeller and fans). Deformation or stress of solid materials are also examined by CFD (Versteeg and Malalasekera, 1995; Xia and Sun, 2002). The general application area of CFD can be summarized in Table 5.1 (Xia and Sun, 2002).

CFD applications in food engineering has been used for nearly 15 years (Scott, 1994). Since the consumer demand for convenient and high quality meals has been growing over the last several years, the development of new food processing practices and technologies is needed to be simulated. CFD application has been applied successfully to understand the presence of extreme physical conditions of thermal, physical and rheological properties in the food processing (Xia and Sun 2002; Norton et al, 2007).

Table 5.1. CFD Application in Various Areas
(Source: Xia and Sun, 2002)

Industrial	Aerospace
	Architecture
	Automotive
	Biomedical
	Chemical and Process
	Combustion
	Electronics and computers
	Glass manufacturing
	HVAC (heat, ventilation and cooling)
	Petroleum
	Power
	Marine
	Mechanical and Metallurgical
	Nuclear
	Train design
	Turbo machinery
Environmental applications	Atmospheric and water pollution
	Climate calculations
	Fire in buildings
	Oceanic flows
	Pollution of natural waters
	Safety
Physiological applications	Cardiovascular flows (heart, major vessels)
	Flow in lungs and breathing passages
Food Applications	UV Disinfection-Photobioreactor
	Temperature distribution in heat exchangers
	Freezing process

Computational simulation methods of fluid dynamic are developed as a basis of development of software and code engineering in computer science. (Norton and Sun, 2006; Versteeg and Malalasekera, 1995). The main advantages of CFD can be classified as (Green et al, 1995; Lazarova et al, 1998; ; Norton et al, 2007; Versteeg and Malalasekera, 1995; Xia and Sun, 200):

- CFD provides a detail understanding of flow distribution, mass and heat transfer in the whole or individual processing system to identify the possible problems.

- CFD helps to evaluate new designs with less time and cost than would be applied in laboratory testing.
- It allows to scale-up of the system using independent scale up models and study of the large systems, which is difficult to be implemented in laboratory.
- It is useful for studying the extreme conditions (high pressure or temperature process of individual units).
- CFD can help to highlight the design errors and approaches needs to used for the new design.
- CFD provides important details for an efficient processing and storage conditions and prevents wasting of food in pre-experiments or optimization studies.
- CFD can be used for designing and processing of a food product having a high quality. Therefore it helps to develope a marketing and consumer strategy by decreasing the operational cost for that food product (Burfoot et al, 1999; Dhanasekharan et al, 2004; Friis and Jensen, 2002).

5.2. CFD Applications in Food Engineering

CFD has been applied in food processing industry, including clean room design, refrigeration and transportation of foods, static mixers and pipe flow (Collins and Ciofalo, 1991; Quarini, 1995; Scott, 1977; Scott, 1994). Besides, food processing operations such as chilling, drying, baking, mixing, freezing, cooking, pasteurization and sterilization are dependent on fluid flow. CFD allows the food engineers to understand the performance of food equipment and to improve the quality or safety of food products (Norton and Sun, 2002; Xia and Sun, 2002; Scott and Richardson, 1997; Xia and Sun, 2002). Several studies, in which CFD was used to determine physical phenomena, has been published in the area of food processing (Asteriadou et al, 2006; Burfoot et al, 1999; Harral and Burfoot, 2005; Unluturk et al, 2004) including clean-room design and storage/transportation of refrigerated foods (Janes and Dalgly, 1996), static mixers (Scott, 1977), pipe flow of food streams (Scott, 1996). treatment of foodborne microorganisms (Siriwattanayotin et al, 2006; Varma and Kannan, 2006), mixing (Song and Han, 2005) and food drying (Huang et al, 2003).

Determination of UV dose distribution in a continuous flow UV system by CFD has also been investigated in the literature. Downey et al, (1998) estimated the residence

time and size distributions of salt particles inside the continuous flow UV reactor using computational fluid dynamics (CFD) and studied the effect of particle number, particle size distribution and hydrodynamic properties of UV reactor on UV dose (Downey et al, 1998). Sozzi and Taghipour, (2006) compared the performance of the flow models by using continuum (Eulerian) and dispersed phase (Lagrangian) approaches integrated with finite and infinite line source UV dose distribution models in the design of continuous flow UV reactor having different inlet and outlet configurations (Sozzi and Taghipour 2006). Demessic et al, (2003) studied the flow dynamics and residence time distribution of the fluid inside the photoreactor by applying numerical methods and compared the effect of the mechanical energy on the homogeneous distribution of fluid in the reactor (Demessic et al, 2003). Taghipour and Sozzi (2005) computed the velocity and time distributions of microbial particles in the wastewater disinfected in the vertical UV reactor having different inlet and outlet configurations by time averaged turbulent flow models combined with CFD and compared the simulation result with the ones obtained from particle imaging system (Taghipour and Sozzi, 2005). Also they numerically investigated the effect of design configurations on particle size and velocity distribution. For this purpose Sozzi and Taghipour, (2005) simulated the flow of wastewater inside a UV reactor designed with two different inlet-outlet configurations by applying Reynolds averaged Navier-Stokes flow model (Taghipour, 2005). Besides, the UV dose distribution in the wastewater containing microbial particles was predicted by CFD considering body forces resulted in turbulent flow regime (Taghipour, 2004; Sozzi and Taghipour, 2006). Elyasi and Taghipour (2010) computed momentum and continuity equations using CFD for the design of a continuous flow UV reactor by considering time independent volumetric based inactivation rate in Eulerian approach (Elyasi and Taghipour, 2010).

Duran et al, (2009) examined the single phase liquid flow including mass transfer phenomena in commercial-type U-shape and L-shape annular reactors both numerically (using FLUENT® 6.3.26) and experimentally. Several hydrodynamic turbulence models of standard k–ε, realizable k– ε, Reynolds stress (RSM), and the Abe-Kondoh-Nagano (AKN-turbulence model with low Re number) were used for different Re numbers in the range of 0 and 11000 (Duran et al, 2009).

Wols et al, (2010) simulated an ozone system by applying several calculation methods using CFD and taking into consideration of residence time distributions, ozone concentrations, and particle trajectories. Eulerian and Lagrangian approaches were applied on fluid flow hydraulics of the system to determine the disinfection rate. Also the effect of

flow regime in different reactor geometry was examined. Wols et al, (2010) applied a CFD model based on a finite-element method (COMSOL3Dv3.4®) for prediction of the flow behaviour, by using an integrated approach to estimate residence time distributions, local velocity measurements and visualization of particle trajectories. For this aim, Reynolds averaged Navier Stokes (RANS) equations combined with standard k–ε turbulence model. Turbulent kinetic energy (k) and turbulent dissipation (ε) were solved by a matrix solver-PARDISO® (Wols et al, 2010). Crapulli et al, (2010) designed a pilot-scale fluoropolymer tube UV photoreactor to disinfect MS2 and T1 bacteriophages by using CFD. During simulation, design parameters such as flow rate, UV intensity rate, microbial inactivation and UV dose distribution were considered in an Eulerian framework in CFD solver. Results were compared biodosimetric data to predict the disinfection efficiency and cost of operation (Crapulli et al, 2010). UV intensity and dose determination studies using CFD modelling approach are summarized in Table 5.2.

In summary, CFD has been used in food industry to improve the quality of food products for decades (Norton et al, 2006; Quarini, 1995; Scott, 1994; Scott and Richardson, 1997; Xia and Sun, 2002; Wang and Sun, 2003). CFD application in the food industry has focused on the solution of the complex physical mechanisms where thermal, physical and rheological properties of food materials has also been taking into account (Janes and Dalgly, 1996; Quarini, 1995; Scott and Richardson, 1997). CFD applications in the food industry are expected to increase in the future because of supplying many benefits (Norton et al, 2006; Xia and Sun, 2002).

Table 5.2 Summary of Studies for Determination of UV Intensity Distribution

Author	Type of UV System	Model Solution	Numerical Method	Solver Program	Flow Model	Particle Tracking	UV Intensity Model	Predicted UV Dose	Exp. UV Dose
Downey et al, 1998	Thin film annular flow U-shaped UV reactor (steady state turbulent flow)	Salt tracer	Finite element	FIDAP 7.62	Navier Stokes, k-ε turbulence model	Pathogenic fungus (DPM with Lagrangian approach)	N/A	N/A	N/A
Chiu et al, 1999	Rectangular vertical UV chamber (turbulent flow)	Water	Finite element	N/A	Navier Stokes, k-ε turbulence model	Laboratory velocity field measurement-Random Walk Model	Multiple Point Source Summation	12-40 mJ/cm^2	N/A
Wright and Hargreaves, 2001	Horizontal S-Shaped thin film annular flow UV reactor (steady/unsteady turbulent flow)	Water	Finite volume	CFX5	Navier Stokes, k-ε turbulence model	DPM with Lagrangian approach	Infinite Line Source	0-60 mJ/cm^2 (steady state) 0-128 mJ/cm^2 (steady state)	N/A
Unluturk et al, 2004	Thin film annular flow UV Reactor (steady state turbulent flow)	Apple cider	Finite volume	FLUENT 5	Navier Stokes (Eqn. of continuity and motion)	DPM with Lagrangian approach (apple cider particles)	Infinite Line Source, Multiple Point Source Summation (with user defined function) Beer-Lambert Law	20-90 mJ/cm^2	18.8-78.8 mJ/cm^2
Taghipour and Sozzi, 2005	Horizontal L-Shaped thin film annular flow UV reactor (steady state, turbulent flow)	Water	Finite volume	FLUENT 6.1	Conservation of mass, momentum and species with k-ε turbulence model	DPM with Lagrangian approach (organic materials) Particle image velocimetry	Infinite Line Source	N/A	N/A
Ducoste et al, 2005a	Thin film annular flow UV reactor (steady state, turbulent flow)	Water	Finite volume	PHONEICS	Navier Stokes, k-ε turbulence model	DPM with Lagrangian and Eulerian approach (microorganisms)	5-point Multiple Point Source Summation,	25-45 mJ/cm^2	N/A
Ducoste et al, 2005b	Closed Conduit UV reactor (Steady state turbulent flow)	Water	Finite volume	PHOENICS, FLUENT RADLSI and UVCalc3D	Navier Stokes, k-ε turbulence model	DPM with Lagrangian and Eulerian approach (microorganisms)	RADLSI and UVCalc3D with Multiple Segment Source Summation	40-200 mJ/cm^2 (Four lamp)	N/A

(**cont. on next page**)

Table 5.2. (Cont.)

Elyasi and Taghipour, 2006	Horizontal U-Shaped thin film annular flow UV reactor (steady turbulent flow)	Water	Finite volume	FLUENT 6.2.26	Conservation of mass and momentum	DPM with Eulerian approach (microbial particles)	A radiation model based on emission of UV lamp, Beer Lambert Law	0-150 mJ/cm^2	0-100 mJ/cm^3
Sozzi and Taghipour, 2006	Horizontal L- and U-Shaped thin film annular flow UV reactors (steady turbulent flow)	Water	Finite volume	FLUENT 6.1.22	Reynolds Averaged Navier Stokes k-ε turbulence model	DPM with Lagrangian approach (organic materials) Particle image velocimetry	N/A	N/A	N/A
Liu et al, 2007	Closed conduit polychromatic UV reactor (steady state, turbulent flow)	Water	Finite volume	UVCalc3D (for UV dose simulation) DaVis6.2 (for particle image) PHOENICS (for flow simulation)	Navier Stokes with k-ε, k-ω, Reynolds stress and two-fluid turbulence models	DPM with Lagrangian approach (microbial population) Digital particle image velocimetry	Multiple Point Source Summation	10-100 mJ/cm^2 (low lamp power) 50-300 mJ/cm^2 (high lamp power)	20-50 mJ/cm^2
Munoz et al. 2007	Closed conduit polychromatic UV reactor (steady state, turbulent flow)	Water	Finite volume	FLUENT 6.1	Navier Stokes, k-ε turbulence model	DPM and Discrete Random Walk with Lagrangian approach	Multiple Segment Source Summation	49.2 mJ/cm^2	N/A
Reichl et al, 2007	Vertical S-Shaped thin film annular flow UV reactor (steady turbulent flow)	Water	Finite volume	FLUENT 6.2	Conservation of mass, momentum and species with k-ε turbulence model	DPM with Random Walk Model (*Bacillus subtilis* spores)	Multiple Point Source Summation, Linear Source Integration	50-200 mJ/cm^2	45-80 mJ/cm^2
Wols et al, 2010a	Horizontal cylindiricalbench top UV reactor (lamps perpendicular to flow axis), steady state turbulent flow	Water	Finite element	COMSOL 3D v3.4	Reynolds Averaged Navier Stokes with k-ε, turbulence model	DPM with Lagrangian approach (passive tracer with potassium permanganate dye)	Multiple Point Source Summation	20-80 mJ/cm^2	N/A
Chen et al, 2011	Closed conduit UV reactor (steady state, turbulent flow)	Water	Finite volume	FLUENT 6.3	Navier Stokes with k-ε, k-ω, Reynolds Stress and two-fluid turbulence models	DPM with Lagrangian approach (microbial population)	Modified P-1 Radiation Model (with user defined function)	50-550 mJ/cm^2	N/A

5.3. Performing a CFD Analysis

There are generally three steps in solving a problem in the CFD analysis. The pre-processing step of the analysis is to formulate the flow problem, to model the geometry, to establish the boundary and initial conditions, and to generate the grid by an appropriate meshing software. In the processing step, a simulation strategy, and input parameters and files are first established. An input data file is created listing the values of the input parameters consisted with the desired strategy. The files for the grid and initial flow solution is generated. Then the simulation is performed by an appropriate CFD solver. As the simulation proceeds, the solution is monitored to determine if a "converged" solution has been obtained. The last step is post processing step. Post-processing involves extracting the desired flow properties from the computed flow field. The computed flow properties are then compared to results from analytic, computational, or experimental studies to establish the validity of the computed results. The performing steps for CFD analysis are summarized in Figure 5.1.

5.3.1. Pre-Processing

In this section, the flow problem is formulated by considering the objective of the physical problem, the geometry of the physical domain, operating conditions, dimensionality of the spatial model (1D, 2D or 3D), modeling approach (steady or unsteady), the nature of the flow (inviscid, laminar, turbulent) e.t.c. The body about which flow is to be analyzed requires modeling. For this purpose, the geometry is modelled with a CAD package. It is fundamental to model the geometry to eliminate any defects formed near the boundaries, critical edges, fillets, bolts, open faces, wall surfaces etc. Since these defects can cause several problems in meshing application complicating the grid structure. The geometry and flow domain are modeled in such a manner as to provide input for the grid generation. Thus, the modeling often takes into account the structure and topology of the grid generation. The model geometry is discreatized into a grid which is called a **mesh**. The grid generation involves defining the structure and topology and then generating a grid on that topology. In most of the cases, multi-block and structured grids are involved.

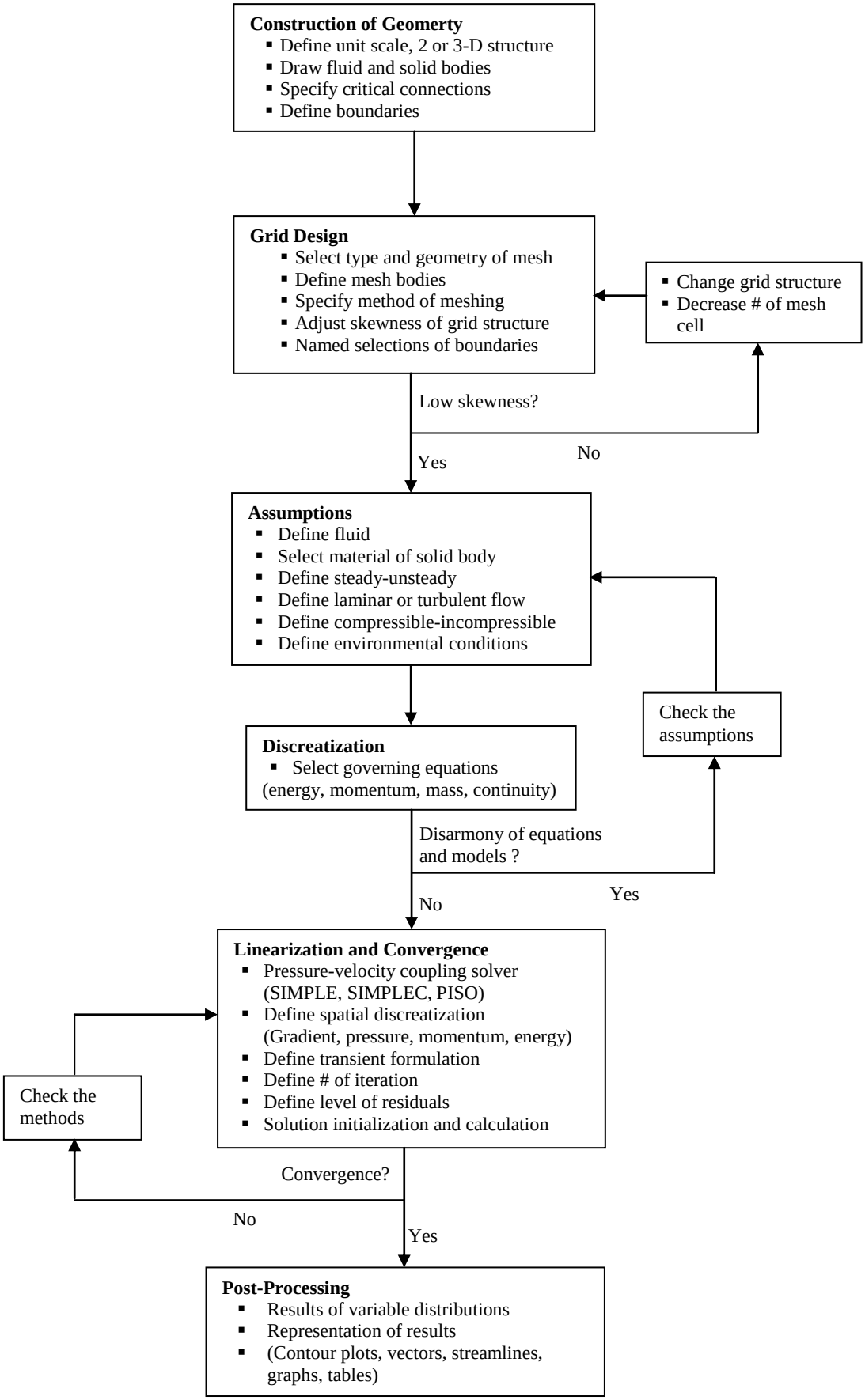

Figure 5.1. Performing of a CFD analysis

A rectangular surface geometry and a structured grid are represented in figure 5.2 a and b.

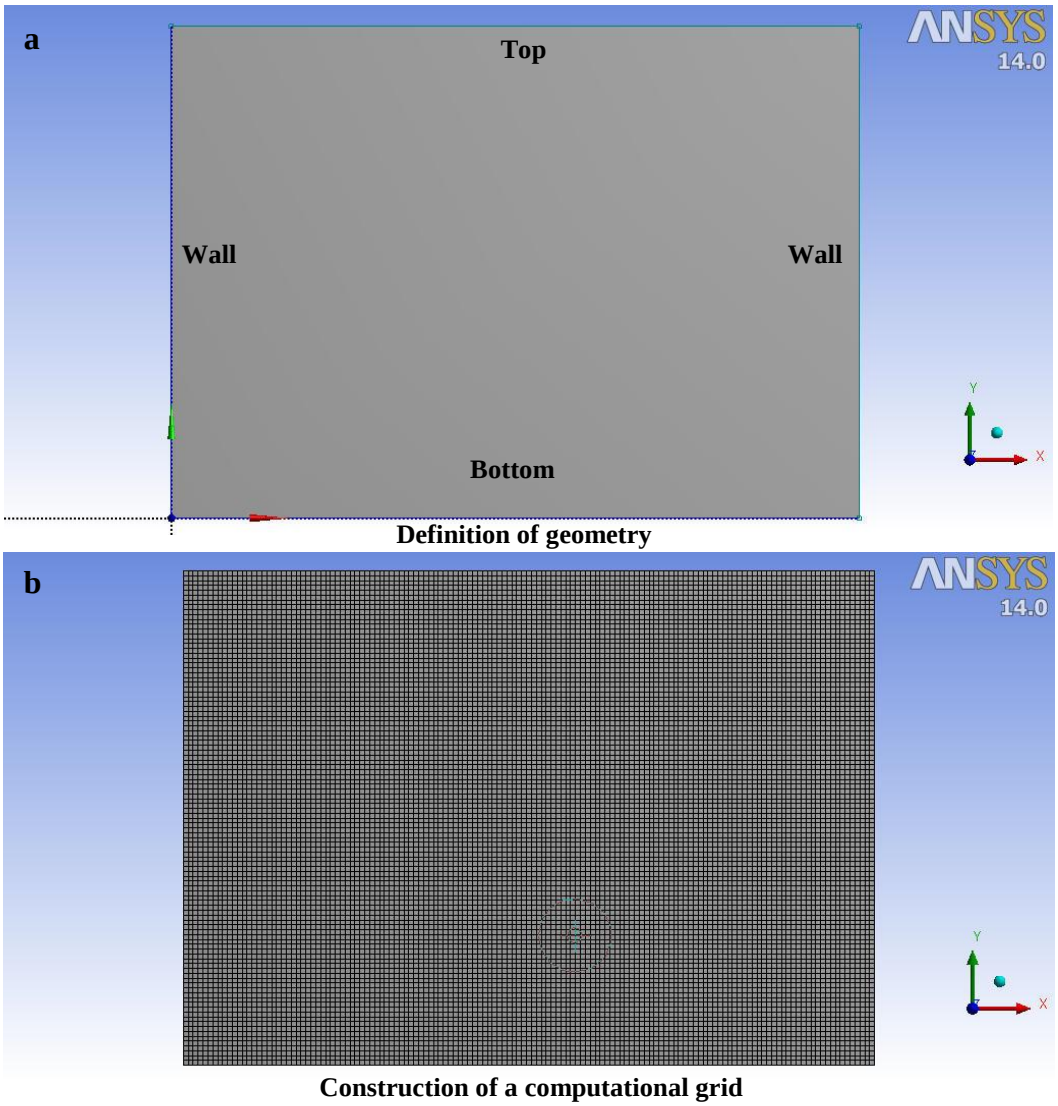

Figure 5.2. (a) Defining geometry for a CFD simulation (b) Computational grid structure of geometry

The maximum spacings should be consistent with the desired resolution of important features such as velocity, pressure, temperature gradients. In creating a grid structure, different types of mesh elements (tetrahedral, hexahedral etc.) are used based on the complexity of the geometry or the presence of non-conformal interfaces. These structured and unstructured mesh elements are depicted in Figure 5.3.

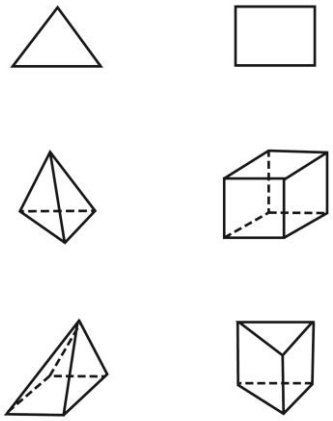

Figure 5.3. Mesh configurations of triangle (up left), quadrilateral (up right), tetrahedron (mid-left), hexahedron (mid-right), pyramid (down-left) and prism/wedge (down-right) (Source: ANSYS 14.0 User's manual).

Mesh skewness is a qualitative or quantitative parameter that decides whether the mesh is having a large amount of skewness or it is an ideal triangle or a square. It can be determined by a measure of the relative distortion of an element compared to its ideal shape and is scaled from 0 (Excellent) to 1 (Unacceptable). Skewness factor can be estimated by the following correlations, based on the structure and dimensions of mesh cell:

By equilaterial volume deviation skewness factor is;

$$Skewness = \frac{Optimal\,cell\,size - cell\,size}{Optimal\,cell\,size} \tag{5.1}$$

This correlation for skewness is applied for meshes configured by triangles and tetrahedrans. By normalized angle deviation, skewness factor can be estimated as;

$$Skewness = \max\left[\frac{\theta_{\max} - \theta_e}{180 - \theta_e}, \frac{\theta_e - \theta_{\min}}{\theta_e}\right] \tag{5.2}$$

where θ_e represents the equiangular face/cell, which is 60 for tetrahedrons-triangular meshes and 90 for quadrilaterals and hexahedron meshes. This method is applied to all cell and faces of prisms and pyramids.

Mesh smoothness describes as to how smooth the mesh is, how is its transition whether it is an abrupt or in a smooth manner. **Mesh aspect ratio** is the ratio of the largest dimensional length of an element to the smallest length.

5.3.2. Processing

5.3.2.1. Finite Volume Method, Discretization and Linearization of The Equations and Convergence

In the processing step, a simulation strategy, and input parameters and files are first established. The strategy for performing the simulation involves determining the use of space-marching or time-marching, the choice of turbulence or chemistry model, and the choice of algorithms. A CFD code generally requires that an input data file be created listing the values of the input parameters consisted with the desired strategy. Further the a grid file containing the grid and boundary condition information is generally required. The files for the grid and initial flow solution need to be generated. Then the simulation is performed by an appropriate CFD solver.

In general, control-volume technique is used in CFD solver to convert the governing equations to algebratic ones. This technique is applied by integrating the governing equations about each control volume by yielding discrete equations as a result of conservation of each quantity on a control volume. The discrete values of any field variable are stored at center of the cells. The face values for these variables, which are used in the discrete form of the equations, interpolated from the cell center values by using an upwind scheme. As a result, the face value of the variable is derived from quantities in the cell upstream relative to the direction of the normal velocity vector. Five upwind schemes are used in CFD solver algorithm: First-order upwind, second-order upwind, power-law, QUICK (Quadratic Upwind Differencing Scheme) and third-order MUSCL (Monotone Upstream-Centered Schemes for Conservation Laws). Time dependent (transient) equations are discreatized in both space and time. The temporal discretization involves the integration of every term in the differential equations over a time step Δt. Backward differencing scheme is used to discretized the time derivative. Both implicit and explicit time integration methods are available in CFD solver.

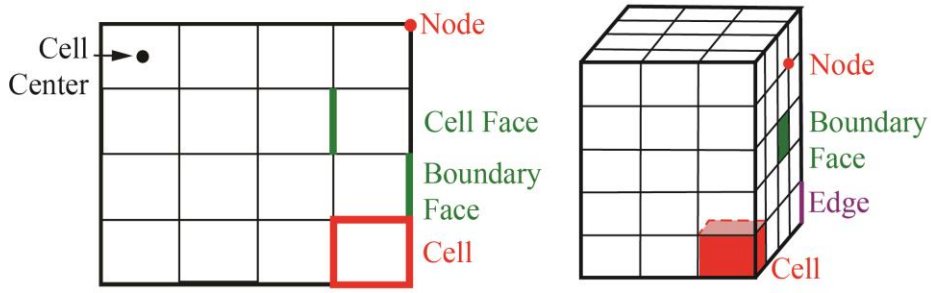

Figure 5.4. Simplifying the 2-D (left) and 3-D (right) meshing configurations based on finite volume element analysis having boundary face and control volume in 3-D meshing configuration (Source: ANSYS 14.0 User's manual).

The discretized equation contains the unknown variable φ at the cell center as well as the unknown values in surrounding neighbor cells. This equation is nonlinear with respect to these variables. In both the segregated and coupled solution methods the discrete, non-linear governing equations are linearized to produce a system of equations for the dependent variables in the computational cells. The resultant linear system is then solved to yield an updated flow-field solution.

In the segregated solution method, each discrete governing equation is linearized implicitly. In other words, the segregated approach is applied for a single variable field solution (e.g., pressure "*p"*) by considering all cells at the same time. It is solved for the next variable field by again considering all cells at the same time, continuously. Solution of the coupled implicit approach is realized for all variables (*p, u, v, w, T*) in all cells at the same time. Similarly the coupled explicit approach is used for solution of the variables (*p, u, v, w, T)* per cell at a time.

A linearized form of equation can be written as:

$$a_p \varphi = \sum_{nb} a_{nb} \varphi_{nb} + b \qquad (5.3)$$

where the subscripts "nb" refers to neighbor cells, and a_p and a_{nb} are determined as the linearized source term. Similar equations can be written for each cell in the grid. This results in a set of algebraic equations. In order to solve these equations Gauss-Siedel linear

equation solver is used in conjunction with an AMG (Algebraic Multigrid) method (FLUENT 14.0 User's manual; Versteeg and Malalasekera, 1995).

Time dependent (transient) equations are discretized in both space and time. The temporal discretization involves the integration of every term in the differential equations over a time step Δt. Backward differencing scheme is used to discretized the time derivative. Both implicit and explicit time integration methods are available in CFD solver.

The pressure field and face mass fluxes are not known as a prior and must be obtained as a part of the solution. CFD solver relates the face value of velocity to the stored values of velocity at the cell centers to find the face flow rate equation. Pressure-velocity coupling is achieved by using these face flow rates to derive an equation for pressure from the discrete continuity equation. Four-pressure velocity coupling algorithms are used in commercial CFD: SIMPLE (Semi Implicid Method for Pressure Linked Equations), SIMPLEC (SIMPLE-Consistent) and PISO (Pressure Implicit with Splitting of Operators).

Convergence can be affected by a number of factors such as large numbers of computational cells, complex flow physics etc. The scaled or normalized residuals are useful indicators of solution convergence. For most problems, the default convergence criterion in CFD solver is that the scaled residuals decrease to 10^{-4} for all equations except the pressure equations for which the criterion is 10^{-6}. If more convergent solutions are to be needed, residual can be adjusted as absolute or independent level of absolute value in CFD solver.

5.3.2.2. Governing Equations for Continuous Phase

Equation of continuity is an equation that describes the transport of a conserved quantity Eqn. 5.4). The principle of this equation is derived from the fact that mass is always conserved in fluid systems regardless of the complexity or direction of flow. (Bird et al, 2002; Sozzi and Taghipour, 2006):

$$\left[\frac{\partial \rho}{\partial t} + \left(\nabla \cdot \rho \vec{v}\right)\right] = 0 \tag{5.4}$$

When it is written for the cylindirical coordinates, it takes the following form (Bird et al, 2002):

$$\frac{\partial \rho}{\partial t}+\frac{1}{r}\frac{\partial}{\partial r}\left(\rho r v_r\right)+\frac{1}{r}\frac{\partial}{\partial \theta}\left(\rho v_\theta\right)+\frac{\partial}{\partial z}\left(\rho v_z\right)=0 \tag{5.5}$$

The generalized form of **conservation of momentum** is represented as (Bird et al, 2002):

$$\rho\frac{Dv}{Dt}=-\nabla p-\left[\nabla\cdot\tau\right]+\rho g+S \tag{5.6}$$

The conservation of momentum for cylindirical coordinates can be written as:

$$\rho\left(\frac{\partial v_r}{\partial t}+v_r\frac{\partial v_r}{\partial r}+\frac{v_\theta}{r}\frac{\partial v_r}{\partial \theta}+v_z\frac{\partial v_r}{\partial z}-\frac{v_\theta^{\,2}}{r}\right)=-\frac{\partial p}{\partial r}-\left[\frac{1}{r}\frac{\partial}{\partial r}\left(r\tau_{rr}\right)+\frac{1}{r}\frac{\partial}{\partial \theta}\tau_{\theta r}+\frac{\partial}{\partial z}\tau_{zr}-\frac{\tau_{\theta\theta}}{r}\right]+\rho g_r+S_r \tag{5.7}$$

$$\rho\left(\frac{\partial v_\theta}{\partial t}+v_r\frac{\partial v_\theta}{\partial r}+\frac{v_\theta}{r}\frac{\partial v_\theta}{\partial \theta}+v_z\frac{\partial v_\theta}{\partial z}-\frac{v_r v_\theta}{r}\right)=-\frac{1}{r}\frac{\partial p}{\partial \theta}-\left[\frac{1}{r^2}\frac{\partial}{\partial r}\left(r^2\tau_{r\theta}\right)+\frac{1}{r}\frac{\partial}{\partial \theta}\tau_{\theta\theta}+\frac{\partial}{\partial z}\tau_{zr}+\frac{\tau_{\theta r}-\tau_{r\theta}}{r}\right]+\rho g_\theta+S_\theta \tag{5.8}$$

$$\rho\left(\frac{\partial v_z}{\partial t}+v_r\frac{\partial v_z}{\partial r}+\frac{v_\theta}{r}\frac{\partial v_z}{\partial \theta}+v_z\frac{\partial v_z}{\partial z}\right)=-\frac{\partial p}{\partial z}-\left[\frac{1}{r}\frac{\partial}{\partial r}\left(r\tau_{rz}\right)+\frac{1}{r}\frac{\partial}{\partial \theta}\tau_{\theta z}+\frac{\partial}{\partial z}\tau_{zz}\right]+\rho g_z+S_z \tag{5.9}$$

where t represents time. υ_r, υ_z and υ_θ are the velocity components in r, θ and z-coordinates. τ_{rz}, τ_{zr}, $\tau_{r\theta}$, $\tau_{\theta r}$, $\tau_{\theta\theta}$ and τ_{rr} are stres tensors based on the flow directions (if flow is present in subscribed coordinate) g is represented as the gravitational acceleration component for different coordinates. S is the source term based on the momentum transfer between particle and liquid phases.

5.3.2.3. Dispersed Phase Model (DPM) for Particle-Liquid Flows

In addition to the equation of continuity, and equation of momentum for continuous phase, a dispersed particle phase is used considering a Lagrangian frame of reference. This particle phase is composed of spherical particles such as suspended solids, microorganisms, hydrophobic droplets or bubbles, dispersed in the continuous phase (Worley and Manbeck, 1995). It is necessary to couple a discrete phase model (DPM) with flow model. The initial position, velocity, size, and initial temperature of particles are the

inputs necessary to initiate the numerical calculation (Predicala and Maghirang, 2003). By the help of an appropriate numerical solution software, such as FLUENT®, the discrete phase model can be easily coupled with a continuous phase flow field model. The effect of the discrete phase on the continuous phase is handled by a source term found in momentum equations. Calculations are continued until a converged coupled solution is achieved (ANSYS-FLUENT® 14.0 User's manual, 2012).

In summary, the fluid phase is treated as a continuum by solving the time-averaged Navier-Stokes equations, while the dispersed phase is solved by tracking a large number of particles through the calculated flow field. The dispersed phase can exchange momentum, mass, and energy with the fluid phase. A fundamental assumption made in this model is that the dispersed second phase occupies a low volume fraction, even though high mass loading is acceptable. The particle or droplet trajectories are computed individually at specified intervals during the fluid phase calculation. This makes the model appropriate for the modeling of spray dryers, coal and liquid fuel combustion, and some particle-laden flows, but inappropriate for the modeling of liquid-liquid mixtures, fluidized beds, or any application, where the volume fraction of the second phase is not negligible (ANSYS-FLUENT® 14.0 User's manual, 2012).

5.3.2.4. Boundary Conditions

At the inlet, liquid phase velocities and at the outlet the pressure (atmospheric) were specified. The direction of the gravity and its magnitude were also specified before starting any calculations. The other variables were extrapolated from the interior. Generally **Newmann conditions** were applied to the velocities;

$$\frac{\partial \vec{u}_c}{\partial n} = 0 \tag{5.10}$$

where n is the normal direction to the outlet cells.

At the wall, **no slip boundary conditions**, i.e., $\vec{u} = 0$ was enforced for continuous liquid phase. For no slip wall conditions, CFD solver can predict the shear stress on the fluid at the wall (FLUENT 14.0® user manual, 2012). For laminar flows, this calculations simply depends on the velocity gradient at the wall:

$$\tau_w = \mu_c \frac{\partial \vec{u}_c}{\partial n} \tag{5.11}$$

When a particle strikes a boundary face throughout the flow volume, one of the following boundary conditions can be chosen:

Reflect boundary condition is used in the case of particles rebound from the boundary with a change in its momentum as defined by the coefficient of restitution (Figure 5.6a). The normal coefficient of restitution can be estimated by ratio of the amount of momentum in the direction normal to the wall that is retained by the particle after the collision with the boundary:

$$e_n = \frac{\upsilon_{2,n}}{\upsilon_{1,n}} \tag{5.12}$$

where υ_n is the particle velocity normal to the wall and the subscripts 1 and 2 refer to before and after collision, respectively. the tangential coefficient of restitution, e_t, defines the amount of momentum in the direction tangential to the wall that is retained by the particle.

$$e_t = \frac{\tan\theta_2}{\tan\theta_1} \tag{5.13}$$

A normal or tangential coeffcient of restitution equal to 1.0 refers that the particle reflects from the wall of flow volume with the same angle (an elastic collision) in case of reflection angles θ_2 is equal to θ_1. A normal or tangential coefficient of restitution equal to zero means that the particle retains none of its normal or tangential momentum after the rebound (ANSYS-FLUENT® 14.0 User's manual, 2012).

Escape boundary condition for particle phase assumes that the particle escapes when it encounters the boundary (Fig. 5.5c). For example when the particle reaches the outlet boundary, trajectory calculation is terminated and particle leaves the system.

Incomplete boundary condition is the one that particle is terminated when the maximum allowed number of time steps is exceeded.

Trapped boundary condition is used when the particle is terminated at a flow boundary. For example, non-volatile material is lost when get in contact with the boundary; volatile material present in the particle or droplet is released to the vapor phase at this point. In the case of evaporating droplets, their entire mass instantaneously passes into the vapor phase and enters the cell adjacent to the boundary (Figure 5.5b).

Evaporated boundary condition includes those trajectories along which the particles are evaporated within the domain.

Aborted trajectories can be used for particles failed to complete their motion in the liquid flow due to numerical/round-off reasons. If there are many aborted particles, it should be recalculated with a modified length scale or different initial conditions (ANSYS-FLUENT® 14.0 User's manual, 2012).

The main inputs for the discrete phase calculations in FLUENT® are the initial conditions that define the starting positions, velocities, and other input parameters for each particle stream. These initial conditions provide the starting values for all of the dependent discrete phase variables that describe the instantaneous conditions of an individual particle. First of all, an injection is created to start particle motion. The **initial conditions** for a particle/droplet stream is to be well-defined by creating an injection and assigning properties to it. FLUENT® has options for several types of injections such as:

- **Single** injection for specifying a single value for each of the initial conditions (Figure 5.7a).
- **Group** injection to define a range for one or more of the initial conditions (e.g., a range of diameters or a range of initial positions, see in Figure 5.6b).
- **Cone** injection to determine hollow spray cone injections in 3D problems only (Figure 5.6c).
- **Surface** injection to release particles from a surface, either a zone surface or a surface it is defined by the user.
- **Atomized** particle injection types such as plain-orifice, pressure-swirl, flat-fan, air-blast and effervescent atomizer injections.
- User defined injection.

Then the following initial conditions of injection are used as input for simulation:

- Position of the particle to *x*, *y*, *z* coordinates.
- Type of injection (solid, droplets or gas bubbles).
- Velocity magnitudes of the particle for *x*, *y*, *z* coordinates at the inlet of flow geometry.

- Diameter of the particle
- Temperature of the particle.
- Mass flow rate of the particle stream that will follow the trajectory of the individual particle/droplet, of which is required only for coupled calculations (ANSYS-FLUENT® 14.0 User's manual, 2012).

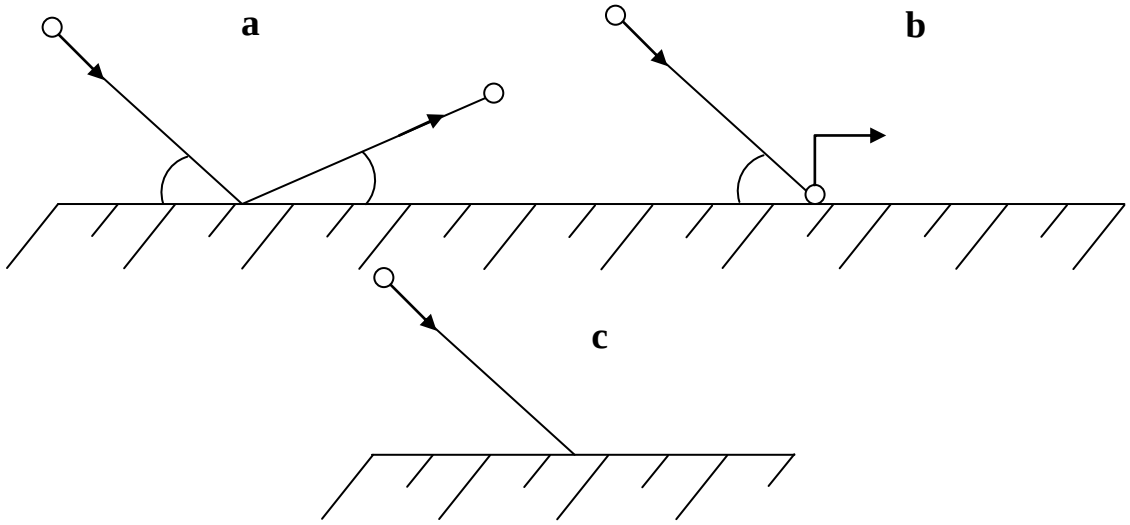

Figure 5.5. Main boundary conditions for particles in discrete phase model (DPM); (a) Reflect (b) Trap (c) Escape (Source: ANSYS-FLUENT® 14.0 User's manual, 2012)

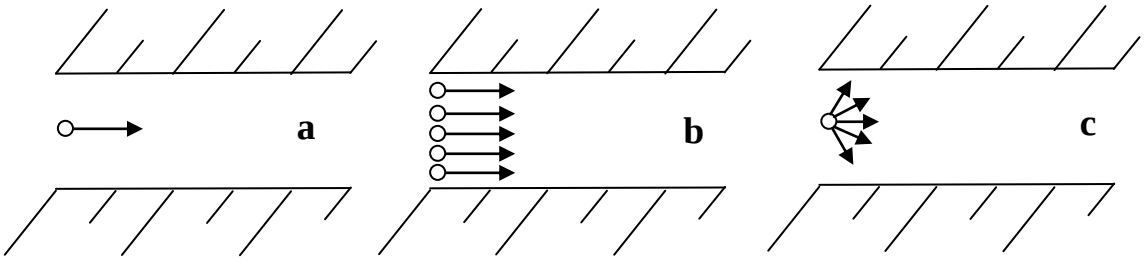

Figure 5.6. Particle injection definition (a) Single (b) Group (c) Cone plate (Source: ANSYS-FLUENT® 14.0 User's manual, 2012)

5.3.2.5. Calculation Procedure

The general summation of procedure for setting up and solving a steady-state discrete-phase problem can be outlined as the following:

- Continuous-phase flow field is solved based on specified initial and boundary conditions.
- The discrete-phase model is introduced for calculation of the trajectory of each injected particle. Recalculate the continous phase flow field using the interphase exchange of momentum determined during the previous particle trajectory calculation.
- Recalculate the particle phase trajectories in the modified continuous phase flow field.
- Repeat the previous two steps until a converged solution is achieved.

5.3.3. Post Processing

The last step of performing of CFD analysis is evaluation of the results of numerical solution. Post-processing involves extracting the desired flow properties from the computed flow field. The post processor of a CFD solver has capabilities include image generation to communicate results visually, qualitative post-processing to display and calculate data, automation to ease repetitive tasks, and the ability to run in batch mode. It is also possible to show data in the form of tables. By this way numerical data might be investigated statistically in a different software to make comparison. Velocity, temperature, pressure distributions can be represented as contour figures Also such properties can be shown as streamlines or vector plots (scaled arrow or points to the direction of flow) if two phase flow is simulated in CFD solver. Also residence time of both liquid and solid particles can be represented (Scott and Richardson, 1997; Versteeg and Malalasekera, 1995). The computed flow properties are then compared to results from analytic, computational, or experimental studies to establish the validity of the computed results.

The process can be repeated to examine the sensitivity of the computed results to understand the possible differences in the accuracy of results and/or performance of the computation with respect to dimensionality, flow conditions, initial conditions, marching strategy, algorithms, grid topology and density, turbulence model, chemistry model, flux model, artificial viscosity, boundary conditions and computer system.

CHAPTER 6

DETERMINATION OF UV DOSE AND INTENSITY BY COMPUTATIONAL FLUID DYNAMICS (CFD)

6.1. Introduction

Computational fluid dynamics (CFD) has been utilized as a helpful method in many processes. CFD considers mathematical physics of rheological and physicochemical properties of materials, iterative methods of numerical solutions of transport equations (heat, mass and momentum) (Norton and Sun, 2006; Scott and Richardson, 1997; Xia and Sun, 2002). CFD is preferred because of saving the time and lowering the cost for construction of a process or individual operation in comparison of conducting complex experimental procedures and optimization studies (Scott and Richrdson, 1997). Computational fluid dynamics (CFD) has also been used in food industry to lower operational and experimental costs (Norton and Sun, 2006; Xia and Sun, 2002).

The objectives of this study were to determine UV intensity and UV dose distribution in an annular type continuous flow UV reactor by numerical analysis. FSOGJ was selected as a model liquid food. It is assumed that grape juice was composed of both liquid and particle phases. Microorganisms was considered to constitute particle phase. Three steps were applied in the CFD simulation. In the first step, the physical geometry of S-shaped continuous flow UV reactor was created to define the flow boundaries and meshed by using ANSYS 14.0®, equipped with Design Modeler® and Mesh®. In the second step, a commercial CFD solver, FLUENT® 14.0, was used. Physical properties (viscosity and density) were introduced as an input to CFD solver. Liquid velocity, determined experimentally, was also used as an inlet boundary condition. Continuity, momentum and mass transfer equations were combined to simulate the flow field. In addition, Discrete Particle model (DPM) was integrated with flow models for simulation of motion of the microbial particles in the flow field. An injection was created for a group of microbial particles having certain density and mass flow rate. For numerical iteration, these models were discretized in terms of finite volume element method and solved by FLUENT® 14.0. In the last step, the results were examined using the post processing

features of the FLUENT ® 14. Graphical and visual inspection of the numerical solution was carried out by particle tracking features and contour graphs.

6.2. Methods

6.2.1. Pre-Processing of The Flow Domain

As mentioned in Chapter 5, the simulation of flow field was started after creating the whole geometry and meshing to form a grid structure. Then, disctreatization of aproppriate governing equations was carried out following linearization step for defined assumptions and boundary conditons. The whole procedure for simulation of the flow inside the S-shaped continuous flow UV reactor was carried out by ANSYS 14.0®, equipped with Design Modeler® for geometry design, Mesh® for construction of grid structure and FLUENT 14.0® for iterative solution and Post Processing® (ANSYS Inc., USA). For simulation, FSOGJ, defined in Chapter 3, was chosen as model opaque liquid food. All the data, geometry, grid structure and simulated results were integrated in a Workbench 14.0® file. Hence, all the modifications about a flow geometry could be done in the same file.

The S-shaped UV reactor system was illustrated previously in Figure 4.1 (Section 4.2.2.3.). Geometry for the S-shaped UV tube was drawn using Design Modeler® and shown in Figure 6.1. The geometrical parameters of the UV system was given in Table 3.1. The flow gap has a thickness of 5 mm. The flow gap was surrounded by a quartz glass having high penetration rate of UV with lower degree of loss of light. The length and thickness of this quartz glass was 400 mm and 2 mm, whereas thickness of the glass at the inlet and outlet of the gap was 1 mm. Solid quartz glass body was meshed seperately from the flow body. Grid structure of these two different bodies were connected by inflation. This application was useful in meshing configuration, especially near the parts that was impossible to connect the critical nodes. Also components of flow domain (flow gap with inlet and outlet pipe) were drawn as one fluid body that is essential for implying boundary conditions and meshing.

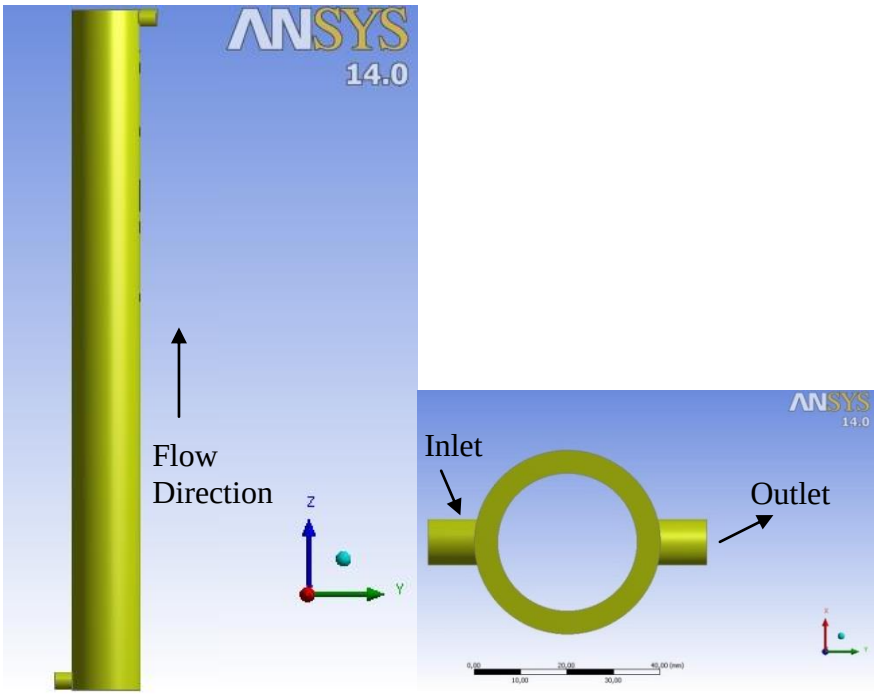

Figure 6.1. Geometry of S-shaped UV reactor flow region drawn by Design Modeler®; (a) Side view (b) Top view

Meshing of UV reactor flow region was complex and difficult to adjust the best grid configuration due to different size of cylindirical bodies, connected vertically. Grid structure was shown in Figure 6.1b. Connected parts of the body resulted dense nodes (especially inlet and outlet of the pipe connections near the main annulus). This kind of phenomena results iteration and convergence problems during numerical analysis. Distribution of skewness factor was estimated by Eqn 5.6 and 5.7 based on the element metrics in such a way that configuration and distribution of mesh size of the whole body was acceptable.

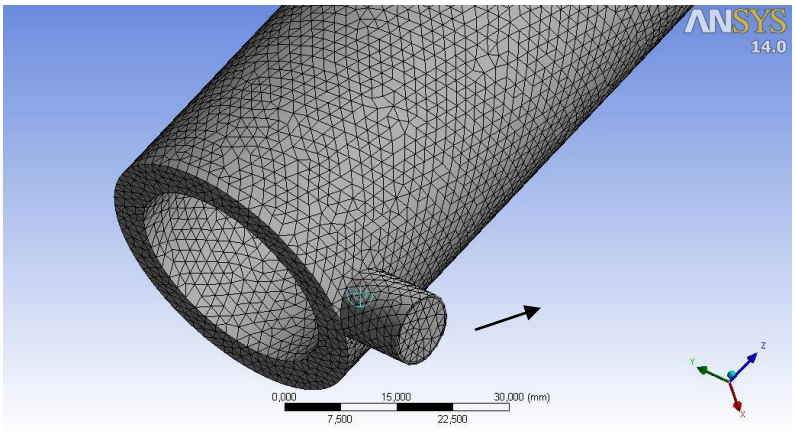

Figure 6.2. Grid structure by Mesh® in ANSYS Workbench 14.0.®

As a result of meshing operation, number of total mesh element was composed of 417.641 cell volumes, including flow gap, thickness of quartz glass and inlet-outlet of S-shaped UV tube. Minimum skewness factor was obtained as "0.84" from equation 5.1. It was examined that triangular mesh volumes were used in fluid body.

6.2.2. Simulation of The Flow Field

6.2.2.1. Initial and Boundary Conditions

FLUENT® 14.0 version was used as numerical solver due to good performance in 3D flow simulations (Asteriadou et al, 2006; FLUENT® User manual, 2012). Equation of continuity and momentum were applied to simulate laminar flow behavior of fluid food. General scale and axial adjustment were done with respect to flow direction. Metric scale and pressure based solver was used for solution. Operational parameters and assumptions used to simulate flow in S-shaped UV tube were summarized in Table 6.1.

The laminar flow regime was selected to maintain better UV inactivation efficiency providing higher residence time of fluid flow. For this aim, Reynolds number was calculated by eqn. 6.1.

$$\mathrm{Re} = \frac{D_{inlet}\, \nu\, \rho_{sample}}{\mu_{sample}} \tag{6.1}$$

In Eqn 6.1, Re is Reynolds number, D_{inlet} is inlet diameter (m), υ refers to average flow velocity at the inlet (m/s), ρ_{sample} is density of sample (kg/m^3) and μ is apparent viscosity (kg/m.s).

The viscosity and density of simulated FSOGJ were measured at process temperature (Table 6.1). Overall UV irradiation process was considered as steady state within no change of properties with respect to time. Numerical solution was initiated on flow region, based on single flow rate (0.0115 m/s) used as inlet boundary condition. Absorption coefficient of grape juice was 2384.7 m^{-1} (from Chapter 3).

Construction of thin film continuous flow UV reactor was well defined in Chapter 4. The flow simulaton of this reactor was carried out considering only one lamp located at the center of flow domain. Power of single lamp was 15 W (Table 6.1).

Table 6.1. Solution Criteria used by FLUENT® Solver

Software	FLUENT 14.0 ®
Discreatization	Pressure-Based Finite Volume
Particle Tracking	Disperse Phase Model
Scheme Method	SIMPLE
Gradient Method	Least Squares Cell Based
Fluid Food	FSOGJ
Viscosity (kg/m.s)	0.021
Density (kg/m^3)	1065.3
A_{254} (m^{-1})	2384.7
Re_{inlet}	5.82
V_{inlet} (m/s)	0.011
Temperature (°C)	20
Lamp Power (W)	15
Flow Gap (m)	0.005
Assumptions	▪ Steady flow ▪ Incompressible flow ▪ Newtonian fluid ▪ Laminar flow ▪ Isothermal system.
# of Finite Volume Element	417.000
Convergence Critetion	10^{-4}-10^{-6}
Type of Mesh	Triangular-tetrahedral
# of Iteration	100

Discrete Particle model (DPM) was also integrated to flow simulation. The injection of inert microbial particles were incorporated into model fluid (FSOGJ) assuming no interaction of microbial particles with fluid phase. Then initial and boundary conditions of injected particles were determined. Diameter of particles,10^{-6} m was chosen in terms of diameter of yeast spheres. Particles were released from the surfaces of the inlet. Injection type was determined as "surface" without any collision or bound on the surface of domain. By this way, particles were easily escaped from the outlet tube (Chapter 5). Total flow rate of injected particles were estimated approximately 0.001 kg/s based on the diameter of one spherical particle. Velocity of particles were determined as 0.009 m/s that was a little less than the initial fluid velocity (0.0115 m/s).

6.2.2.2. Compilation of UDF

UV intensity distribution gives information about the UV intensity applied in different regions of a flow domain. UV dose is defined as independent of the flow field but dependent on the distance of UV light source, absorptivity of the fluid and incident intensity of UV light (Blatchley, 1997; Koutchma, 2006; Sozzi and Taghipour, 2005). In order to define the points, where UV light is poorly penetrated, the estimation of the UV intensity and UV dose distribution in UV reactor (in mW/cm^2) is essential.

A user defined function (UDF) can be determined as the single or a group of function that is represented by an appropriate computational algorithm to enhance the standard features of the solver code. Using UDFs, specific material properties, boundary conditions, source terms or specified flow or transport models can be enhanced and customized into standard discreatization and linearization operation. For FLUENT®, UDFs can only be written on C, C+ or C++ algorithm in order to be integrated in flow and DPM model used in ANSYS FLUENT® solver. UDFs can be interpreted, complied or executed FLUENT® solver based on the geometry and transport properties. Prior to flow simulation, user defined function (UDF) compilation was carried out in order to simulate the UV intensity distribution in the flow volume.

6.2.2.3. Multiple Point Source Summation (MPSS) Model

The UV intensity and dose distribution must be considered in the design of a UV reactor. This is due to the fact that homogeneous UV dose and intensity distribution in a UV reactor are limited by presence of some material components having different absorptive or reflective properties. There are several model expressions for determination of UV intensity distribution. Finite Line Source and Multiple Point Source Summation (MPSS) models are developed based on division of the UV lamp into many number of point sources within equally-spaced throughout the lamp axis. MPSS model is used to compute UV radiation intensity field as a summation of trajected particles' received radiation from a series of co-linear point source. The light emission occurred through all the UV reactor volume (Amos, 2007; Blatchley, 1997; Jacob and Dranoff, 1970; Kucuk, 2002; Suidan and Severin, 1986; Unluturk et at. 2004). In this model, intensity rate changes over the length of the lamp and overprediction of diffused radiation occurs at the

end point of the light sources and near the light sources (Liu et al, 2004; Sozzi and Taghipour, 2005). The fluence rate (UV intensity) at a random point in the flow domain is estimated from equation 6.2 by the summation of the fluence rate values of all point sources,:

$$E(r,z)=\sum_{i=1}^{n}\frac{\Phi}{4\pi l_i^{\,2} m}\exp\left[-a_{254}(r-r_L)\frac{l_i}{r}\right] \tag{6.2}$$

l_i refers to the distance from the current location (cm) to the ith number of point source out of *m* sources and estimated from the Pisagor theorem;

$$l_i^{\,2}=(r^2+z_i^{\,2}) \tag{6.3}$$

Generally, single lamp configuration (at the center of UV tube) was studied in the literature (Amos, 2007; Blatchley, 1997; Jacob and Dranoff, 1970; Kucuk, 2002; Sozzi and Taghipour, 2005, 2006; Suidan and Severin, 1986; Unluturk et at. 2004). Hence, in this study, the UV intensity distribution is simulated by using a single lamp, placed at the center of annulus. Flow domain of S-shaped continuous flow UV reactor was shown in Figure 6.3.

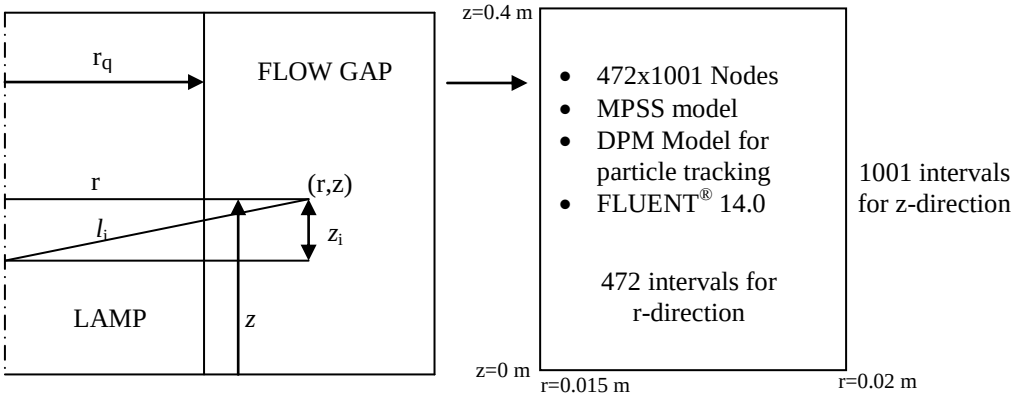

Figure 6.3. MPSS model parameters on flow gap (left) and number of intervals for numerical solution of UV intensity (right)

6.2.2.4. CFD Analysis for UV Intensity Distribution

Initially, FLUENT standalone setup file was connected to grid structure on Workbench®. FLUENT was started in 4 parallel core of CPU and double precision for best and fast calculation. Initial velocity was assigned as inlet boundary. Solver was initiated for computational simulation. Convergence monitors and solver settings were set in order to follow iteration. Equation of continuity was used for laminar flow conditions in the simulation (Eqns. 5.4 and 5.5 in Section 5.3.2.2). In addition, momentum (Eqns. 5.7, 5.8 and 5.9 in Section 5.3.2.2) equations were applied. SIMPLE and least squares cell based solution methods were selected to obtain best pressure-velocity coupling along with first order upwind solution method.

Discrete Particle model (DPM) was activated to determine residence time distribution of particles. An injection was created for particle tracking. Initial conditions for DPM (positioning, mass flow rate and type of particle track) were defined. Particles were assumed as inert microbial spheres, moving as a group throughout the domain. Escape boundary condition was chosen for particle flowing from inlet to outlet of domain. User defined function (UDF), written in C++ algorithm was compiled for MPSS model for simulation of UV intensity in a cylindrical annular UV tube. (Kucuk, 2002). UDF was integrated into DPM by building libudf source file. 100 iterations were determined to achieve low convergence at a level of 10^{-4}-10^{-6}.

After the numerical simulation and calculation, numerical data of UV intensity and dose distribution were saved as the output files (Microsoft Notepad and Microsoft Excel, Microsoft Co. USA). At the end of the simulation, 5 data were estimated: Radius (r), UV intensity, ($I_{r,z}$), axial distance (z), residence time and UV dose estimated based on the particle residence time and UV intensity of a given location. Finally contour plots and vectors based on r and y-direction in outlet of flow region were illustrated using MATLAB R2011b (Mathworks® Inc, USA). Contour graphs were plotted based on intensity distribution in both r and z-directions.

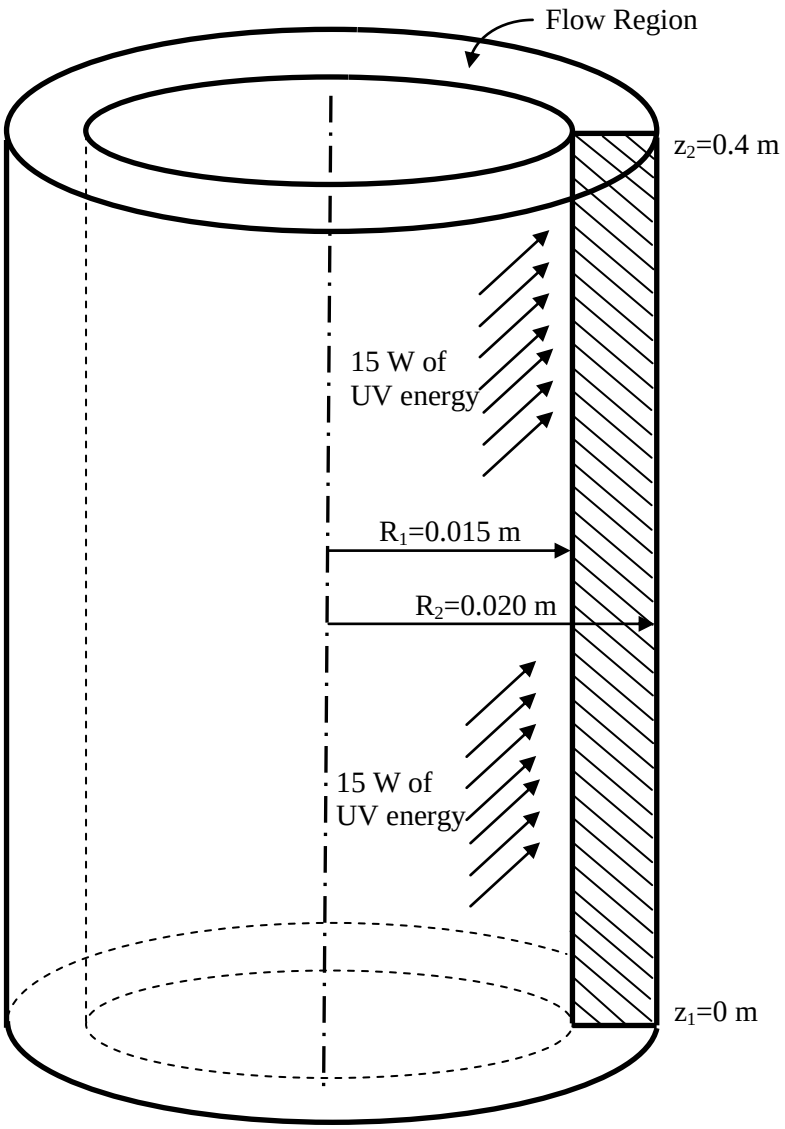

Figure 6.4. Computational fuid dynamics (CFD) analysis for 3-D domain of flow region

6.3. Results and Discussion

UV intensity and dose distributions of microbial particles and fluid flow with respect to radial and axial directions were simulated. Besides, the residence time distribution of particles were estimated by flow and DPM model. Streamlines of microbial particles through the flow volume was depicted in Figure 6.5. Total 101 microbial particles were injected as a group from the inlet surface and 92 particles completed their movement in the fluid and ejected from outlet.

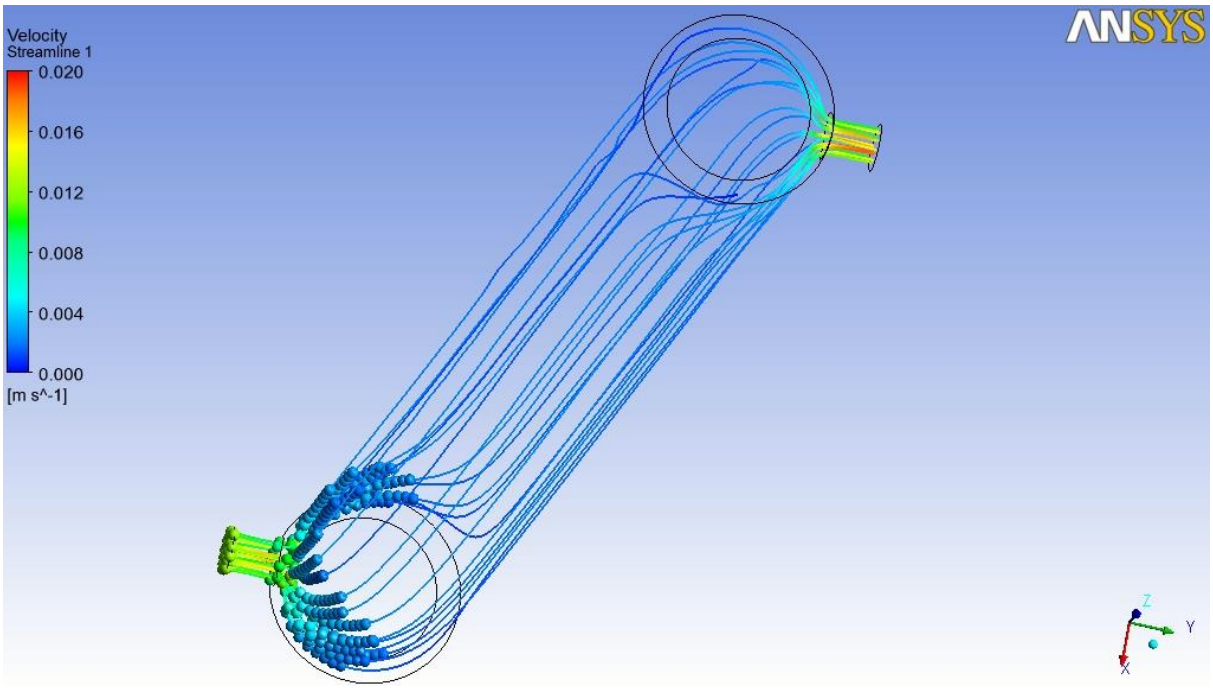

Figure 6.5. Streamline representation of velocity for fluid and microbial particle

The position of particles in the fluid flow volume is represented in figure 6.6. It was seen that particles are distributed randomly in 5 mm gap.

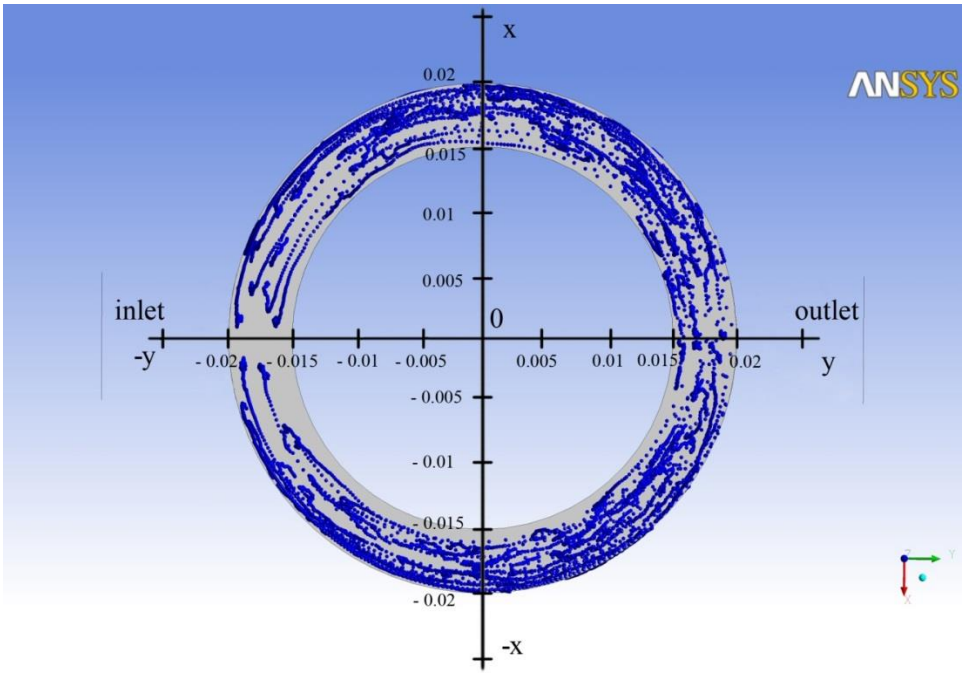

Figure 6.6. Particle distribution in the fluid domain (top view)

The velocity profiles of particles and fluid were also examined at the middle section of the flow domain (z=0.2 m) in Figure 6.7. It was seen that maximum velocity of fluid (0.0136 m/s) was greater than that of particles (0.009 m/s). It was determined that, the velocity distribution of fluid phase and particle phase did not exhibit a symmetrical parabolic profile in the annular region i.e., the maximum of the parabolic curve was shifted to the boundary surface of the inner pipe.

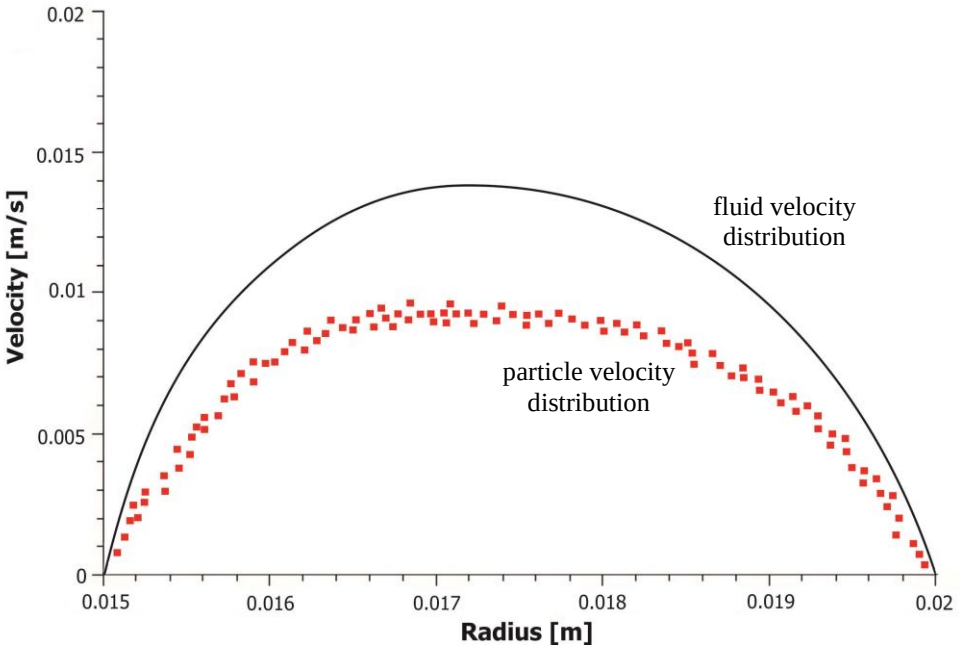

Figure 6.7. Velocity profiles of fluid and particles

6.3.1. Residence Time Distribution

Residence time distribution within particle pathlines throughout flow domain is shown in figure 6.8. It was noticed that there was no vortex formation that causes interrupting particle motion at defined flow conditions. Also histogram of residence time distribution was depicted in figure 6.9. Residence time distribution did not exhibit normal distribution. There was no particle having residence time less than 165 seconds. The residence time of 75 particles was in the range of 165-300 seconds. Approximately, only 17 of the particles were completed transition from the tube in 350 and 475 seconds. This time difference between particles might be as a result of the velocity profile of the fluid in the annular region and the drag force exerted on the particles near the wall. Mean residence

time of 92 particles were estimated as 241.2±77.96 s. This average time was very close to the one recorded manually (244 s) at the same flow rate.

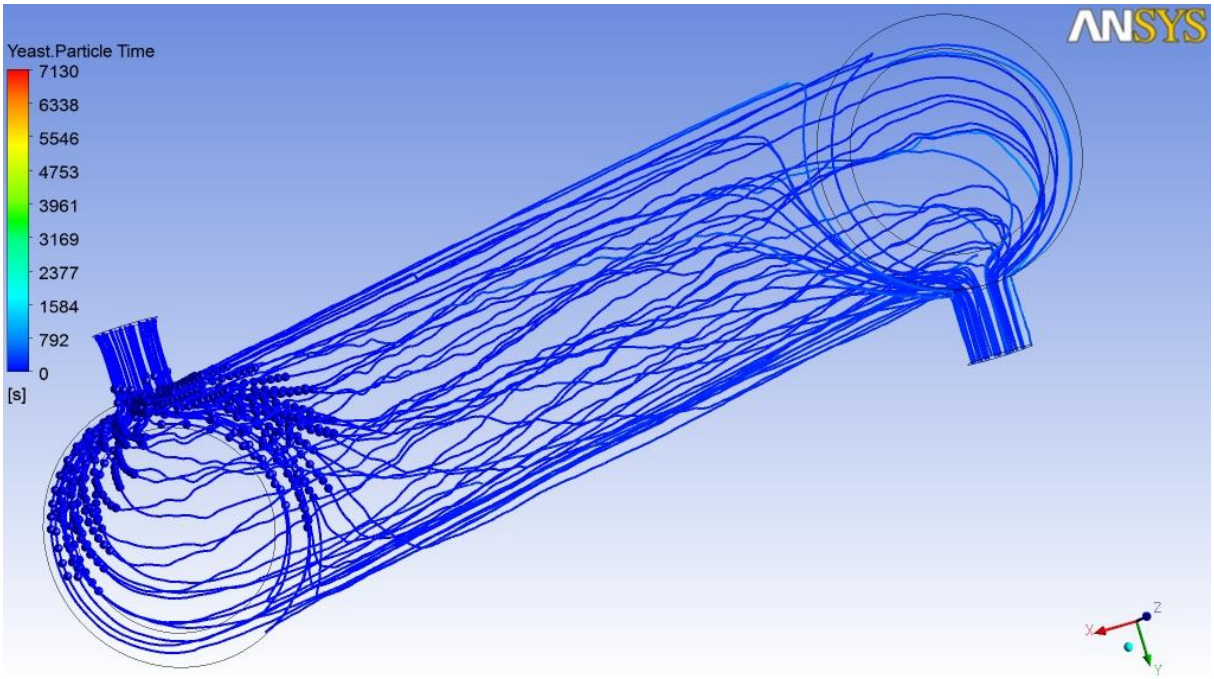

Figure 6.8. Residence time distribution of particles in flow domain

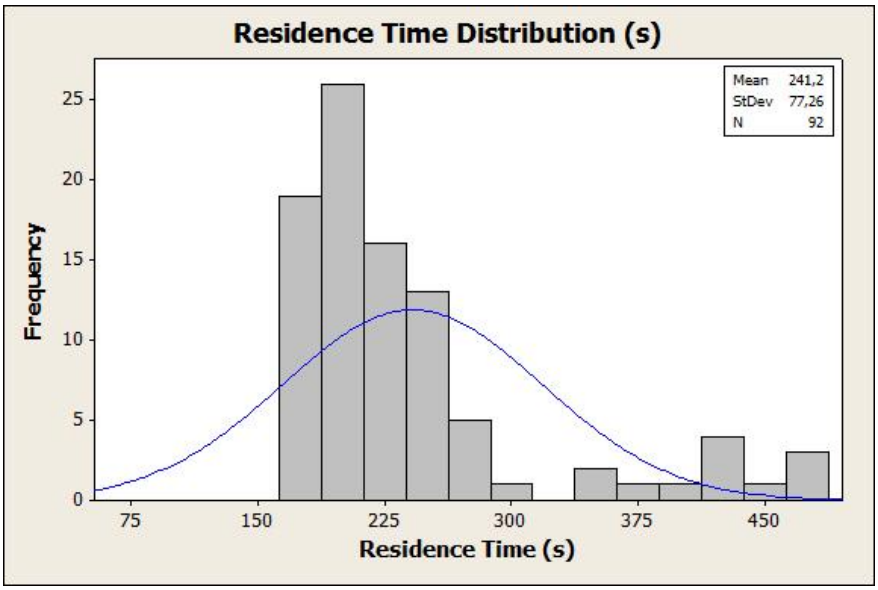

Figure 6.9. Histogram of residence time distribution of the simulated microbial particles

6.3.2. UV Intensity Distribution in Flow Domain

UV intensity distribution of the whole domain was estimated by MPSS model. Intensity values were calculated for the UV light emitted from the UV lamp in the axial and radial direction of the flow gap by using MPSS model (see eqns 6.2 and 6.3). Hence, the UV intensity was decreased by increasing of distance to each point source of the lamp (Blatchley, 1997; Liu et al, 2004; Sozzi and Taghipour, 2005; Unluturk et al, 2004). Results were shown in figüre 6.10a, b and c. It was found that intensity distribution decreased by increasing the radial direction away from the light source. It was predicted that UV light emission was symmetrical in the axial direction of the lamp i.e., from the middle point of the lamp to the edges. Near the lamp surface (r=0.015 m), UV intensity was calculated by MPSS model as 0.326 mW/cm^2. The highest UV intensity (41.092 mW/cm^2) was estimated at the middle of the lamp (z=0.2 m) and close to UV lamp surface (r=0.015 m) as. In other words, it was observed that high UV emission occured in the middle of the lamp. Average intensity rate throughout axial direction at the point where r =0.015 was calculated as 35.87 mW/cm^2. Figure 6.10a represents distribution of UV intensity along the axial (z) direction and radial direction where r is chaning between 0.015 and 0.016 m i.e., UV penetration lenght was 1 mm. It was shown that UV lights were able to penetrate up to 1 mm distance from UV source in flow gap (Unluturk et al, 2004). Decrease of UV intensity rate as a function of radial distance might be explained due to the low UV emissivity of opaque fluid food (Koutchma et al, 2004; Unluturk et al, 2004).

Figure 6.10b shows UV intensity distribution for the region lie between 0.015 and 0.0175 m (i.e., half of the flow gap). UV emissivity converged to zero after radial direction was greater than 0.0165 m. UV intensity level of the whole flow domain was depicted in figure 6.10c The average intensity values at different axial and radial positions were summarized in Table 6.2. The highest UV intensity was predicted as 41.092 mW/cm^2 in the region very close to the lamp surface at the position where r=0.015 and z=0.2. Average UV intensity values were computed as 35.87 mW/cm^2 for near the lamp surface (r=0.015 m), 1.770 mW/cm^2 at r=0.016 m, 0.034 mW/cm^2 at the center of flow gap (r=0.0175) and 4.23x10^{-5} mW/cm^2 for r=0.02 throughout z-direction. On the other hand, the mean UV intensity values at different axial distances was estimated based on averaging the values predicted along the radial direction at the given locations. For example at the inlet point (z=0.0004 m), average UV intensity rate was computed as 0.013 mW/cm^2.

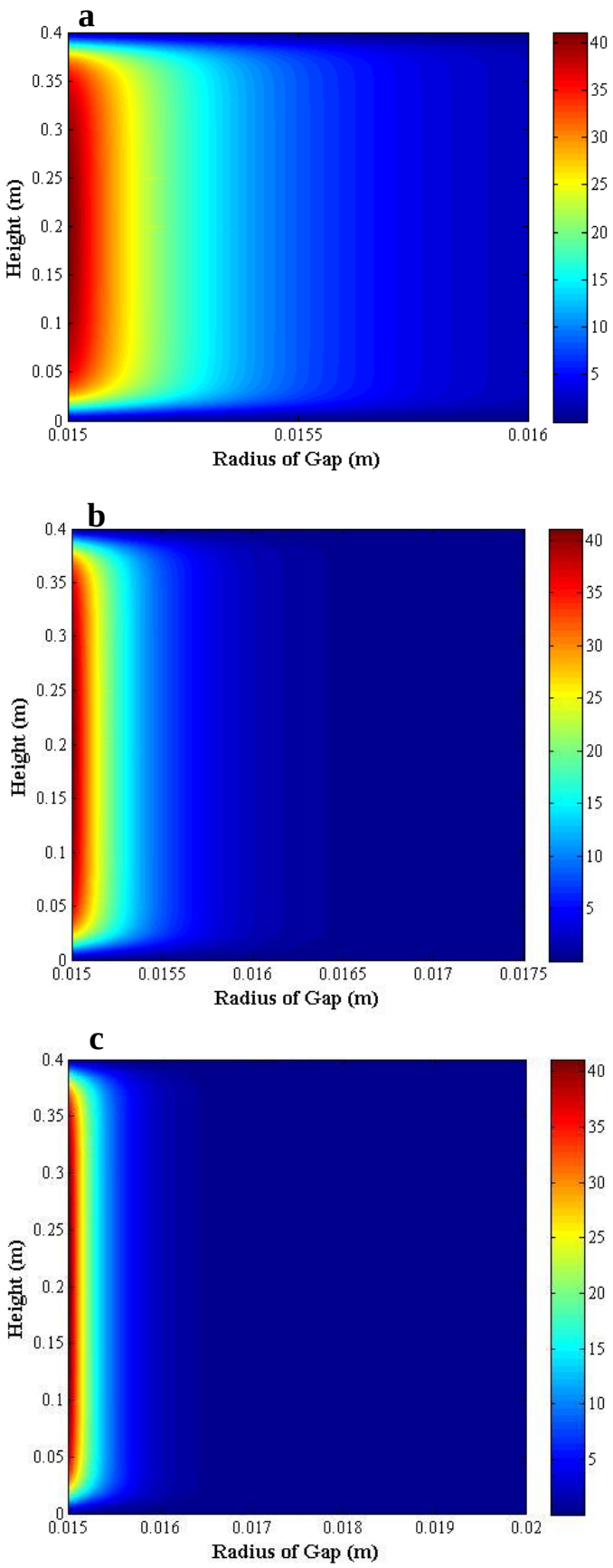

Figure 6.10. UV intensity distribution of the flow domain estimated by MPSS model at (a) 0.015 < r < 0.016 m (b) 0.015 < r < 0.0175 m (c) 0.015 < r < 0.020 m

Table 6.2. UV Intensity Values of Critical Points in Flow Boundary

	UV Intensity (mW/cm^2)				
	r-direction				
z-direction	**r=0.015**	**r=0.016**	**r=0.0175**	**r=0.02**	**Ave**
0.0004	0.326	0.020	$5.4x10^{-4}$	$1.8x10^{-6}$	0.013
0.1	39.888	2.080	0.035	$4.3x10^{-5}$	1.415
0.2	41.092	2.080	0.035	$4.34x10^{-5}$	1.429

At 0.1 m height of the flow domain, average UV intensity was 1.41 mW/cm^2, whereas mean UV intensity was estimated as 1.43 mW/cm^2 at the middle of axial direction (z=0.2 m). The decrease of UV intensity distribution throughout the flow gap in radial direction might be due to the high absorption coefficient of simulated fluid (Duran et al, 2010; Koutchma et al, 2004, 2009; Koutchma, 2009; Unluturk et al, 2004).

It was seen that the irradiance at the wall had a symmetrical flat profile covering 95 % of the irradiated domain (between z = 0 m and z = 0.04 m), Moreover, a step decrease was obtained for UV intensity distribution at the edges (z=0-0.01 m and z=0.39-0.4 m) (Duran et al, 2010; Unluturk et al, 2004). This result might be explained with existence of non-irradiated volume at the edges of the lamp due to inefficient lamp emission besaue of the presence of glass lamp diodes (dead points).

The maximum UV intensity obtained at r=0.015, close to lamp surface, was also checked by calculating UV intensityfrom equations 6.4 and 6.5;

$$I_{calculated} = \frac{Power\ of\ UV source}{Area\ of\ UV source} \tag{6.4}$$

$$I_{calculated}\ (mW/cm^2) = \frac{15W}{\pi * D_{lamp} * L_{lamp}} * \frac{1000mW}{1W} * \frac{1m^2}{10000cm^2} \tag{6.5}$$

where diameter of lamp was 0.025 m and length of UV source was 0.4 m. The surface area of lamp was 311 cm^2. Average irradiance was estimated as 45.74 mW/cm^2 from Eqn 6.5. Maximum UV intensity, at which close to lamp surface (r=0.015 m) was estimated by MPSS model as 41.092 mW/cm^2 which is approximately >11 % different than the one calculated from Eqn 6.5.

6.3.3. UV Dose Distribution

UV dose distribution of the particles were also calculated during simulation by multiplying the residence time of each particle obatined from DPM model with the UV intensity estimated from MPSS model. Figure 6.11 shows the UV dose distribution of 92 particles. UV dose of particles were very high. High UV dose estimation was due to a low flow rate and the small gap resulted in having high residence time and UV emission.

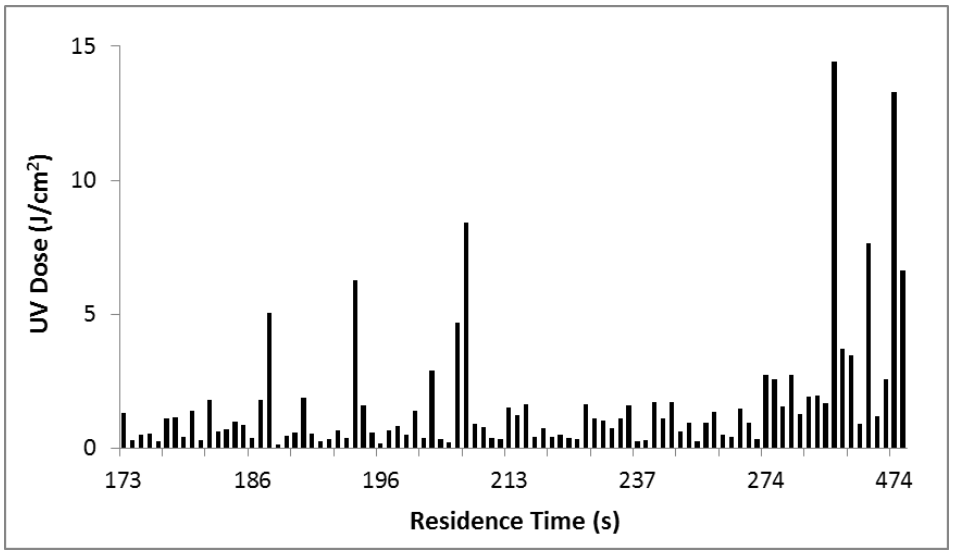

Figure 6.11. UV dose distribution of 92 particles using MPSS model and DPM model

83 of 92 particles (% 90 of total) received UV dose less than 3 J/cm^2. There are two reasons for this. First one is the position of the particles during traveling in the flow volume. Those of particles travelled near the outer wall of the annular flow domain has not been exposed to UV light compared to those passed near the UV light source. Particle tracking, depicted in figure 6.6 showed that microbial particles mostly travelled far from UV light source. This was also supported by findings of Unluturk et al (2004). She was pointed out the importance of the particle positions exposed to UV light in a similar manner. The second reason might be high absorbance coefficient (2384.7 m^{-1}) of simulated opaque fluid food. UV penetration throughout the fluid phase having high absorption coefficient might result in a low UV dose delivery to the particles moved close to outer wall. MPSS model estimated maximum 14 J/cm^2 UV dose for 2 particles (% 2.1 of total) having higher residence time in the flow domain and passing close to lamp surface. Thus, these particles emitted higher UV light resulting higher UV dose delivery. Unluturk et al, (2004) studied laminar flow in thin film continuous flow UV reactor. The thickness of flow

gap was 1 mm. Unluturk et al, (2004) estimated UV dose received by particles having residence time interval between 3-13 seconds. As a result of the simulation, 75% of the particles received UV dose in the range of 30-100 mJ/cm^2. Unluturk et al, (2004) described the reasons of low UV dose level as low residence time and particles at central region of flow where highest velocity was obtained.

6.3.4. UV Intensity Distribution

UV intensity distribution in the flow domain was estimated by MPSS model. Results were shown in figure 6.12. UV intensity distribution that particles had been exposed during their transition from the UV reactor was varied between 0.802 and 40.627 mW/cm^2. 10 % of this particles received UV intensity at 13-41 mW/cm^2 level. Instead, 90 % of these particle had exposed to UV intensity below 10 mW/cm^2. Mean intensity received by92 particles was estimated as 6.328±7.429 mW/cm^2. According to figure 6.9, it was found that different particles received different amount of UV light. For example, intensity values of particles having the residence time range of 450-470 seconds were expected to be higher than that of particles having 250-270 seconds of UV exposure time. Maximum UV emission of simulated microbial particles was 40.627 mW/cm^2. Average UV intensity of particles at 450-470 seconds of residence time were approximately 28 mW/cm^2, whereas average UV intensity level was 36 mW/cm^2 for particles with 270 seconds of residence time. This might be explained by taking different position of particles during flow simulation. Some of the particles might complete their motion throughout the flow volume near by the wall boundry close to the UV light source, of which the UV light penetration was higher. Even though these particles had less residence time, UV intensity levels was higher than those particles having greater residence time but passed far away from UV light source. This result was also supported by Unluturk et al (2004). They applied CFD for UV intensity distribution through thin film continuous flow UV reactor, based on apple cider as model liquid food having laminar flow condition. They also found that UV intensity of several particles having higher residence time was lower than those of having lower residence time.

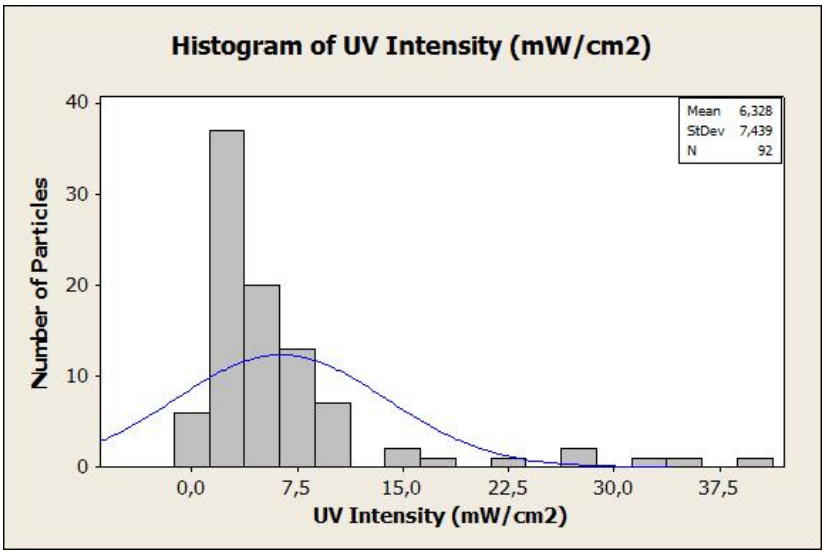

Figure 6.12. UV intensity distribution calculated from MPSS model and DPM model

The average UV intensity, UV dose and residence time obtained by means of biodosimetric method, chemical actinometry and CFD modelling were summarized in Table 6.3. The great difference in UV dose obtained from biodosimetric method was observed in comparison to that of actinometric and CFD results. The calculated UV dose levels were high with great standard deviation (1597±2310 mJ/cm^2), compared to dose values observed from biodosimetry study (247.302 mJ/cm^2). Blatchely and Hunt, (1994) and Unluturk et al, (2004) found that the dose distribution maintained from biodosimetry method was lower than those calculated numerically from the MPSS model. It was mentioned in Chapter 2 and 3 in details that the biodosimetry method is applied by a static, bench top collimated beam UV apparatus by providing good mixing for the irradiated sample. The aim of this operation was to create a dose-response curve by logarithmic reduction versus UV dose (mW/cm^2). Irradiation of sample is maintained at controlled time intervals. Besides, average UV intensity was estimated by Beer Lambert Law (see Equation 2.1) by the relation of sample depth, incident intensity from radiometric measurement and absorptivity of irradiated sample. Finally, a single UV dose is estimated by the multiplication of average UV intensity with time for each sampling (see equation 2.2). Observed UV dose response curve is then used to compare the inactivation of the same sample in continuous flow UV reactor. Inactivation rate at the same time intervals are matched with that of UV dose level in dose response curve.

It is assumed that dose level obtained in disinfection was uniform with well mixing of the samples in a closed batch system. Compared with bench top apparatus, continuous

flow systems have great variations in the flow pattern of multiphase fluid. This means that, motion of liquid food, possible suspended particles microbial distribution are to be considered with respect to their positioning and residence time throughout the flow volume.

Table 6.3. Overall Results of Average UV Intensity, UV Dose and Residence Time

	UV Intensity (mW/cm^2)	**UV Dose Delivery (mJ/cm^2)**	**Residence Time (sec.)**
Biodosimetry	-	247.302	244
Chemical Actinometry	2.33±1.91	570	244
CFD	6.32±7.43	1597±2310	241.2±77.96

The dose and UV intensity values of both bench top and continuous flow systems are mismatched. The reason of this is the presence of single average intensity which is used to calculate single UV dose by mutliplication of limited time intervals in bench top collimated beam apparatus. Moreover, continuous flow systems contain UV intensity variations for each point into flow domain with the function of axial and radial position. As mentioned above, flow simulations of the present study resulted the variations in UV intensity and UV dose on microbial particles.

6.4. Conclusions

MPSS and DPM models were used for computation of UV intensity and UV dose distribution in an annular UV reactor where grape juice containing microbial particles was subjected to UV irradiation. FLUENT 14.0.® was used as CFD program. It was observed that residence time distribution of simulated particles was varied between 180 and 480 seconds. UV intensity distribution in both radial and axial positions were depicted. UV intensity was distributed symmetrically along the axial direction of the lamp. It was also found that UV intensity was decreased in radial directionin the flow gap. In radial direction, UV intensity close to the surface of light source was predicted as very high. High UV intensity was observed in the first 1 mm of the flow gap close to the light source. But in contrast, the rest of the domain (4 mm) had received low UV intensity due to high absorbance coefficient of opaque liquid food. At the edges of the lamp, UV intensity rate was converged to zero due to low emission of UV light at these points. Average UV

intensity values were estimated at different axial and radial points of the domain. Finally, average UV intensity values calculated from equation 6.5 and estimated from CFD simulation were compared and found reasonable close values. On the other hand, estimation of UV dose was done by the multiplication of UV intensity from MPSS model and residence time from DPM model. 90 % of particles received UV dose between 0-3 J/cm^2. High UV dose level was related with the high residence time distribution of the particles having very low velocities in the flow domain.

CHAPTER 7

UV INACTIVATION EFFICIENCY OF A CONSTRUCTED UV SYSTEM

7.1. Introduction

Food and Drug Administration (FDA) states that a fruit juice processing is required to be subjected to regulations of Hazard Analysis Critical Control Point (HACCP) programme (Federal Register [FR], 2001) and related regulation (21 CFR 110). 5 log reduction in the number of target microorganism (i.e., *E coli*) is necessary to meet the requirment of fruit juice pasteurization (USFDA, 2001). The main objective of this study was to investigate the efficiency of UV-C irradiation as a non-thermal pasteurization process for PCGJ and FSOGJ. Three different studies were designed to evaluate the effect of UV-C irradiation on the microbial inactivation and physical properties of grape juices. In the first study, PCGJ was inoculated with *S.cerevisiae* (NRRL Y-139) as target microorganism. In the second study, FSOGJ was fermented to provide the growth of spoilage microorganisms, i.e., yeast and lactic acid bacteria. S-shaped continuous flow UV reactor designed for opaque liquid foods was used in this study. Inoculated or fermented grape juice samples were exposed to a UV-C irradiation in the UV reactor having 5 mm of flow gap. Different UV doses, three different volumetric flow rates (0.90, 1.75 and 3.70 mL/s) corresponding to three different Re_{inlet} numbers (38.48, 80.24, 159.13 for PCGJ and 36.38, 75.87, 150.46 for FSOGJ) were used for UV inactivation of grape juice samples. In the third study, the efficiency of UV-C irradiation was examined using *E.coli* K-12 (ATCC 25253) which is a surrogate strain of *E.coli* O157:H7 by inoculating both PCGJ and FSOGJ. UV dose delivered in continuous flow UV reactor was determined based on biodosimetric method conducted by a bench top collimated beam apparatus. The UV dose response curves of target microorganisms were already given in Chapter 3. In order to find the delivered UV dose in irradiated FSOGJ, the maximum inactivation rate of spoilage yeast and lactic acid bacteria was marked and UV dose necessary for these inactivaton rate was read from the UV-dose response curve.

7.2. Experimental Study

Commercial PCGJ and FSOGJ obtained from Sultana type Turkish white grapes (seedless) were used as liquid medium. In the first part of the study, *S.cerevisiae* was selected as target microorganism for PCGJ. Besides, yeast and lactic acid bacteria (LAB) suspended in FSOGJ were irradiated by continuous flow UV reactor. Additionally, *E.coli* K-12 (ATCC 25253) was inactivated in both PCGJ and FSOGJ.

7.2.1. Materials

Commercial PCGJ (Kavaklıdere, Ankara), produced from seedless Sultana type traditional Turkish grapes (*V.vinifera*) were purchased from a local market. Pasteurized juice was selected since it does not contain significant level of background flora. Juice samples in the size of 200 mL bottles were stored at room temperature temperature (20 ºC) until it was used. FSOGJ was obtained according to Section 3.2.2.1.

7.2.2. Physical and Optical Measurements of Grape Juices

pH of PCGJ and FSOGJ samples were measured by a bench top pH meter (HANNA Instruments, United States) at room temperature (20 ºC). Calibration of pH meter was done using buffer 1 (pH=7) and buffer 2 (pH=4), respectively. On the other hand, density of grape juices were measured by portable density meter (Kyoto Electronics DA, Japan) at temperatures ranging from 5 to 90 ºC.

The absorbance coefficient of PCGJ and FSOGJ samples were measured using UV-visible spectrophotometer (Carry 100, Varian Inc.,bCA, United States) set at a wavelength of 254 nm. Absorbance coefficient was determined from several dilutions of samples (1:1, 1:2, 1:5, 1:10, 1:25, 1:50, 1:100, 1:200, 1:250 and 1:500).

Turbidity of the grape juice samples were measured by turbidimeter (HACH 2100AN IS. HACH Company, United States). Results were given as Nephelometric Turbidity Unit (NTU).

CIE colour parameters e.g., L* (brightness-darkness), a* (redness-greenness), b* (yellowness-blueness), were determined (Konica Minolta CR 400 Chromometer, Konica

Inc, Japan). According to these parameters, total colour difference (ΔE) and browning index (BI) of the samples were calculated from the Equations 7.1 and 7.2:

$$\Delta E = \sqrt{\left(\Delta L^*\right)^2 + \left(\Delta a^*\right)^2 + \left(\Delta b^*\right)^2} \tag{7.1}$$

$$BI = 100 * \frac{\frac{0.31\left(a^* + 1.75L^*\right)}{\left(5.645L^* + a^* - 3.012b^*\right)}}{0.172} \tag{7.2}$$

White grape juice samples in the amount of 10 mL from each variety was poured into quartz glass petri dishes. Measurements obtained from three different places of the samples were recorded. All the measurements related to physical and optical properties were repeated at least three times.

Brix was measured using bench top refractometer (Mettler-Toledo RE40D, AEA Investors Inc., USA). 3-4 drops of treated and untreated grape juice samples were poured into the reading cell. Data were collected at 20 ºC. Moreover, the amount of the titratable acidity was determined by titrametric method (Hakguder, 2009). 15 ml of sample was poured in a flask and titrated against standardized 0.1N of NaOH up to pH 8.1 (phenolphthalein indication point). The volume of NaOH used was recorded. Dominant organic acids in grape juices are tartaric and citric acid. Thus, results were expressed as grams of tartaric or citric acid per 100 mL of fruit juice, by the following formula:

$$\text{TA (\%)} = (V)\,(f)\,(E)\,(100) / M \tag{7.3}$$

where, V refers to the volume (mL) of 0.1 N NaOH used for the titration f is the normality factor, E is the miliequivalent weight of citric or tartaric acid in grams and M is the sample volume in mL.

The amount of ascorbic acid per liter of sample was determined by L-ascorbic acid test kit (Boehringer Mannheim-R-Biopharm, Roche, Germany) based on colorimetric method. Two quartz cuvettes were used. 1 ml of sodium phosphate/citrate buffers+MTT [3-(4,5-dimethylthiazoyl-2)-2,5-diphentyltetrazolium bromide] was mixed with 1.5 ml of ultrapure water and 0.1 ml of grape juice, equivalently. Then one of the cuvette was allowed to react with oxygen to produce dehydroascorbate by shaking a spatula conatining

ascorbate oxidase for 6 min. Oxygenated (sample) and unreacted (sample blank) mixture were incubated at 37 ºC. Then both cuvettes were used to read in the visible range of MTT-formazan at 578 nm and absorbances were recorded as A_1 and $A_{1\text{sample blank}}$. At pH 3.5, enzymatic reaction of L-ascorbic acid in grape juice sample was carried out by adding 0.1 ml of electron carrier PMS (5-methylphenazinium methosulfate). The sample was incubated again at 37 ºC for 15 minutes. Finally, absorbances were recorded as A_2 and $A_{2\text{sample blank}}$ at 578 nm. The absorbance differences for both sample and sample blank were calculated as:

$$\Delta A = (A_2\text{-}A_1)_{\text{sample}} - (A_2\text{-}A_1)_{\text{sample blank}} \tag{7.4}$$

The calculation was done with the aid of the extinction coefficient of MTT-formazan by the following equation:

$$c = \frac{V * MW}{\varepsilon * d * v * 1000} * \Delta A\,(g/l) \tag{7.5}$$

where V is final volume of the cuvettes (mL), v refers to sample volume (mL), MW is the molecular weight of the substance to be assayed (g/mol), d is the light path (cm) and ε is known as the extinction coefficient for MTT-formazan at 578 nm (L mol^{-1} cm^{-1}). The ascorbic acid concentration (in g L-ascorbic acid/L of sample solution) was calculated by the following expression:

$$c = \frac{2.7 * 176.13}{16.9 * 1.0 * 0.1 * 1000} * \Delta A\,(g/l) = 0.2814 * \Delta A \tag{7.6}$$

7.2.3. Target Microorganism and Cultivation

In the first study, *S.cerevisiae* was inactivated in PCGJ. Cultivation of *S.cerevisiae* was well defined in Chapter 3. In the second study, natural microflora (yeast and lactic acid bacteria) was determined as target microorganism for FSOGJ (Otezia et al, 2010; Fredericks et al, 2011; Ochoa-Velasco and Guerrero-Beltran, 2012). In order to investigate the efficiency of UV-C irradiation on FSOGJ, samples prepared in previous section were

first thawed and stored at the refrigerator for overnight. Then, 100 mL of FSOGJ was fermented under the conditions mentioned in Section 3.2.2.2. 60 mL fermented FSOGJ was mixed with 440 mL FSOGJ in order to provide a initial inoculum level of 5-6 Log CFU/mL to be used for UV treatments.

In the third study, *E.coli* K-12 (ATCC 25253) was used to determine the efficiency of continuous flow UV reactor. Preparation and acid adaptation of *E.coli* K-12 (ATCC 25253) strain was well defined in Chapter 3. *E.coli* K-12 was first adapted to pH 3.6 by malic and tartaric acid following several steps, as mentioned in Chapter 3 (Koutchma et al, 2007; Pala and Toklucu, 2013). After adaptation of *E.coli* K-12 to pH 3.6, single colony was transferred into 100 ml of TSB supplemented with 0.75% (w/v) glucose (Merck, Germany) having pH of 7.0. Then incubated at 37 ºC for overnight. Enriched TSB adjusted to 4 pH was used to inoculate FSOGJ having pH of 3.90-3.94. Moreover, enriched TSB adjusted to 4 pH was used for inoculation of PCGJ (pH = 2.90-2.92). 100 mL of enriched TSB broth was centrifuged at 3000 RPM for 5 min and seperated cells were inoculated into 500 ml of grape juice samples to obtain a concentration about 10^{6-7} CFU/mL for Enumeration of *E.coli* K-12 (ATCC 25253) was done by plating on tryptone soy agar using appropriate dilutions of phosphate buffered peptone water (Merck, Germany). All the plates were incubated at 37 ºC for 18 h.

Before UV inactivation study, the culture adapted to acidic environment i.e., pH 4.0 and 3.6, was tested by inoculating into grape juice samples (Pala and Toklucu, 2013). In order to determine the possible inactivation effect caused by high acidic environment of grape juice, both acid adapted TSB broth was centrifuged at 764 g for 5 min at 4 ºC and supernatant was separated. Cells were inoculated into 100 ml of FSOGJ and PCGJ with initial concentration of 10^{7-8} CFU/mL. Inoculated grape juices were then incubated at 37 ºC for 24 h and microbal count was done after 2, 4, 6, 7, 10 and 24 hours by plating on tryptone soy agar (TSA, Merck, Germany).

In order to eliminate total microbial backflora, FSOGJ was pasteurized by thermal treatment before inoculation of *E.coli* K-12. For this aim, 500 ml of FSOGJ was pasteurized at 72 °C, of which is defined as optimum pasteurization temperature for grape juice (Sanchez-Moreno et al, 2004; Timmermans et al, 2011). Temperature was controlled by a thermocouple, placed into the center of sample. Moreover, grape juice sample was shaked continuously to maintain homogeneous temperature distribution during heating. After 10 minutes, center of sample was reached to 72 °C. Then sample was hold at 10-20

seconds to complete pasteurization. Finally grape juice sample was immediately placed into ice bath for cooling.

7.2.4. Continuous Flow UV Study

Inoculated FSOGJ and PCGJ samples were placed into the glass tank equipped with a cooling jacket. UV treatments were carried out by continuous flow UV reactor described in Section 4.2.2.3. by applying three flow rates (0.90, 1.75 and 3.70 mL/s) and circulating five times. UV inactivation of *E.coli* K-12 (ATCC 25253) was carried out at only 0.90 mL/s of flow rate. Residence time for each flow rate was determined by a chronometer by recording the time of the liquid flowing between the inlet and outlet of UV reactor. Nonetheless, the total processing time of one cycle for each flow rate was estimated for 500 ml of grape juice. The whole flow volume was collected in the glass sample tank at the end of completion of one cycle. Then, the next cycle was started to be recorded. UV experiments were repeated twice for each flow rate. Reynolds numbers were estimated for grape juice by Eqn. 6.1 (Chapter 6). UV dose was given in two different units i.e., J/ml and J/cm^2 in the literature. UV dose was calculated by the relation of lamp power and volumetric flow rate following the equation (Tran and Farid, 2004, Keyser et al, 2008):

$$UV\ Dose = \frac{P}{Q} \tag{7.7}$$

In Eqn 7.7, P is referred to total UV-C output of the lamp (W) and Q is the volumetric flow rate (mL/s). Flow parameters and applied UV dose levels of PCGJ and FSOGJ used in UV reactor are given in Table 7.1. 5 mL of samples were collected before and after each UV cycle and plated on TSA, PDA and MRS agar for enumeration of total aerobic count, yeast count and lactic acid bacteria count, respectively.

UV dose delivered to inactivate spoilage microorganisms (yeast and lactic acid bacteria) can be also given in J/cm^2 unit. For this purpose, UV dose response curves obtained in bench top collimated beam apparatus were used (Figure 3.2. in Chapter 3). Moreover, UV dose response curve, depicted in Figure 3.2 was non-linear. For this aim, determination of dose delivery for continuous flow UV reactor was estimated by using a

non-linear inactivation kinetic model such as Hom and Weibull models, of which was defined in Chapter 2.

Table 7.1. Flow Parameters of Grape Juices on UV Inactivation Procedure

Type of Grape Juice	Power of Pump (RPM)	Velocity (mm/s)	Volumetric Flow Rate (mL/s)	Residence Time (s)	Re_{inlet}	UV Dose (J/mL)
PCGJ	17	1.64	0.90	244	38.48	116. 7
	33	3.15	1.75	127	80.24	60.0
	70	6.77	3.70	59	159.13	31.1
FSOGJ	17	1.64	0.90	244	36.38	116. 7
	33	3.15	1.75	127	75.87	60.0
	70	6.77	3.70	59	150.46	31.1

7.2.5. Statistical Analysis

All the experimental data was analyzed statistically by Student's t-test (Microsoft Excel, USA) for determination of significancy of property change during UV treatment.

7.3. Results and Discussion

7.3.1. Inactivation of *S.cerevisiae* in Pasteurized Clear Grape Juice (PCGJ)

Continuous flow UV treatment was performed for inactivation of *S.cerevisiae* in PCGJ, at flow rates of 0.90, 1.75 and 3.70 mL/s. The logarithmic inactivation curves were drawn by plotting log (N/N_0) versus UV exposure time (min) at the end of each cycle (Figure 7.1). For PCGJ samples, microbial reduction was decreased from 6.498 to 4.209 Log CFU/mL when the flow rate increased from 0.90 to 3.70 mL/s. It was seen that 0.3 Log CFU inactivation was observed per cycle for yeast at minimum flow rate. At medium and maximum flow rates, 0.2 Log CFU inactivation was obtained per each cycle. At maximum flow rate (3.70 mL/s), inactivation rate slowed down from cycle 2 to cycle 5 (Table 7.2). Applied UV dose, calculated by Eqn. 7.7 was between 0-116.7 J/mL for both grape juice samples. *S.cerevisiae* was completely inactivated at 0.90 and 1.75 mL/s of flow

rates. The highest level of inactivation might be related with low absorbance coefficient (3.895±0.006 cm^{-1}) and high residence time provided at the lowest flow rate (Table 7.2).

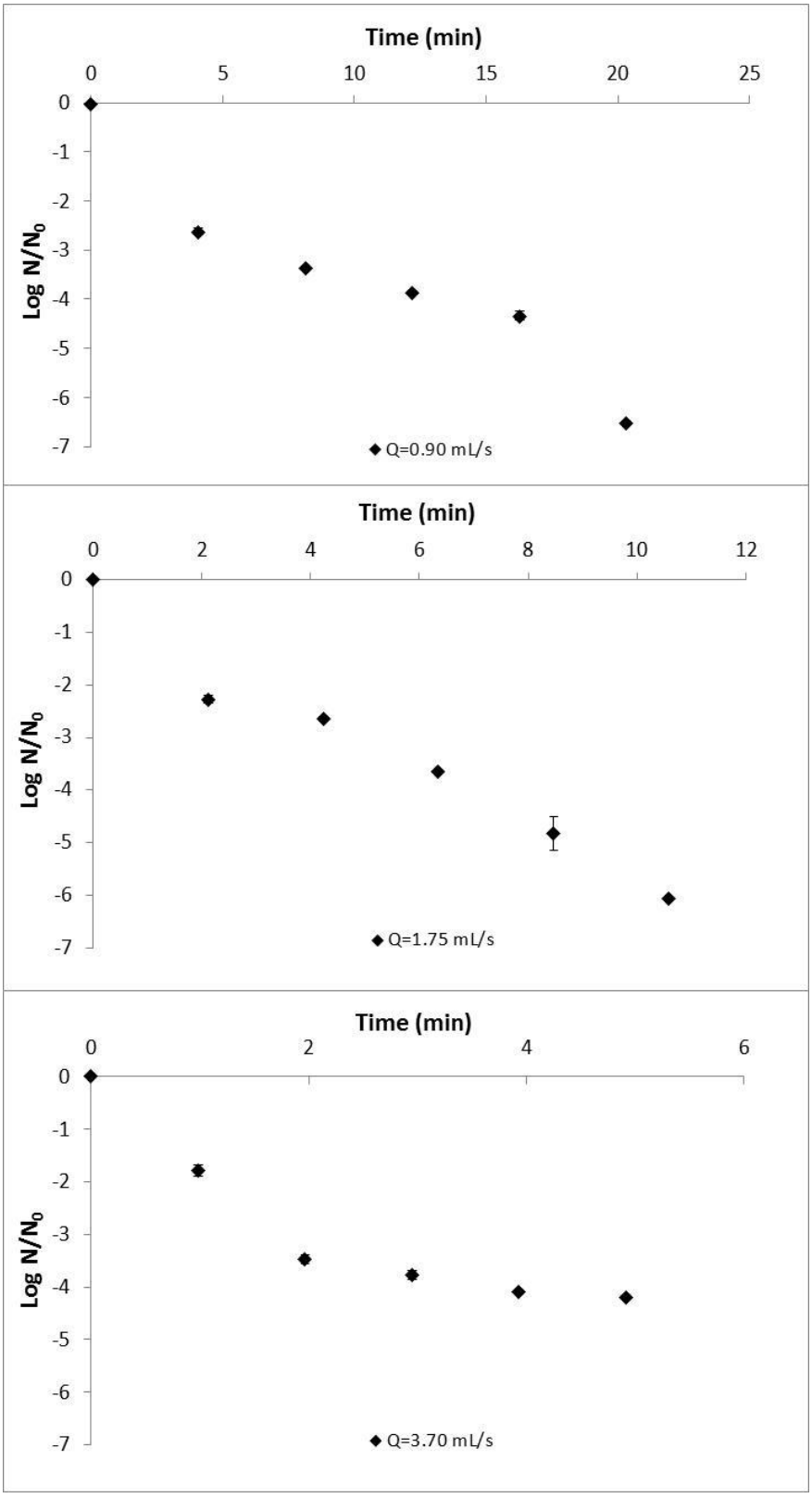

Figure 7.1. UV inactivation of *S.cerevisiae* (Y-139) strain in PCGJ

Table 7.2. Average Logarithmic Reduction Levels of Yeast and Lactic Acid Bacteria in FSOGJ and *S.cerevisiae* in PCGJ after UV Inactivation

	FSOGJ						**PCGJ**		
	Yeast			Lactic Acid Bacteria			*S.cerevisiae*		
Flow Rate / **Cycles**	0.90 mL/s	1.75 mL/s	3.70 mL/s	0.90 mL/s	1.75 mL/s	3.70 mL/s	0.90 mL/s	1.75 mL/s	3.70 mL/s
C_{1in}	0	0	0	0	0	0	0	0	0
C_{1out}	0.338±0.095	0.418±0.148	0.762±0.714	2.557±0.579	2.197±0.586	0.708±0.177	2.619±0.066	2.281±0.078	1.790±0.109
C_{2out}	0.626±0.139	0.600±0.181	0.913±0.764	3.043±0.625	2.387±0.397	1.362±0.225	3.352±0.027	2.650±0.039	3.469±0.083
C_{3out}	0.984±0.121	0.803±0.087	1.189±0.741	3.611±0.648	3.366±0.518	1.650±0.140	3.845±.0.180	3.659±0.016	3.779±0.090
C_{4out}	1.367±0.303	1.080±0.154	1.446±0.701	3.957±0.679	3.696±0.430	1.843±0.195	4.326±0.092	4.818±0.321	4.091±0.047
C_{5out}	1.604±0.321	1.313±0.245	1.643±0.667	4.133±0.679	3.966±0.497	2.335±0.034	6.498±0.010	6.057±0.016	4.209±0.024

Additionally, microorganisms might be in good contact with UV light in PCGJ samples which does not haveany suspended particles (i.e., solid particles, inactivated microorganisms or precipitates). UV dose estimated by Hom model was 1001.618 mJ/cm^2, which was necessary to achieve 6.498 Log CFU/mL reduction of *S.cerevisiae* suspended in PCGJ.

7.3.2. Inactivation of Spoilage Microorganisms in Freshly Squeezed Opaque Grape Juice (FSOGJ)

The number of spoilage yeast was reduced by only 1.604, 1.313 and 1.643 Log CFU/mL in fermented FSOGJ when the same flow rates (0.90, 1.75 and 3.70 mL/s) were applied. On the other hand, higher number of lactic acid bacteria was inactivated under the same conditions (4.133, 3.966 and 2.335 log CFU/mL). Inefficient reduction of yeast can be explained with the higher absorbance coefficient (23.847±0.248 cm^{-1}) and turbidity (131.500±7.778 NTU) of FSOGJ. 247.302 mJ/cm^2 of UV dose (from Hom model) was needed to reduce 1.604 logarithmic unit of yeast per ml. Besides, UV dose which was required to inactivate 4.133 logarithmic unit of lactic acid bacteria per ml was found as 301.113 mJ/cm^2. UV light penetration in FSOGJ might be poor due to suspended particles causing scattering of UV light during treatment. Char et al, (2010) studied single and combined treatment effect of *E.coli* and *S.cerevisiae* by ultrasound and UV-C disinfection in apple and pulp orange juice. As a result of suspended particles and colored compounds, UV-C disinfection was found to be inefficient for orange juice (Char et al, 2010).

It was found that five complete cycle of UV inactivation in continuous flow UV reactor was not enough for complete inactivation of spoilage yeast and lactic acid bacteria for FSOGJ. It was found that the maximum inactivation was 1.643±0.667 Log CFU/ml for yeast. Besides, 4.133±0.679 Log CFU/ml inactivation rate was achieved for lactic acid bacteria at minimum flow rate (0.90 mL/s) (Figure 7.2 and Table 7.2).

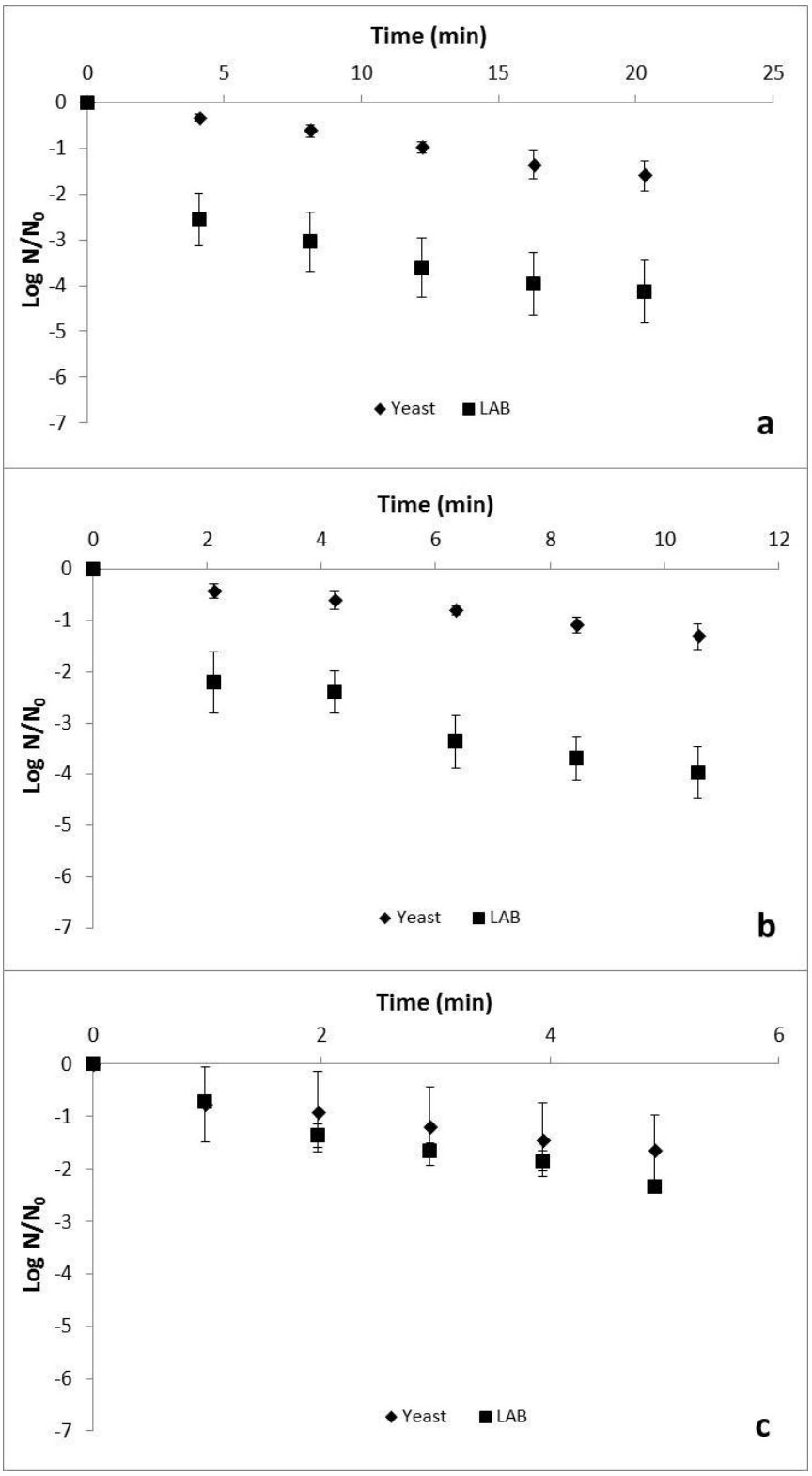

Figure 7.2. UV inactivation of yeast and lactic acid bacteria in FSOGJ; (a) Q=0.90 mL/s (b) Q=1.75 mL/s (c) Q=3.70 mL/s

Additionally, the background flora might be another reason. Because lactic acid bacteria found in fermented juice also compete with yeast found in the background flora to get enough UV-C light. Since lactic acid bacteria is much smaller than yeast cells and have different DNA material, they have a higher chance than yeast to be inactivated when exposed to UV-C irradiation. Another reason might be due the fact that natural spoilage flora is more resistant to UV-C irradiation than inoculated microorganisms. Besides, the shadowing effect caused by aggregation of microorganisms or suspended particles and large size of yeast resulting an increase in absorption coefficient of juice product were also other factors affecting the efficiency of UV irradiation. (Koutchma and Parisi, 2004; Linden and Darby, 1998; Otezia et al, 2009; Tran and Farid, 2004). Consequently, it was suggested to increase the cycling number to reach 5 logarithmic unit inactivation. Eight cycles (41 min of UV exposure time) were applied on fermented FSOGJ at 0.90 mL/s. Cycle number was limited to eight in order to prevent negative effect of the high UV dose on physicochemical and optical quality parameters of FSOGJ. Figure 7.3 represents the inactivation rate of spoilage microorganisms after UV inactivation of FSOGJ after 8 cycle. Maximum 2.194±0.135 Log CFU/ml of inactivation was obtained for spoilage yeast after 8 cycles of operation. But the number of lactic acid bacteria was reduced by 3.564±0.049 Log CFU/ml which was lower than the inactivation rate obtained after application of 5 cycles. The main reason of obtaining different logarithmic reduction levels for LAB in the application of different cycles might be explained by the differences between absorption coefficients and solid contents of FSOGJ samples used in these experiments. The sample irradiated by 8 cycles of operation had more suspended solids and turbid structure than that of irradiated by 5 cycles of UV treatment. By applying Hom model to UV dose response curve and inactivation data, it was concluded that 247.3 mJ/cm^2 UV dose was needed in order to achieve 1.604±0.327 Log CFU/ml reduction of spoilage yeast suspended in FSOGJ. On the other hand 301.1 mJ/cm^2 was required to obtain 4.133±0.679 Log CFU/ml of lactic acid bacteria reduction suspended in FSOGJ. Approximately 152.62 mJ/cm^2 UV dose (D_{10}) was necessary to inactivate 1 logarithmic unit of spoilage yeast. Also 48.47 mJ/cm^2 UV dose was applied to determine 1 logarithmic unit inactivation of lactic acid bacteria.

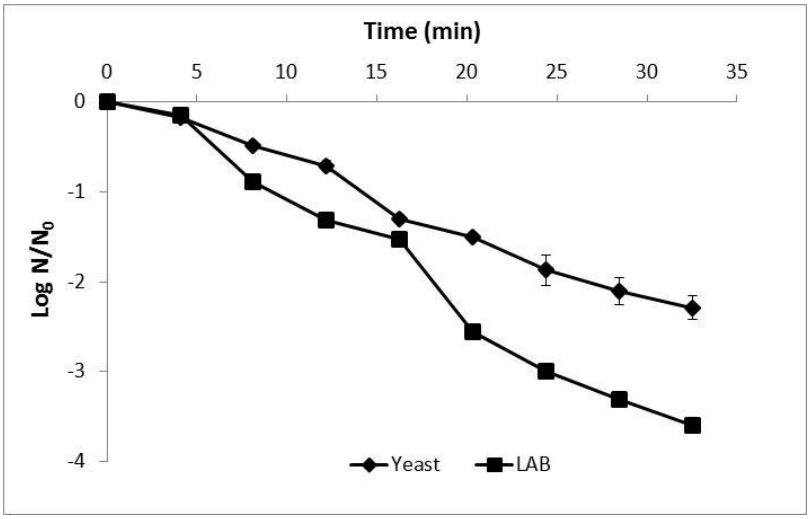

Figure 7.3. Cycle determinaton of continuous flow UV study with FSOGJ to reach 5-Log CFU/ml reduction

7.3.3. Inactivation of *E.coli* K-12 in Freshly Squeezed Opaque (FSOGJ) and Pasteurized Clear Grape Juice (PCGJ)

After application of 8 cycles (41 min of operation time) in the continuous flow UV reactor, 5.341±0.016 Log CFU/ml reduction was achieved for *E.coli* K-12 (ATCC 25253) suspended in FSOGJ. Nonetheless, 5.986±0.077 Log CFU/ml of reduction was observed in PCGJ (Figure 7.4). Murakami et al, (2004) found that decrease in UV inactivation efficiency of *E-coli* K-12 was seen, when suspended particles increased in fruit juices, such as turbid apple juice. This was due to lack of penetration of UV light reaching to target microorganism. Moreover, Koutchma et al, (2004) treated apple juice to inactivate *E.coli* K-12 as target microorganism by continuous flow UV reactor and applying 14.5 mJ/cm^2 of UV dose. They used turbulent flow regime and reached 3-4 Log CFU/ml of inactivation. Besides, Koutchma et al, (2004) also inactivated *E.coli* K-12 in high turbid apple juice by UV treatment and obtained < 1 Log CFU/ml of reduction at 21.5 mJ/cm^2 of UV dose. Due to different physical and chemical properties of the turbid and clear apple juices, they observed that absorbance coefficient of juice products was directly affected inactivation efficiency of *E.coli* K-12. Similarly, Geveke, (2008) applied UV irradiation in liquid egg white in order to inactivate *E.coli* K-12. Due to high absorptive property of liquid egg white, the author applied 44 J/ml of UV dose to reduce the number of *E.coli* K-12 by 4.3 CFU/mL.

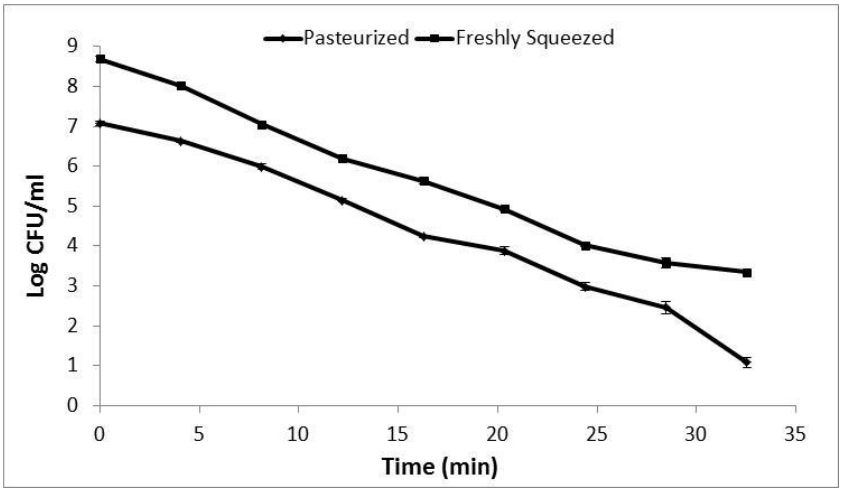

Figure 7.4. Logarithmic reduction of *E.coli* K-12 (ATCC 25253) in grape juices after continuous flow UV irradiation

UV dose was determined by using both biodosimetric method and equation 7.7., as given in Table 7.3 and 7.4. As a result of Weibull model for inactivation kinetics, 273.520 mJ/cm^2 was necessary to have 5.341 logarithmic reduction of *E.coli* K-12 per ml in FSOGJ. Nonetheless 577.245 mJ/cm^2 was needed to inactivate 5.986±0.077 Log CFU/ml of *E.coli* K-12 per ml in PCGJ (Table 7.4.)

Table 7.3. Estimation of Dose Delivery in Terms of Hom Model

Type of Grape Juice	**M.orgn**	**k'**	**h**	**log (N/N_0)**	**UV Dose (mJ/cm^2)**	**UV Dose (J/ml)**
FSOGJ	Yeast	0.156	0.934	-1.604	**247.302**	116.7
	LAB	0.311	0.961	-4.133	**301.113**	116.7
PCGJ	*S.cerevisiae*	0.300	0.952	-6,498	**1001.618**	116.7

Table 7.4. Estimation of Dose Delivery in Terms of Weibull Model

Type of Grape Juice	**M.orgn**	**α**	**β**	**log (N/N_0)**	**UV Dose (mJ/cm^2)**	**UV Dose (J/ml)**
FSOGJ	*E.coli* K-12	1.045	0.990	-5.431	**273.520**	116.7
PCGJ	*E.coli* K-12	1.005	0.981	-5,986	**577.245**	116.7

In summary, yeasts were more resistant than bacteria in FSOGJ. Tran and Farid (2004) studied the effect of UV-C treatment of bacteria, yeast and mold populations in orange juice. They explained the difference between inactivation data of bacteria and yeast in a similar manner. Yeast have larger surface area than bacteria, that causes inefficient UV penetration throughout yeast cell. On the other hand, genetic information of eucaryotic yeast is enclosed into cytoblast, and cytoblast is covered with its own

membrane in addition to cell wall. Nonetheless genetic material disperses in cytoplasm of bacterial cell and covered only by cell wall. Effect of UV light on bacterial cell is higher since UV light only penetrates through the cell wall to damage DNA. But in contrast UV light is needed to be penetrated through the cell wall of yeast and wall of cytoblast. Consequently, yeast are more resistant to UV treatment compared to bacteria (Tran and Farid, 2002, 2004). Palgan et al, (2011) inactivated *E.coli* bacteria and *P. fermentans* yeast using non-thermal technologies i.e., high intensity light pulses, ultraviolet light, pulsed electric fields and ultrasound in single or combined manner for a fresh blend of apple and cranberry juice. They also showed the same trend and determined lower inactivation rate for yeast than that of *E.coli* (~ 6 Log CFU/mL).

The flow rate is also an important factor influencing the efficiency of continuous flow UV-C treatment. Koutchma et al, (2004) applied UV light to apple cider to inactivate *E.coli* K-12 using laminar flow and turbulent flow UV reactor systems. The authors stated that UV dose ranges between 90 and 150 mJ/cm^2 rate was necessary for a decimal reduction in turbulent UV reactor system at flow rate of 1250 mL/s. Nonetheless, UV dose in the range of 18.8-25.1 mJ/cm^2 was required in the thin film laminar UV reactor for one decimal reduction at a flow rate of 56.8 mL/s. The authors determined that turbulent flow was not appropriate for high turbid fruit juices such as apple cider. Also Geveke and Torres, (2012) studied UV inactivation of *E.coli* K-12 in grapefruit juice by centrifugal continuous flow UV reactor. They applied 0-24 mJ/cm^2 of UV dose and obtained >5.0 Log CFU/ml of inactivation. High inactivation rate with low UV dose level was due to perfect mixing and good penetration of UV light produced in the thin film generated by centrifugation.

7.3.4. The Effects of UV Irradiation on Physical and Optical Properties

Physical and optical properties including absorbance coefficient, pH, color and turbidity of grape juice samples were measured before and after UV treatment and summarized in Table 7.5. pH, brightness (L*), total soluble content (Brix %) of PCGJ and FSOGJ did not change significantly by the effect of UV treatment ($p<0.05$). The main reason of low pH for commercial PCGJ (2.90±0.01) was due to addition of citric acid during processing juice to maintain microbial stability. Clarification process was applied on FSOGJ after pressing. FSOGJ was kept at refrigeration temperature (6°C) for

detartarization. As a result, tartaric acid and tartarate compounds such as potassium hydrogen tartartares could be removed. This was resulted in lower titratable acidity level in FSOGJ than that of PCGJ.

On the other hand, change in absorbance coefficient level of PCGJ was significant. Absorbance coefficients of untreated PCGJ was 3.895±0.006 cm^{-1} and reduced to 3.292±0.097 cm^{-1} after UV treatment. Decrease in absorbance coefficient might be due to degradation of vitamin C (ascorbic acid) by UV irradiation (Koutchma, et al, 2009). Tran and Farid (2004) found 17% loss of vitamin C in orange juice at 100 mJ/cm^2 of UV exposure. The decrease in titratable acidity of juice samples might be also explained by reduction in the amount of ascorbic acid by UV light and volatile acids by the effect of temperature increase during UV irradiation. Yellowness (a*) and redness (b*) of grape juice samples also affected by UV treatment. Higher yellowness of fresh squeezed opaque grape juice might be due to the presence of caretonoid. PCGJ had less carotenoid pigment due to degradation occured during thermal pasteurization (Fratianni et al, 2010). Another reason to have more yellowness could be due to the suspended particles and skin residuals found in FSOGJ. Redness (a*) was higher in the PCGJ than that of FSOGJ. High redness level might be due to non-enzymatic browning of the FSOGJ by the presence of melanoidin (Ibarz et al, 2005). Enzymatic activity in the FSOGJ samples could not be stopped during detartarizaton step and enzymatic browning occured in the absence of thermal inactivation. Color pigments of juice might be also affected by non-enzymatic browning (Maillard reaction) occured during UV treatment (Chia et al, 2012; Ibarz et al, 2005; Klim and Nagy, 1988; Moyer and Aitken, 1980). Also turbidity levels of irradiated juice variety were much higher than untreated samples. High inoculation rate of yeast, LAB or *S.cerevisiae* of juice samples before UV treatment might be another reason resulted in an increase in turbidity of juice products (Otezia et al, 2009; Tran and Farid, 2002, 2004).

Table 7.5. Physical and Optical Properties of Grape Juices after Continuous Flow UV Treatment

	PCGJ		FSOGJ	
	Untreated	**UV Treated**	**Untreated**	**UV Treated**
pH	2.905±0.007	2.900±0.000	3.945±0.007	3.915±0.007
Turbidity (NTU)	0.567±0.011	12.175±0.176*	38.575±3.358	131.500±7.778*
Absorbance coefficient(cm^{-1})	3.895±0.006	3.292±0.097*	23.847±0.248	23.921±0.360
L*	28.795±0.049	29.073±0.038	28.807±0.230	28.550±0.001
a*	0.045±0.007	-0.105±0.002*	-0.273±0.033	-0.312±0.012
b*	3.395±0.026	3.062±0.021*	2.567±0.009	1.910±0.023*
ΔE	28.994±0.052	29.234±0.035*	28.922±0.231	28.615±0.001
BI	59.660±0.028	59.118±0.031*	58.448±0.036	57.696±0.016*
Brix (%)	16.905±0.007	16.935±0.007	18.420±0.014	18.258±0.007
Ascorbic Acid (g/L of juice)	0.008±0.0003	0.008±0.000	0.309±0.001	0.291±0.001*
Titratable Acid (%)	5.561±0.000	5.685±0.035*	2.483±0.070	2.706±0.035

*Significant (p-value<0.05)

7.4. Conclusions

Inactivation efficiency of UV-C irradiation treatment in PCGJ was better than FSOGJ. Maximum inactivation of *S.cerevisiae* (6.498±0.010 Log CFU/ml) was obtained at minimum (0.90 mL/s) flow rate in PCGJ. This was due to the low absorption coefficient of PCGJ that was related with low turbid structure allowing high penetration and effective contact of microorganisms with UV light. Moreover, the high turbid structure of FSOGJ caused by presence of suspended particles was resulted in a shadowing effect preventing UV light penetration through microorganisms. High residence time (at 0.90 ml/s) was resulted in a great microbial reduction in FSOGJ (4.133±0.679 Log CFU/ml for lactic acid bacteria and 1.604±0.321 Log CFU/ml for yeast). It was concluded that significant changes in optical properties was observed for both types of juice before and after UV inactivation. Also no changes in pH and Brix was observed after UV treatment of juice products.

E.coli K-12 (ATCC 25253) was completely inactivated in UV treated FSOGJ and PCGJ by continuous flow UV reactor. The population of *E.coli* K-12 (ATCC 25253) in FSOGJ was reduced after 41 min of exposure by 5.341±0.016 Log CFU/ml. Besides, 5.986±0.077 Log CFU/ml of inactivation was achieved for *E coli* K-12 suspended in PCGJ irradiated at flow rate of 0.90 mL/s. These inactivation levels were

higher than that of spoilage microorganisms (yeast and lactic acid bacteria). Because, the sensitivity of surrogate pathogenic microorganisms (*E.coli* K-12) was very high for UV irradiation.

UV dose delivered in continuous flow UV reactor was determined using both UV dose response curve of yeast and lactic acid bacteria obtained by biodosimetric method (Chapter 3) and estimated from power of the lamp and flow rate (Eqn. 7.7). By applying Hom and Weibull models to inactivation data, it was concluded that 247.3 mJ/cm^2 UV dose was needed in order to achieve 1.604±0.321 Log CFU/ml reduction of spoilage yeast suspended in FSOGJ. On the other hand 301.1 mJ/cm^2 was required to obtain 4.133±0.679 Log CFU/ml of lactic acid bacteria reduction suspended in FSOGJ. Approximately 152.62 mJ/cm^2 UV dose (D_{10}) was necessary to inactivate 1 logarithmic unit of spoilage yeast. Also 48.47 mJ/cm^2 UV dose was applied to determine 1 logarithmic unit inactivation of lactic acid bacteria. 577.245 mJ/cm^2 UV dose was required to inactivate 5.431 Log CFU/ml of *E.coli* K-12 in FSOGJ. Additionally, 1001.6 mJ/cm^2 and 273.5 mJ/cm^2 of UV dose were necessary to inactivate 6.498 Log CFU of *S.cerevisiae* and 5.986 Log CFU of *E.coli* K-12 in PCGJ.

CHAPTER 8

MICROBIAL SHELF LIFE OF UV TREATED GRAPE JUICE

8.1. Introduction

Freshly squeezed fruit juices have shelf-life of maximum 5-6 days. They are usually packed and delivered to retailers within 24 hours. The shelf life of fruit juice depends on a variety of factors such as the type of product, the ingredients (water, sugar content), acidity (ascorbic acid content), storage period and storage temperature**.** Freshly squeezed juice has a shorter shelf life than pasteurized juice and must be kept chilled. Commercially, fruit juice products are pasteurized by thermal treatment based on high temperature-low time treatment method to increase the storage time in appropriate conditions (Mansfield, 1962). But in contrast the deterioration of many quality and nutritional attributes e.g., change of color and loss of essential aroma and vitamin content were reported during thermal pasteurization of fruit juice (Brown 2001; Mazotta, 2001; Choi and Nielsen, 2005; Shewfelt 1986).

Consumption of minimally processed, high quality fruit juices have been increased recently. But in contrast, product safety is difficult to be maintained in these products without using conventional thermal preservation methods like pasteurization or sterilization (Heinz et al, 2003; Mertens and Knorr, 1992). Non-thermal preservation methods such as PEF, HHP, ultrasound and UV-C light have been shown to be potential applications for minimally processed juice in keeping their microbial, physicochemical and sensorial quality during storage in addition to reduction of operational energy costs (Daoudi et al, 2002; Heinz et al, 2003; Pala and Toklucu, 2013; Patil et al, 2009; Tikekar et al, 2011; Tiwari et al, 2010; Toepfl et al, 2007).

There are several avantages of application of non-thermal UV-C radiation as a pasteurization process of fruit juices. None of the study was reported for production of toxic or significant nontoxic byproducts during UV-C treatment. Also no taste or odor change produced by UV-C inactivation was reported (Keyser et al, 2008; Pala and Toklucu, 2011, 2013a, 2013b; Tran and Farid 2004) Besides, germicidal effect of UV-C

light (200-280 nm range) on spoilage microorganisms including yeasts, moulds and LAB in fruit juices were cited in many studies (Caminiti et al, 2012; Franz et al, 2009; Fredericks et al, 2011; Guerrero-Beltrán et al, 2009; Keyser et al, 2008; Noci et al, 2008; Pala and Toklucu, 2011; Tran and Farid 2004). According to study conducted by Tran and Farid (2004), fruit juices can not be consumed when the numbers of spoilage yeast and total aerobic count are above 1000 CFU/ml and 5000 CFU/ml, respectively (Tran and Farid, 2004).

The objective of this study was to follow the microbial stability of UV treated FSOGJ during storage period at refrigerated temperature (4 ºC). Additionally, the changes in quality parameters of grape juice (such as absorbance coefficient, turbidity, color, brix (%), pH, vitamin C content and total titratable acidity) were determined during storage.

8.2. Experimental Study

8.2.1. Materials

FSOGJ was used as a treatment medium. Physical and chemical changes in UV-C treated juice and microbial stability i.e., yeast and LAB growth in UV treated grape juice were examined throughout the storage period. Since the total aerobic count and LAB count were shown to be very similar in our previous studies, only LAB was determined in this study. This was also supported by the microscopical examination of the samples.

8.2.2. Methods

8.2.2.1. Preparation of Sample

10 kg of Sultana variety of white grapes (*V.vinifera*) were purchased to produce freshly squeezed opaque white grape juice. Before squeezing, the grapes were washed to eliminate mold from the surface. A household table top fruit juice extractor (Moulinex, France) was used to mash the grapes. White grapes were pressed and the

juice was strained twice by a cheese cloth. By this way, most of the cloud structure and solid particles were eliminated. Besides, 600 mg/kg L-ascorbic acid (Merck, Germany) was added as an antioxidant agent to maintain the original color of juice during preperation step. Bitartrate particles formed in white grape juice were precipitated by shaking at 100 RPM and 4°C for 2-3 hours in the shaker (Thermo Electron Corp., Ohio, United States). Following the straining and removal of the bitartrates, approximately 6 lt of juice samples were stored in 12 of 500 ml sterile plastic bottles at -18 ºC until used.

8.2.2.2. Continuous Flow UV Irradiation of FSOGJ

The residence time of grape juice in UV tube was determined at the minimum flow rate (0.90 mL/s) in order to achieve the best microbial inactivation. The operational parameters are depicted in Table 8.1.

Table 8.1. Flow Parameters of PCGJ and FSOGJ on UV Inactivation Procedure for Shelf Life Study

Power of Pump (RPM)	Velocity (mm/s)	Volumetric Flow Rate (ml/s)	# of cycle	Total Operation Time	Residence Time/cycle (s)	Re_{inlet}
17	0.16	0.90	8	68 m	244	36.38

The frozen white grape juice in the aseptic plastic bottles was first thawed by keeping at room temperature (25ºC) for over night and stored at refrigeration temperature (4-6ºC) to remove the suspended particles (potassium bitartrate or potassium hydrogen tartrate) by sedimentation. Before UV inactivation experiment, the clear part of the FSOGJ was drawn, aseptically by a pipette without disturbing the sediment. Then 500 ml of grape juice was UV treated by applying 8 cycles. Microbial growth was followed during storage. For yeasts and LAB, Potato Dextrose Agar (PDA, Difco Corp, United States) acidified with 10% tartaric acid and De Man Rogosa-Sharp Agar (MRS, Merck, Germany) were used. Yeasts were incubated at 25 ºC for 2 days. Incubation for LAB was carried out at 30 ºC for 2 days. Untreated FSOGJ was used as a control. All UV treated and untreated grape juice samples were stored using aseptic bottles at 4 °C in refrigerator.

8.2.2.3. Physical and Optical Measurements

Physical and optical properties including pH, soluble sugar (%Brix), ascorbic acid, total titratable acidity, absorbance coefficient, turbidity and color were carried out according to the procedures outlined in chapter 7, section 7.2.1.2. All the experimental data were analyzed statistically by Student's t-test (Microsoft Excel, Microsoft Inc, USA) for determination of significancy of property change during storage.

8.3. Results and Discussion

Total 8 cycles of continuous flow UV treatment was performed to extend the shelf life of FSOGJ. For this aim, treated and untreated samples were analyzed microbiologically, optically, physically and chemically during storage period. All the experiments were carried out in two replicates. It was found that the sensorial properties of the fruit juice were acceptable by consumers when the total microbial count was less than 5000 CFU/ml (Tran and Farid, 2004). Hence, analysis were stopped after 14 days, since fermentation was observed after this point. The growth curve of yeast and LAB in FSOGJ samples during storage is shown in Figure 8.1. In the first 5 days, no yeast or LAB growth was observed. The yeast population increased up to 1.900±0.077 Log CFU/ml in UV treated samples at 7^{th} day of storage. Meanwhile, yeast level in untreated sample was determined as 3.058±0.023 Log CFU/ml at the 7^{th} day of storage. At the end of 14^{th} days of storage, the level of yeast was determined as 4.360±0.049, whereas LAB increased to 3.062±0.085 Log CFU/ml in UV treated samples. UV treatment was able to double the shelf life of FSOGJ.

The effect of UV on optical and physicochemical properties was determined and shown in Table 8.2.

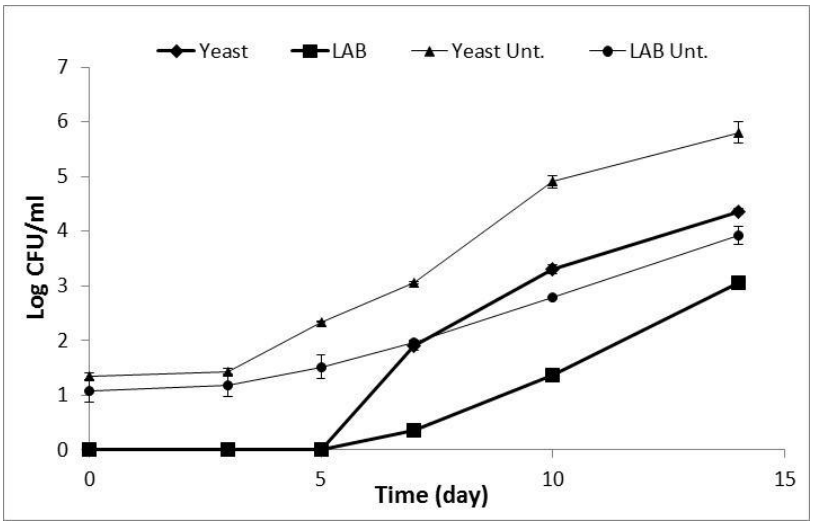

Figure 8.1. Growth of yeast and LAB in UV treated and untreated FSOGJ during storage

Table 8.2. Overall Physicochemical and Optical Properties of FSOGJ before and after UV Treatment during Storage

	Day 0		**Day 3**		**Day 5**	
	Untreated	**Treated**	**Untreated**	**Treated**	**Untreated**	**Treated**
pH	3.955±0.01	3.94±0.00	3.94±0.01	3.93±0.00	3.88±0.014	3.91±0.014
Turbidity (NTU)	98.22±3.00	118.75±2.47*	110.75±3.89	165.25±1.77*	115.75±1.77	181.25±3.18*
Abs Coeff. (cm^{-1})	12.13±1.78	7.69±0.16*	10.55±0.14	8.11±0.43*	9.02±0.86	8.36±0.19
L*	27.74±0.08	26.48±0.15*	25.91±0.05	26.26±0.29	26.63±0.10	26.07±0.12*
a*	0.05±0.02	0.40±0.016*	1.58±0.03	0.77±0.02*	1.75±0.01	1.16±0.04*
b*	2.98±0.03	4.60±0.05*	4.23±0.03	4.76±0.06*	5.81±0.32	6.50±0.021
Brix (%)	18.57±0.13	18.23±0.02	17.88±0.11	18.20±0.014	17.86±0.03	17.87±0.014*
Ascorbic Acid (g/L of juice)	0.56±0.03	0.01±0.006*	0.036±0.002	0.027±0.007*	0.015±0.006	0.016±0.003*
Titratable Acid (%)	2.08±0.07	2.16±0.03	2.53±0.07	2.34±0.03	2.75±0.03	2.48±0.07*
	Day 7		**Day 10**		**Day 14**	
	Untreated	**Treated**	**Untreated**	**Treated**	**Untreated**	**Treated**
pH	3.79±0.007	3.88±0.02*	3.73±0.014	3.85±0.014*	3.64±0.02	3.78±0.01*
Turbidity (NTU)	122.25±3.18	196.50±5.66*	136.75±6.01	310.50±10.61*	228.75±3.89	348.75±13.79*
Absorbance Coefficient (cm^{-1})	8.89±0.21	8.81±0.01	8.87±0.60	10.10±0.65	9.58±0.08	12.95±3.58
L*	26.31±0.05	25.96±0.29	25.50±0.20	24.98±0.11	24,51±0.06	25,54±0.15*
a*	1.90±0.03	1.21±0.02*	2.05±0.050	1.27±0.002*	2.34±0.05	1.85±0.06*
b*	6.41±019	6.40±0.03	6.55±0.02	6.53±0.005	6.84±0.07	6.58±0.02*
Brix (%)	17.76±0.03	17.69±0.05*	17.45±0.08*	17.56±0.02	16.79±0.03	17.08±0.06*
Ascorbic Acid (g/L of juice)	0.004±0.002	0.002±0.001*	0.002±0.0005	0.001±0.0005*	0.000	0.000*
Titratable Acid (%)	2.90±0.03	2.68±0.07	3.57±0.21	3.00±0.10	9.06±0.53	5,36±0.28*

*Significant change ($p<0.05$)

Besides the increase in the number of microorganisms, pH decreased both in the treated and untreated grape juice samples throughout 14 days. This was due to the increase of acidity as a result of metabolic activity of microorganisms (Figure 8.2 and Table 8.2). pH of treated grape juice samples decreased from 3.940 to 3.790 after 14 days. pH of the untreated grape juice samples decreased from 3.955 to 3.645 due to increase in microbial population. Unlikely, Donahue et al, (2004) inactivated *E.coli* O157:H7 strain in apple cider by UV light and no significant change was found on pH of apple ciders during storage. The change in pH of grape juice (treated and untreated) was significant throughout storage period in this study ($p<0.05$). But the change of pH in untreated juice samples was more pronounced in comparison to irradiated samples.

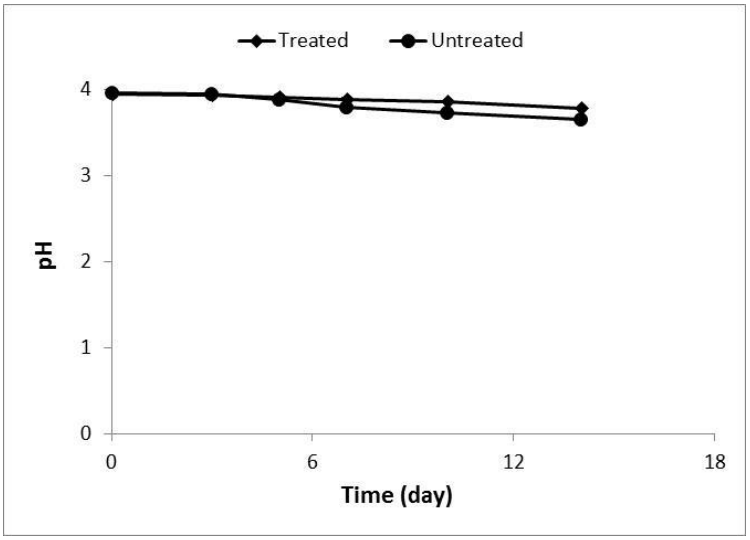

Figure 8.2. Change in pH for UV treated and untreated FSOGJ

Change in turbidity and absorbance coefficient levels were directly related with the quality properties of grape juice. Change in color of grape juice when exposed to UV light caused a decrease in absorbance coefficient of the sample (Table 8.2). At the end of 14 days, it was observed that turbidity level of treated samples increased from 118.75±2.47 NTU to 348.75±13.79 NTU. The level of turbidity was increased gradually after UV treatment. At the end of 14^{th} day of storage, turbidity of untreated samples were measured as 228.75±3.89 NTU increased from initial level of 98.22±3.00 NTU. (Figure 8.3a). Cloud structure was observed upon microbial increase. Tandon et al, (2003) determined significant changes in turbidity of UV-irradiated (14 mJ/cm^2 at 254 nm) apple cider during storage. It was expected that the untreated and UV-treated samples showed an increase in turbidity during storage time due to increase in the

number of spoilage yeast and bacteria producing visible sediment and cloud in juice products (DiGiacomo and Gallagher, 1959; Tandon et al, 2003; Chia et al, 2012).

At the end of 14th day, the absorbance coefficient of untreated grape juice decreased from 12.13±1.78 to 9.58±0.08 cm^{-1} and leveled off around 9.58±0.08 cm^{-1}. For UV treated samples, the absorbance coefficient was increased from 7.69±0.16 cm^{-1} to 12.95±3.58 cm^{-1}. This was probably due to the degradation of color compounds by UV treatment causing an increase in the turbid structure.

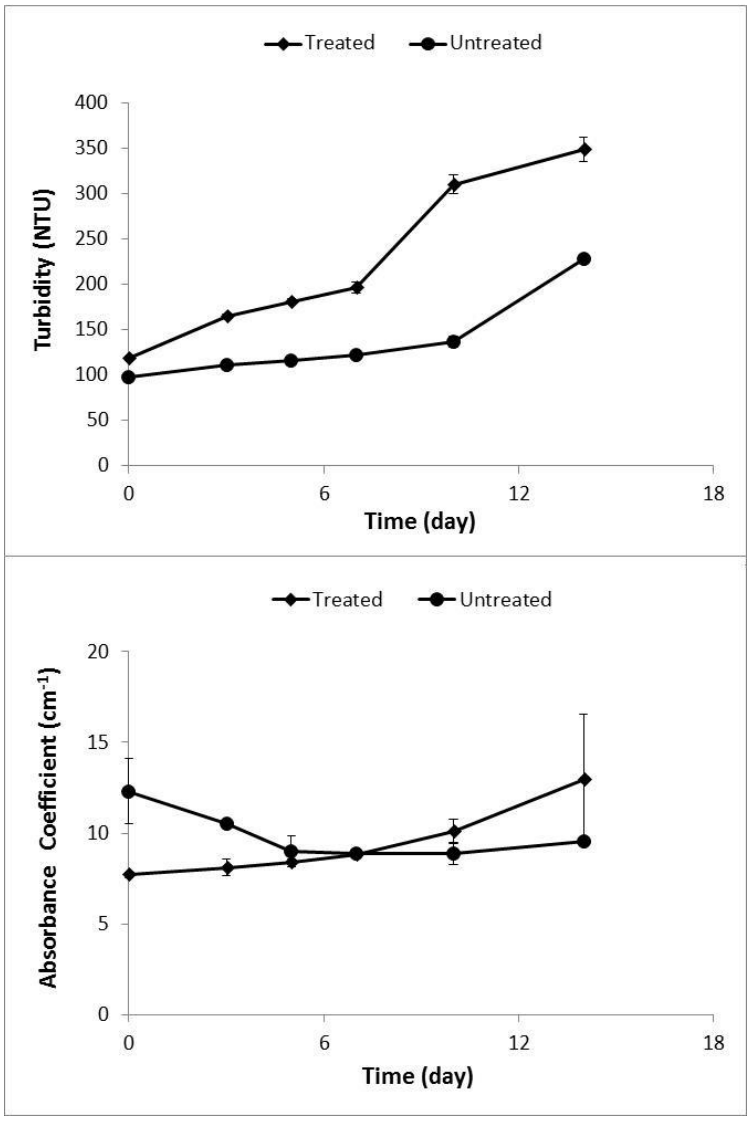

Figure 8.3. Change in; (a) Turbidity (b) Absorbance coefficient of UV treated and untreated FSOGJ

Ibarz and Pérez-Teijón (1990) applied sunlight exposure to clarified apple juice to study the changes in absorbance. The findings revealed that there was a decrease in

the absorbance at 420 nm due to degradation of the juice pigments. It was also stated that the significant change in turbidity was due to the effect of storage time and presence or absence of UV irradiation process during storage. Unlikely, it was not observed any change by the effect of exposure time or UV treatment. ($P>0.05$). The interaction between these two factors directly affected the absorbance coefficient of FSOGJ. On the other hand, a high absorption coefficient might be due to presence of the polymeric fruit derivatives, e.g., melanin and melanoidin, providing the brown colour of fruit juice. Absorptivity property of melanoidin pigments during UV inactivation of various enzymes was reported in the literature (Seiji and Iwashita, 1965). The results of the experiments revealed that degradation of melanoidins occured by long exposure of the fruit juice samples to UV light (Kwak et al, 2004).

Color parameters i.e., brightness (L*), redness-greenness (a*) and yellowness-blueness (b*) were measured before and after the UV treatment. L* values of the UV treated samples slightly decreased from 26.48±0.15 to 25.54±0.15 during storage period (Figure 8.4a). Also L* values for untreated samples decreased from 26.48±0.15 to 25.54±0.15 at the end of 14^{th} day of storage. Chia et al, (2012) found that L* was decreased in untreated, UV treated and heat treated pineapple juice during storage. Genovese et al, (1997) reported that the suspended particles were resulted in a partial precipitation in juice and decrease in L* values. Aguilo-Aguayo et al, (2009) showed that the brightness of heat treated strawberry juice was decreased at 4°C of storage.

The color parameters a* and b* are combine for indication of the physical characteristics of the visual colour (Patras et al, 2009). Parameter a* of UV treated samples had a significant increase from 0.40±0.02 to 1.85±0.06 at the end of 14 day storage period (Figure 8.4b). But in contrast, b* of UV treated samples were increased from 4.60±0.07 to 6.58±0.02 (Figure 8.4c). The significant effect of storage in UV treated samples was seen in brightness (L*), yellowness (a*) and redness (b*) of grape juice samples. Color degradation in FSOGJ might have been due to non-enzymatic Maillard browning formed after interaction of soluble sugars, amino acids and organic acids (Chia et al, 2012; Ibarz et al, 2005; Klim and Nagy, 1988; Moyer and Aitken, 1980). Nonetheless, the colour of juice might have been also affected by some of the factors including irradiation energy, heating, air and light etc. which led to degradation of carotenoids by causing oxidation, cis/trans changes and decomposition of epoxide rings during storage (Esteve and Frigola, 2007; Fratianni et al, 2010). Another reason of having more yellowness in treated samples was due to suspended particles and skin

residuals left in the freshly squeezed white grape juice after straining step. Significant effects of storage time and UV irradiation was observed in three of the color parameters. Guerrero-Beltrán et al. (2009) reported that increasing the flow rate inthe treatment of grape juice by UV-C light, and decreasing the contact time between UV-C light and the liquid food preserved the color of juice.

Ibarz et al, (2005) studied the effect of exposure of apple, peach and lemon juices to UV light in 250-650 nm wavelength range onon color parameters. Brightness (L*) increased but a significant decrease occurred in redness-greenness (a*) and yellowness-blueness (b*). This was due to degradation of brown coloration pigments by UV light. Guerrero-Beltrán and Barbosa-Cánovas (2005) observed a significant decrease for a* and b* in apple juice samples after UV irradiation. This finding indicates that there is a photodegradation of apple juice pigments. Besides, clarified apple, peach and lemon juices had significant changes of color parameters as a result of melanins and melanoidin destruction when expose to UV light (Ibarz et al, 2005).

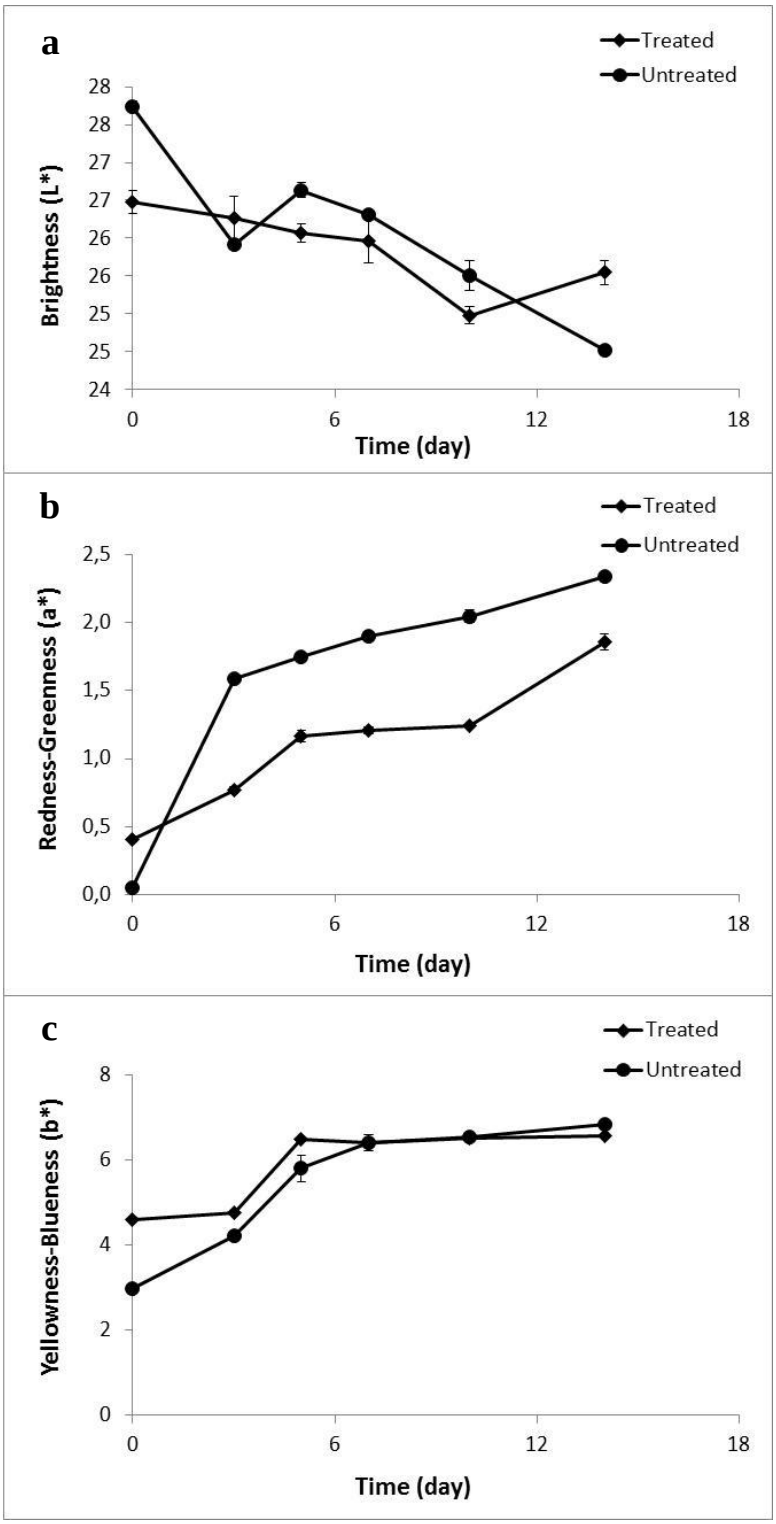

Figure 8.4. Change in; (a) Brightness-L* (b) Redness-greenness-a* and (c) Yellowness-blueness-b* of UV treated and untreated FSOGJ

The changes in total soluble content (% of Brix), titratable acidity and ascorbic acid before and after UV exposure and during storage period were examined. It was noticed that total soluble content decreased in both untreated and UV treated samples.

For UV treated sample, brix % reduced from 18.23±0.02 to 17.08±0.06 (Figure 8.5a). At the end of storage, the brix % of untreated samples was measured as 16.79±0.03 decreased from 18.57±0.13. After 5^{th} day of storage, significant changes in brix levels of both UV treated and untreated samples were observed ($p<0.05$). Chia et al, (2012) reported a decrease in the total soluble solids for untreated and UV treated pineapple juice samples throughout the storage. It was speculated that the change in total soluble solids is the result of the microbial activiy that cause sugar fermentation (Rivas et al, 2006; Rosen and Gothard, 2010; Chia et al, 2012).

Ascorbic acid (Vitamin C) level was also measured in untreated and UV treated samples. 0.56±0.03 g of ascorbic acid/lt of grape juice was found before storage. After 14 days, all vitamin C content was degraded by the effect of UV-C light (Figure 8.5b). Chia et al (2012) also analyzed the ascorbic acid content of untreated and UV treated pineapple juice. Significant decrease was found in ascorbic acid content due to UV-C light. The presence of ascorbic acid is indicated as the quality assurance of the juice product (Plaza et al, 2006). Storage time and UV treatment had significant effect on degradation of ascorbic acid ($p<0.05$). Shaw (1992 a and b) investigated vitamin C content of stored fresh mandarin and orange fruits. At the end of their shelf life, 50% retention of initial ascorbic acid content was reported.

It was supported that the degradation of Vitamin C during storage was due to atmospheric oxygen (Odriozola-Serrano et al, 2008) and other factors such as light exposure, hydrogen peroxides, storage temperature, type of processing and packaging materials, and enzymes (ascorbate oxidase and peroxidase) (Ayhan et al, 2001; Davey et al, 2000). Titratable acidity level was detected as higher (5.36±0.28 %) than that of the initial level (2.16±0.03 %), which supports the decrease in pH level caused by microbial metabolic activity throughout the storage (Figure 8.5c). Titratable acidity level was changed significantly by the effect of storage time ($p<0.05$).

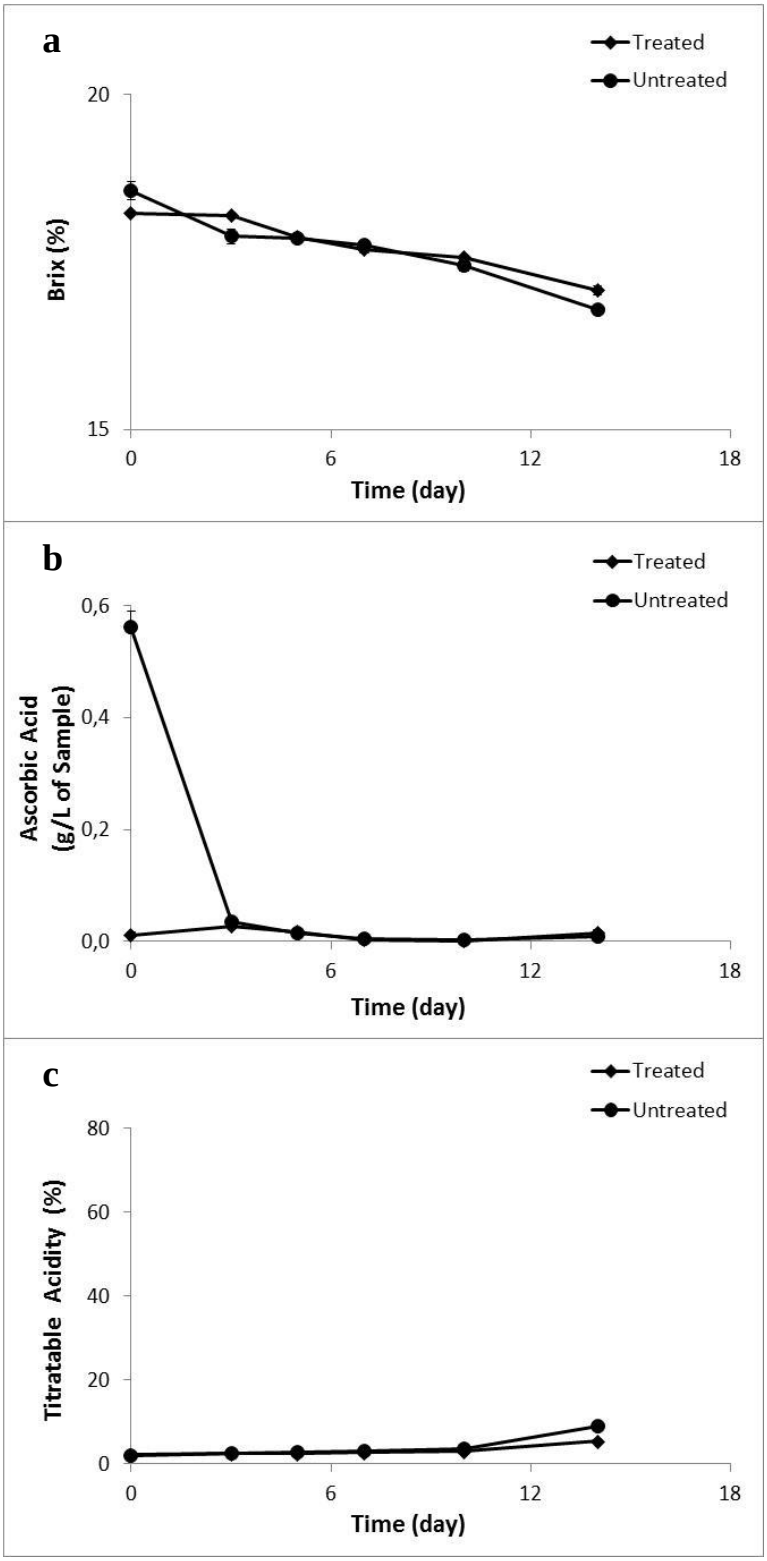

Figure 8.5. Change in; (a) Brix (b) Ascorbic acid and (c) Titratable acidity of UV treated and untreated FSOGJ

8.4. Conclusions

It could be concluded that, the shelf life of grape juice was determined as 14 days for UV-C treated FSOGJ. The number of yeast and LAB in irradiated juice was increased up to 4.360±0.049 and 3.062±0.085 Log CFU/ml in 14 days. Nonetheless, the number of yeast and LAB were reported as 5.804±0.199 and 3.924±0.163 at the end of 7^{th} day of storage for untreated grape juice. In other words, untreated grape juice samples were spoiled at the end of 7^{th} day of storage since total microbial count was above 5000 CFU/ml. As a result of this, it was commented that the shelf life of FSOGJ was doubled. Complete degradation of vitamin C was noticed during storage period. Although, pH, brix and titratable acidity were not affected during UV-C treatment their level changed significantly due to microbial increase and formation of the fermentation byproducts during storage. By the effect of sugar degradation, brix level reduced significantly after 5^{th} day. Color properties and turbidity were affected significantly in UV irradiated juice due to photodegradation of color compounds and reduction in the amount of carotenoid. After 14 days, turbidity was quite higher than initial level since cloud structure was observed based on increase in the number of microorganisms and metabolic by-products.

CHAPTER 9

CONCLUSIONS

The overall accomplishment of this Ph.D. study was to design a UV reactor by means of a computational fluid dynamics (CFD) modelling for opaque liquid foods in which minimum 5 log microbial reduction can be achieved. One of the most important issue in the design of a UV system is the modelling of UV intensity and/or UV dose distribution received by liquid material during UV processing. Generally, average UV dose in an UV reactor is calculated based on the biodosimetric method conducted in a bench top static system. But this method is a very crude method. So, it is fundamental to determine the exact UV dose distribution in the UV reactor system for evaluation of its efficiency. The details regarding the death spots and areas exposed to low UV dose helped to improve the system design. Application of CFD to a UV reactor is necessary to compute the exact UV intensity or UV dose distribution across the UV lamps.

The first objective of this study was to determine UV dose response curves for different target microorganisms (e.g., spoilage microorgansims (yeast and LAB), *S.cerevisiae* and *E.coli* K-12) suspended in the PCGJ and FSOGJ using a bench top collimated beam apparatus and investigate the efficiency of UV-C irradiation as a non-thermal pasteurization process for clear and opaque grape juices. For this purpose samples were UV treated in bench top collimated beam apparatus for 0-40 min. UV dose up to 1588 mJ/cm^2 was applied to grape juice samples. Non linear inactivation kinetics of UV dose response curves were modelled by using different kinetic models e.g., Hom, Weibull and Modified Chick-Watson. The populations of *E.coli* K-12, spoilage yeast and LAB suspended in FSOGJ were reduced after 40 min of exposure by 5.431±0.064, 3.539±0.123 and 5.501±0.042 log CFU respectively. 5.986±0.077 and 6.498±0.010 log CFU reduction were obtained for *E.coli* K-12 and *S.cerevisiae* suspended in PCGJ. The inactivation kinetics of *E.coli* K-12 was best described by Weibull model with the smallest root mean squared error (RMSE) ($R^2 \geq 0.99$). Hom model represented the best results for determination of non-linear inactivation kinetics for *S.cerevisiae*, spoilage yeast and lactic acid bacteria.

The second objective of the Ph.D. study was to measure the UV intensity and UV dose in the both collimated beam apparatus and S-shaped continuous flow UV reactor by using chemical actinometry. For this purpose, a S-shaped, thin film, continuous flow UV reactor was designed and constructed in the Department of Food Engineering, IZTECH, Izmir, Turkey. Iodide/iodate was used as a chemical actinometer. Two different studies were applied. The first study was designed to compare the UV intensity recorded by a radiometer and measured by chemical actinometry in the bench top collimated beam apparatus. The second study was applied to determine UV intensity in continuous flow UV reactor by the help of triiodide (I_3) formation from the potassium iodide (KI) solution reacting under UV exposure. It was observed that results of UV intensity measurements obatined from chemical actinometry (1.790 mW/cm2) and radiometer reading (1.792 mW/cm2) were comparable and concluded that 6.28 minutes of UV exposure time was enough for determination of UV intensity when the chemical actinometry method was applied. When the center lamp was working, incident UV intensity was estimated as 9.1 mW/cm^2 after 6.28 minutes of UV exposure. When the six surface lamps were switched on, incident UV intensity was measured as 50.9 mW/cm^2. The average UV intensities (calculated based on Beer Lambert law) were estimated as 2.33±1.91 mW/cm^2 (center lamp was on) and 13.05±10.69 (surface lamps on) for FSOGJ. On the other hand, average UV intensities of PCGJ were calculated as 6.06±1.45 mW/cm^2 (center lamp was on) and 33.90±8.12 (surface lamps on). One of the drawback of the chemical actinometry is that the iodide/iodate chemicals react with the phenolic compounds of the fruit juices. During this reaction, the color of the juice turns to dark brown which prevents the penetration of light and adversly affects the spectrophotometrical measurements. Because of this, it is commented that the iodometric method needs to be modified if it is to be used for fruit juices.

The third objective of the Ph.D. study was to develop a general approach by integrating a flow model, UV intensity distribution model and DPM model for prediction of UV dose distribution in a UV reactor. For this purpose, FLUENT® 14.0 was used as a commercial finite volume CFD solver. For numerical solution, continuity equation, equations of momentum and mass are integrated to solver. In addition to this, discrete particle model (DPM) was applied to simulate the residence time (exposure time) of microbial particles in model fluid food (i.e., opaque grape juice) in laminar flow conditions. The integrated models were used to simulate the flow field, particle

motion and UV dose in the continuous flow UV reactor. The simulated UV dose results were compared with the data obtained from biodosimetric and iodometric studies. It was observed that average UV dose predicted by CFD analysis was much higher than the values measured by biodosimetric or actionometric method. 90 % of particles had UV dose level changing between 0 and 3 J/cm^2. The high UV dose level was related with the high residence time and the location of the simulated particles in the UV reactor. 80 % of the particles had the residence time interval of 165-300 seconds whereas 20 % of those particles completed their motion in 350-475 seconds. Besides, intensity values of some particles having 450-470 seconds of residence time were lower than that of particles having 250-270 seconds of UV exposure time. Consequently, some particles received much more UV energy than the others due to high residence time and having a position close to the lamp surface. The variations in the particle exposure time and location directly affected the average UV dose delivery and residence time resulted in the higher average UV dose value with a high standard deviation. On the other hand, it was predicted that the average residence time of microbial particles was comparable with the manually recorded one (244 s). It was concluded that the prediction of UV dose by CFD analysis can be improved by taking into account of the other factors such as reflection, refraction, fouling, and lamp aging.

The fourth aim of Ph.D study was to investigate the efficiency of UV-C irradiation in PCGJ and FSOGJ at different volumetric flow rates (0.90, 1.75 and 3.70 mL/s). For this purpose, a newly designed S-shaped, thin film, continuous flow UV reactor was used. Three different studies were designed to evaluate the effect of UV-C irradiation on the microbial inactivation and physical properties of grape juices. In the first study, PCGJ was inoculated with *S.cerevisiae* (NRRL Y-139) as target microorganism. In the second study, FSOGJ was fermented to increase the number of spoilage microorganisms, i.e., yeast and lactic acid bacteria. Inoculated or fermented grape juice samples were exposed to a UV-C irradiation in the continuous flow UV reactor. In the third study, the efficiency of UV-C irradiation was examined using *E.coli* K-12 (ATCC 25253) which is a surrogate strain of *E.coli* O157:H7 in both PCGJ and FSOGJ. UV dose delivered in continuous flow UV reactor was determined based on the biodosimetric method. FSOGJ, contaminated with spoilage yeast and lactic acid bacteria were treated by continuous flow UV reactor. Then, maximum inactivation level was defined and UV dose, necessary for these inactivaton rate was estimated from the UV dose response curve obtained by using bench top collimated beam apparatus. The

reduction of *S.cerevisiae* was very high (6.498±0.010 log CFU/ml) in PCGJ when the flow rate was 0.90 mL/s. Maximum inactivation of lactic acid bacteria and spoilage yeast were 4.133±0.679 log CFU and 1.604±0.321 log CFU respectively, in FSOGJ at the same conditions. Spoilage yeasts were found to be more UV resistant microorganisms than bacteria in FSOGJ. The population of *E.coli* K-12 (ATCC 25253) in PCGJ and FSOGJ was reduced after 41 min exposure by 5.986±0.077 and 5.341±0.016 log CFU respectively. By applying Hom model to UV dose response curve and inactivation data, it was concluded that 247.302 mJ/cm^2 UV dose was needed in order to achieve 1.604±0.321 Log CFU/ml reduction of spoilage yeast suspended in FSOGJ. On the other hand 301.113 mJ/cm^2 was required to obtain 4.133±0.679 Log CFU/ml of lactic acid bacteria reduction suspended in FSOGJ. Approximately 152.62 mJ/cm^2 UV dose (D_{10}) was necessary to inactivate 1 logarithmic unit of spoilage yeast. Also 48.47 mJ/cm^2 UV dose was applied to determine 1 logarithmic unit inactivation of lactic acid bacteria. 577.245 mJ/cm^2 UV dose was required to inactivate 5.431 Log CFU/ml of *E.coli* K-12 in FSOGJ. Additionally, 1001.6 mJ/cm^2 and 273.5 mJ/cm^2 of UV dose were necessary to inactivate 6.498 Log CFU of *S.cerevisiae* and 5.986 Log CFU of *E.coli* K-12 in PCGJ. Compared to spoilage yeast and lactic acid bacteria, inactivation rate of *E.coli* K-12 was higher due to high sensitivity to UV irradiation. It was concluded that the absorption coefficient, the turbidity, and color of the juice play an important role in UV light penetration and effective inactivation of microorganisms in a UV reactor.

The last objective of the PhD study was to evaluate the microbial shelf life of UV treated FSOGJ. For this purpose, two studies were conducted. The first study was designed to provide a microbial stability in FSOGJ by exposing to UV-C irradiation and extend its shelf life at refrigerated storage conditions. The second study was designed to investigate any changes in physicochemical properties of grape juice (such as absorbance coefficient, turbidity, color, brix (%), pH, vitamin C content and total titratable acidity) throughout the storage period. The number of yeast and LAB in irradiated juice was increased up to 4.360±0.049 and 3.062±0.085 Log CFU/ml in 14 days. Nonetheless, the number of yeast and LAB were reported as 5.804±0.199 and 3.924±0.163 at the end of 7th day of storage for untreated grape juice. In other words, untreated grape juice samples were spoiled at the end of 7th day of storage since total microbial count was above 5000 CFU/ml. As a result of this, it was commented that the shelf life of FSOGJ was doubled. Complete degradation of vitamin C was noticed

during storage period. Although, pH, brix and titratable acidity were not affected during UV-C treatment their level changed significantly due to microbial increase and formation of the fermentation byproducts during storage. By the effect of sugar degradation, brix level reduced significantly after 5th day. Color properties and turbidity were affected significantly in UV irradiated juice due to photodegradation of color compounds and reduction in the amount of carotenoid. After 14 days, turbidity was quite higher than initial level since cloud structure was observed based on increase in the number of microorganisms and metabolic by-products.

REFERENCES

Adhikari, C.; Koutchma, T.; Beecham-Bowden, T. Evaluation of HHEVC (4,4'4" tris-di-B-hydroxylethyl aminotriphenylacetonitrile) Dye as a Chemical Actinometer in Model Buffers for UV Treatment of Apple Juice and Cider. *Food Science and Technology* (LWT) **2005**, 38, 717-725

Aguilo-Aguayo, I.; Oms-Oliu, G.; Soliva-Fortuny, R.; Martin-Belloso, O. Changes in Quality Attributes Throughout Storage of Strawberry Juice Processed by High-Intensity Pulsed Electric Fields or Heat Treatments. *Food Science and Technology* **2009**, 42, 813-818.

Albert, I.; Mafart, P.;. A Modified Weibull Model for Bacterial Inactivation. *International Journal of Food Microbiology* **2005**, 100, 197-211.

ANSYS CFX release 13.1 Technical Specifications. **2012**. Public Notice, ANSYS, Inc., Southpointe, Canonsburg, PA, USA.

Antonelli**,**A.,; Chinnici, F.; Masino, F. Heat-Induced Chemical Modification of Grape Must as Related to its Concentration During the Production of Traditional Balsamic Vinegar: A Preliminary Approach. *Food Chemistry* **2004**, 88(1), 63-68

Ball, H.R. Jr.; Hamid-Samimi, M.; Foegeding, P.M.; Swartzel, K.R. Functionality and Microbial Stability of Ultrapasteurized, Aseptically Packaged Refrigerated Whole Egg, *Journal of Food Science* **1987**, 52, 1212-1218.

Bandla, S.; Choudhary, R.; Watson, D.G.; Haddock, J. UV-C Treatment of Soymilk in Coiled Tube UV Reactors for Inactivation of *Escherichia coli* W1485 and *Bacillus cereus* Endospores. *LWT* **2012**, 46, 71-76.

Bank, H.L.; Schmehl, J.L.; Dratch, R.J. Bacteriocidal Effectiveness of Modulated UV Light. *Applied and Environmental Microbiology* **1990**, 56, 3888-3889.

Basaran, N.; Quintero-Ramos, A.; Moake, M.M.; Churey, J.J.; Worobo, R.W. Influence of Apple Cultivars on Inactivation of Different Strains of *Escherichia coli* O157:H7 in Apple Cider by UV Irradiation. *Applied Environmental Microbiology* **2004**, 70(10), 6061-6065.

Battey, A.; Duffy, S.; Schaffner, D. Modeling Yeast Spoilage in Cold-Filled Readyto-Drink Beverages with *Saccharomyces cerevisiae*, *Zygosaccharomyces bailii*, and *Candida lipolytica*. *Applied and Environmental Microbiology* **2002**, 68(4), 1901–1906.

Baumann, A.R.; Martin, S.E.; Feng, H. Power Ultrasound Treatment of *Listeria monocytogenes* in Apple Cider. *Journal of Food Protection* **2005**, 68(11), 2333-2340.

Bazhal, M. I.; Vorobiev. E. I. Electric Treatment of Apple Slices for Intensifying Juice Pressing. *Journal of the Science of Food and Agriculture*. **2000**, 80, 1668-1674

Benabbou, A.K.; Derriche, Z.; Felix, C.; Lejeune, P.; Guillard, C. Photocatalytic Inactivation of *Escherischia coli*: Effect of Concentration of TiO_2 and Microorganism, Nature, and Intensity of UV Irradiation. *Applied Catalysis B: Environmental* **2007**, 76, 257-263.

Bennett, A.F. A Lagrangian Analysis of Turbulent Diffusion. *Reviews of Geophysics* **1987**, 25(4), 799-822.

Bermúdez-Aguirre, D.; Barbosa-Cánovas, G.V. Inactivation of *Saccharomyces cerevisiae* in Pineapple, Grape and Cranberry Juices Under Pulsed and Continuous Thermo-Sonication Treatments. *Journal of Food Engineering* **2012**, 108(3), 383–392

Bermudez-Aguirre, D.; Corradini, M.C.; Mawson, R.; Barbosa-Canovas, G.V. Modeling the Inactivation of *Listeria innocua* in Raw Whole Milk Treated Under Thermo-Sonication. *Innovative Food Sciences and Emerging Technologies* **2009**, 10, 172-178.

Bialka K.L.; Demirci, A. Decontamination of *Escherichia coli* O157:H7 and *Salmonella enterica* on Blueberries using Ozone and Pulsed UV-Light. *Journal of Food Science* **2007**, 72(9), M931-M936.

Bialka, K.L.; Demirci, A.; Puri, V.M. Modeling the Inactivation of *Escherichia coli* O157:H7 and *Salmonella enterica* on Raspberries and Strawberries Resulting From Exposure to Ozone or Pulsed UV-Light. *Journal of Food Engineering* **2008**, 85, 444-449.

Bintsis, T.; Tzanetaki, E.L.; Robinson, R.K. Existing and Potential Applications of Ultraviolet Light in the Food Industry-A Critical Review. *Journal of Food Science and Application*, **2000**, 80, 637-645.

Bird, R.B.; Steward, W. E.; Lightfood, E.N. Shell Momentum Balances and Velocity Distributions in Laminar Flow In: Bird (Ed.). *Transport Phenomena* **2002**, United States, John Wiley Sons, Inc., pp. 40-61.

Blatchley III, E.R. Numerical Modelling of UV Intensity Application to Collimated-Beam Reactors and Continuous-Flow Systems. *Water Resources* **1997**, 31(9), 2205-2218.

Blume, T.; Neis, U. Improved Wastewater Disinfection by Ultrasonic Pre-Treatment. *Ultrasonics Sonochemistry* **2004**, 11, 333-336.

Bohrerova, Z.; Shemer, H.; Lantis, R.; Impellitteri, C.A.; Linden, K.G. Comparative Disinfection Efficiency of Pulse and Continuous-Wave UV Irradiation Technologies. *Water Research* **2008**, 42, 2975-2982.

Bolton, J. R. Calculation of Ultraviolet Fluence Rate Distributions in an Annular Reactor: Significance of Refraction and Reflections. *Water Resources* **2000**, 34, 3315-3324.

Bolton, J.R.; Linden, K.G., Standardization of Methods for Fluence (UV dose) Determination in Bench-Scale UV Experiments. *ASCE: Journal of Environmental Engineering* **2003**, 129(3), 209-215.

Bukhari, Z.; Hargy, T.M.; Bolton, J. R.; Dussert, B.; Clancy, J. L. Medium Pressure UV Light for Oocyst Inactivation. *J. American Water Works Associacion* **1999**, 91, 86-94.

Buzrul, S.; Alpas, H. (2007). Modeling Inactivation Kinetics of Foodborne Pathogens at a Constant Temperature. *LWT* **2007**, 40, 632–637.

Cadet, J.; Sage, E.; Douki T. 2005. "Ultraviolet Radiation-Mediated Damage to Cellular DNA. *Mutation Research* **2005**, 571, 3-17.

Caminiti, I.; Palgan, I.; Muñoz, A.; Noci, F.; Whyte, P.; Morgan, D.; Cronin, D.; Lyng, J. The Effect of Ultraviolet Light on Microbial Inactivation and Quality Attributes of Apple Juice. *Food Bioprocess Technology* **2012**, 5(2), 680-686.

Char, C.D.; Mitilinaki, E.; Guerrero, S.N.; Alzamora, S.M. Use of High-Intensity Ultrasound and UV-C Light to Inactivate Some Microorganisms in Fruit Juices. *Food Bioprocess Technology* **2010**, 3, 797-803.

Chen, H. Use of Linear, Weibull, and Log-Logistic Functions to Model Pressure Inactivation of Seven Foodborne Pathogens in Milk. *Food Microbiology* **2007**, 24(3), 197-204.

Chen, J.; Deng, B; Kim, C.N. Computational Fluid Dynamics (CFD) Modeling of UV Disinfection in a Closed-Conduit Reactor. *Chemical Engineering Science* 2011, 66, 4983-4990

Cheng, L.H.; Soh, C. Y.; Liew, S.C. The, F. F. Effects of Sonication and Carbonation on Guava Juice Quality. *Food Chemistry* **2007**, 104, 1396-1401.

Chia, S. L.; Rosnah, S.; Noranizan, M. A.; Wan Ramli, W. D. The Effect of Storage on the Quality Attributes of Ultraviolet-Irradiated and Thermally Pasteurised Pineapple Juices. *International Food Research Journal* **2012**, 19(3),1001-1010.

Chiu, K.; Lyn, D. A.; Blatchley III, E.R. Integrated UV Disinfection Model Based on Particle Tracking. *Journal of Environmental Engineering* **1999**, 125(1),7-16.

Chick, H. An Investigation into the Laws of Disinfection. *Journal of Hygiene (Cambridge)* **1998**, 8, 92-158.

Chiu, K.; Lyn, D.A.; Savoye, P.; Blatchley, E.R. Integrated UV Disinfection Model based on ParticleTracking. *Journal of Environmental Engineering* **1999**, 125(1), 7-16.

Chmiel, H.; Kaschek, M.; Blöcher, C.; Noronha, M.; Mavrov, V. Concepts for the Treatment of Spent Process Water in the Food and Beverage Industries. *Desalination,* **2002**, 152, 307-314.

Cho, M.; Chung, H.; Yoon, J. Disinfection of Water Containing Natural Organic Matter by using Ozone-Initiated Radical Reactions. *Applied and Environmental Microbiology* **2003**, 69(4), 2284-2291.

Choi, L.H.; Nielsen, S.S. The Effect of Thermal and Non-Thermal Processing Methods on Apple Cider Quality and Consumer Acceptability. *Journal of Food Quality* **2005**, 28, 13-29.

Choi, M.S.; Cheigh, C I.; Jeong, E.A.; Shin, J.K.; Chung, M.S. Nonthermal Sterilization of *Listeria monocytogenes* in Infant Foods by Intense Pulsed-Light Treatment. *Journal of Food Engineering*, **2010**, 97, 504–509.

Choudhary, R.; Bandla, S. Ultraviolet Pasteurization for Food Industry. *International Journal of Food Science and Nutrition Engineering* **2012**, 2(1), 12-15

Choudhary, R.; Bandla, S.; Watson, D.G.; Haddock, J.; Abughazaleh, A.; Bhattacharya, B. Performance of Coiled Tube Ultraviolet Reactors to Inactivate *Escherichia coli* W1485 and *Bacillus cereus* Endospores in Raw Cow Milk and Commercially Processed Skimmed Cow Milk. *Journal of Food Engineering* **2011**, 107, 14-20.

Christiensen, J.; Linden, K. Ultraviolet Disinfection of Unfiltered Drinking Water: Particle Impacts. *Proceedings of the IUVA* **2001**, 1st International Congress, June 14-16, Washington D.C.

Cieminis, K.G.K.; Rančelien, V.M.; Prijalgauskien, A.J.; Tiunaitien, N V.; Rudzianskait, A.M.; Jančys, Z.J. Chromosome and DNA Damage and Their Repair in Higher Plants Irradiated with Short-Wave Ultraviolet Light. *Mutation Research-Fundamental and Molecular Mechanisms of Mutagenesis* **1987**, 181 (1), 9-16.

Collins, M.W.; Ciofalo, M. Computational Fluid Dynamics and its Application to Transport Processes. *Journal of Chemical Technology and Biotechnol*ogy **1991**, 52(l) 5-47

Cortella, G.; Manzan, M.; Comini, G. 1998. Computation of Air Velocity and Temperature Distributions in Open Display Cabinets. In: *Advanced in the Refrigeration Systems, Food Technologies and ColdChain* **1998**, International Institute of Refrigeration, Paris, France, pp. 617–625.

Cortella, G.; Manzan, M.; Comini, G. CFD simulation of refrigerated display cabinets. *International Journal of Refrigeration* **2001**, 24 (3), 250–260.

Courant, R.; Friedrichs, K.O.; Lewy, H. (1928). Uuber die Partiellen Differenzen-gleichungen der Mathematischen Physik, *Partielle Differenzengleichungen der Physik.* **1928**, 100, 32-74.

Crapulli, F.; Santoro, D.; Haas, C.N.; Notarnicola, M.; Liberti, L. Modeling Virus Transport and Inactivation in a Fluoropolymer Tube UV Photoreactor using Computational Fluid Dynamics. *Chemical Engineering Journal* **2010**, 161(1–2), 9-18.

Çinlar, E.; Kao, J. Particle Systems on Flows. *Applied Stochastic Models and Data Analysis* **1991**, 7, 3-15.

Dávalos**,** A.; Bartolomé, B.; Gómez-Cordovés, C. Antioxidant Properties of Commercial Grape Juices and Vinegars. *Food Chemistry* **2005**, 93(2), 325-330

Davis, R.E. On relating Eulerian and Lagrangian Velocity Statistics: Single Particles in Homogeneous Flows. *Journal of Fluid Mechanics* **1982**, 114, 1-26.

Demirci, A.; Panico, L. Pulsed Ultraviolet Light. *Food Science and Technology International* **2008**, 14, 443–446.

Department of Health, Education and Welfare. **1966.** Division of Environmental Engineering and Food Protection: policy statement on the use of the ultraviolet process for disinfection of water. U.S. Department of Health, Education and Welfare, Washington, D.C.

Dhanasekharan, K.M.; Grald, E.W.; Mathur, R. How Flow Modelling Benefits the Food Industry. *Food Technology* **2004**, 58(3), 32-35.

Donahue, D. W.; Canitez, N.; Bushway, A.A. UV inactivation of *E.coli* O157: H7 in Apple Juice: Quality, Sensory and Shelf-Life Analysis. *Journal of Food Processing and Preservation* **2004**, 28, 368-387.

Downey, D.; Giles D.; Delwiche M. Finite Element Analysis of Particle and Liquid Flow Through an Ultraviolet Reactor. *Computers and Electronics in Agriulture* **1998**, 21, 81-105.

Ducoste, J.; Liu, D.; Linden, K. Alternative Approaches to Modeling Fluence Distribution and Microbial Inactivation in Ultraviolet Reactors: Lagrangian versus Eulerian. *Journal of Environmental Engineering* **2005**, 131(10). 1393-1403.

Ducoste, J.; Linden, K.; Rokjer, D.; Liu, D. Assesment of Reduction Equivalent Fluence Bias using Computational Fluid Dynamics. *Environmental Engineering Science* **2005**, 22(5). 615-628.

Duran, J.E.; Taghipour, F.; Mohseni, M. CFD Modeling of Mass Transfer in Annular Reactors. *International Journal of Heat and Mass Transfer* **2009**, 52. 5390-5401.

Elyasi, S.; Taghipour, F. Simulation of UV Photoreactor for Degradation of Chemical Contaminants: Model Development and Evaluation. *Environmental Science & Technology* **2010**, 44, 2056-2063

Emperor Aquatics' web site, (accessed in **2007**) http://www.uvcomparison.com/images/scienceUV-Cspectrum.jpg.

Emperor Aquatics' web site, (accessed in **2007**) http://aquafineuv.com/uvtechnology/index.

Esteve, M.J.; Frigola, A.; Rodrigo, C.; Rodrigo, D. Effect of Storage Period Under Variable Conditions on the Chemical and Physical Composition and Colour of Spanish Refrigerated Orange Juices. *Food and Chemical Toxiology* **2005**, 43, 1413-1422.

Fernández, A.; Lópeza, M.; Bernardoa, A.; Condón, S.; Raso, J. Modelling Thermal Inactivation of *Listeria monocytogenes* in Sucrose Solutions of Various Water Activities *Food Microbiology* **2010**, 24, 372-379

Folts, J.D.; Maalej, N.; Osman, H.; Grape Juice but not Orange or Grapefruit Juice Significantly Inhibits *in vivo* Platelet Activity and Thrombosis in Stenosed Canine Coronary Arteries. *Journal of the American College of Cardiology* **1997**, 29, 180A.

Forney, L.J.; Pierson, J.A.; Andz, Y.E. Juice Irradiation with Taylor-Couette flow: UV Inactivation of *Escherichia coli*. *Journal of Food Protection* **2004**, 67(11), 2410-2415.

Frankel, E.N.; Bosanek C.A.; Meyer, A.S.; Silliman, K.; Kirk, L.L. Commercial Grape Juices Inhibit the *in vitro* Oxidation of Human Low-Density Lipoproteins. *Journal of Agricultural and Food Chemistry* **1998**, 46, 834-838

Franz, C.M.A.P.; Specht, I.; Cho, G.; Graef, V.; Stahl, M.R. UV-C-Inactivation of Microorganisms in Naturally Cloudy Apple Juice Using Novel Inactivation Equipment Based on Dean Vortex Technology. *Food Control* **2009**, 20, 1103-1107.

Fratianni, A.; Cinquanta, L.; Panfili, G. Degradation of Carotenoids in Orange Juice During Microwave Heating. *LWT* **2010**, 43(6), 867-871.

Fredericks, I.N.; Du Toit, M.; Krügel, M. Efficacy of Ultraviolet Radiation as an Alternative Technology to Inactivate Microorganisms in Grape Juices and Wines. *Food Microbiology* **2011**, 28, 510-517.

Friis, A.; Jensen, B.B.B. Prediction of Hygiene in Food Processing Equipment using Flow Modelling. *Food and Bioproducts Processing* **2002**, 80(4), 281–285.

Gabriel, A.A. Inactivation of *Escherichia coli* O157:H7 and Spoilage Yeasts in Germicidal UV-C-Irradiated and Heat-Treated Clear Apple Juice. *Food Control* **2012**, 25, 425-432

Gabriel, A.A.; Nakano, H. Inactivation of *Salmonella, E.coli* and *Listeria monocytogenes* in Phosphate-Buffered Saline and Apple Juice by Ultraviolet and Heat Treatments. *Food Control* **2009**, 20, 443-446.

Garde-Cerdán, T.; Arias-Gil, M.; Marsellés-Fontanet, A.R.; Ancín-Azpilicueta, C.; Martín-Belloso, O. Effects of Thermal and Non-Thermal Processing Treatments on Fatty Acids and Free Amino Acids of Grape Juice. *Food Control* **2007**, 18, 473-479.

Garibaldi, A.; Minuto, A.; Grasso, V.; Gullino, M.L. Application of Selected Antagonistic Strains against *Phytophthora cryptogea* on Gerbera in Closed Soilless Systems with Disinfection by Slow Sand Filtration. *Crop Protection*, **2003**, 22(8), 1053-1061.

Genovese, D.B.; Elustondo, M.P.; Lozano, J.E. Color and Cloud Stabilization by Steam Heating During Crushing in Cloudy Apple Juice. *Journal of Food Science* **1997**, 62, 1171–1175.

Geveke D.J. UV Inactivation of Bacteria in Apple Cider. *Journal of Food Protection*, **2005**, 68(8),1739-1742.

Geveke, D.J. UV Inactivation of *E.coli* in Liquid Egg White. *Food Bioprocess Technology* **2008**, 1, 201-206.

Geveke, D.J.; Torres, D. Pasteurization of Grapefruit Juice Using a Centrifugal Ultraviolet Light Irradiator. *Journal of Food Engineering* **2012**, 111(2), 241-246

Giese, N.; Darby, J. Sensitivity of Microorganisms to Different Wavelengths of UV Light: Implications on Modeling of Medium Pressure UV Systems. *Water Resources* **2000**, 34. 4007-4013.

Goldstein, S.; Rabani, J. The Ferrioxalate and Iodide-Iodate Actinometers in the UV Region. *Journal of Photochemistry and Photobiology A: Chemistry* **2008**,193, 50-55.

Gómez, N.; García, D.; Álvarez, I.; Condón, S.; Rasot, J. Modelling Inactivation of *Listeria monocytogenes* by Pulsed Electric Fields in Media of Different pH. *International Journal of Food Microbiology* **2005**, 103, 199-206.

Góngora-Nieto, M.M.; Pedrow, P.D.; Swanson, B.; Barbosa-Cánovas, G.V. Energy Analysis of Liquid Whole Egg Pasteurized by Pulsed Electric Fields. *Journal of Food Engineering* **2003**, 57, 209-216.

Gouws, P.A.; Gie, L.; Pretorius, A.; Dhansay, N. Isolation and Identification of *Alicyclobacillus acidocaldarius* by 16S rDNA from Mango Juice and Concentrate. *International Journal of Food Science and Technology* **2005**, 40, 789-792.

Green F.B.; Lundquist, T.J.; Oswald, W.J. Energetics of Advanced Integrated Wastewater Pond Systems. *Water Science and Technology* **1995**, 31(12), 9-20.

Guerrero-Beltrán, J. A.; Barbosa-Cánovas, G.V. Reduction of *Saccharomyces cerevisiae*, *Escherichia coli*, and *Listeria innocua* in Apple Juice by Ultraviolet Light. *Journal of Food Process Engineering* **2005**, 28, 437-452.

Guerrero-Beltrán, J.A.; Barbosa-Cánovas, G.V. Inactivation of *Saccharomyces cerevisiae* and Polyphenoloxidase in Mango Nectar Treated with UV Light. *Journal of Food Protection* **2006**, 69, 362-368.

Guerrero-Beltran, J.Á.; Welti-Chanes, J.; Barbosa-Cánovas, G.V. Ultraviolet-C Light Processing of Grape, Cranberry and Grapefruit Juices to Inactivate *Saccharomyces cerevisiae*. *Journal of Food Process Engineering* **2009**, 32, 916-932.

Haas, C.N.; Sakellaropoulos, G. P. Rational Analysis of Ultraviolet Disinfection Reactors, p. 540-547. *In Proceedings of the National Conference on Environmental Engineering* **1979**, American Society of Civil Engineers, Washington, D.C.

Haas, C.N.; Joffe, J. Disinfection Under Dynamic Conditions: Modification of Hom's Model for Decay. *Environmental Science Technology* **1994**, 28, 1367-1369.

Hachard, C.G.; Parker, C.A. A New Sensitive Chemical Actinometer. II. Potassium Ferrioxalate as a Standard Chemical Actinometer. *Proceedings of the Royal Society A* **1953**, 235(1203), 518-536.

Hargy, T.M.; Clancy, J.L.; Bukhari. Z. Shedding UV Light on the *Cryptosporidium* Threat. In *NSF Proceedings of the Small Drinking Water and Wastewater Systems* **2000**, International Symposium and Technology Expo: Phoenix, Arizona.

Harrington, W.O.; Hills. C.H. Reduction of the Microbial Population of Apple Cider by Ultraviolet Irradiation. *Food Technology* **1968**, 22, 117-120.

Harris, D.G.; Adams, D.V.; Sorensen, L.D.; Curtis, M. Ultraviolet Inactivation of Selected Bacteria and Viruses with Photoreactivation of Bacteria. *Water Resources* **1987**, 21, 687-692.

Hassen, A.; Mahrouk, M.; Ouzari, H.; Cherif, M.; Boudabous, A.; Damelincourt, J.J. UV Disinfection of Treated Wastewater in a Large-Scale Pilot Plant and Inactivation of Selected Bacteria in a Laboratory UV Device. *Bioresource Technology*, **2000**, 74, 141-150.

Hermawan, N.; Evrendilek, G.A.; Dantzer, W.R.; Zhang, Q.H.; Richter, E.R. "Pulsed Electric Field Treatment of Liquid Whole Egg Inoculated with *Salmonella enteritidis*, *Journal of Food Safety* **2004**. 24, 71-85.

Hijnen, W.A.M.; Beerendonk, E.F.; Medema, G.J. Inactivation Credit of UV Radiation for Viruses, Bacteria and Protozoan (oo)cysts in Water; A Review. Water Resources **2006**, 40(1), 3-22.

Huang, L. Thermal Inactivation of *Listeria monocytogenes* in Ground Beef Under Isothermal and Dynamic Temperature Conditions. *Journal of Food Engineering* **2009**, 90, 380-387.

Huff, C.B.; Smith, H.F.; Boring, W.D.; Clarke, N.A. Study of Ultraviolet Disinfection of Water and Factors in Treatment Efficiency. *Public Health Reports* **1965**, 80, 695-705.

Ibarz, A.; Pagán, J.; Panadés, R.; Garza, S. Photochemical Destruction of Color Compounds in Fruit Juices. *Journal of Food Engineering* **2005**, 69, 155-160.

Jacob, S.M.; Dranoff, J.S. Light Intensity Profiles in a Perfectly Mixed Photoreactors. *Jour. A.I.Ch.E*. **1970**, 16, 359-363.

Jin, S.; Modifi, A.A.; Linden, K.G. Polychromatic UV Fluence Measurement using Chemical Actinometry, Biodosimetry, and Mathematical Techniques. *Journal of Environmental Engineering* **2006**, 32(8), 831-841.

Johnson, J.D.; Qualls, R.G. Ultraviolet Disinfection of Secondary Effluent: Measurement of Dose and Effects of Filtration. *Report of EPA project R 804770010* **1981**, Municipal Environmental Research Laboratory, Cincinnati, Ohio.

Keevil, J.G.; Osman, H.E.; Reed, J.D.; Folts, J.D. Grape Juice, but not Orange juice or Grapefruit Juice, Inhibits Human Platelet Aggregation. *Journal of Nutrition* **2000**, 130(1), 53-56.

Keyser, M.; Müller, I.; Cilliers, F. P.; Nel, W.; Gouws, P.A. UV Radiation as a Non-Thermal Treatment for the Inactivation Microorganisms in Fruit Juice. *Innovative Food Science Emerging Technology* **2008**, 9(3), 348-354.

Kieviet, F.G.; Van, R.J.; De Moor, P.P.E.A.; Kerkhof, P.J.A.M. Measurement and Modelling of the Air Flow Pattern in a Pilot-Plant Spray Dryer. *Chemical Engineering Research and Design* **1997**, 75 (A3), 321–328.

Klim, M.; Nagy, S. An Improved Method to Determine Nonenzymic Browning in Citrus Juice. *Journal of Agricultural and Food Chemistry* **1988**, 36(6), 1271-1274.

Koivunen, J.; Heinonen-Tanski, H. Inactivation of Enteric Microorganisms with Chemical Disinfectants, UV Irradiation and Combined Chemical/UV Treatments. *Water Research* **2005**, 39, 1519-1526.

Koutchma T.N.; Keller, B.; Parisi, B.; Chirtel, S. Ultraviolet Disinfection of Juice Products in Laminar and Turbulent Flow Reactors. *Innovative Food Science Emerging Technology* **2004**, 5, 179-189.

Koutchma, T. Advances in Ultraviolet Light Technology for Non-Thermal Processing of Liquid Foods. *Food and Bioprocess Technology* **2009**, *2*(2), 138-155.

Koutchma, T.; Parisi, B. Evaluation of UV Dose in Flow-Through Reactors for Fresh Apple Juice and Cider. *Chemical Engineering Communication*. **2006**, 193, 715-728.

Koutchma, T., and Parisi, B. Biodosimetry of *Escherichia coli* UV inactivation in Model Juices with regard to Dose Distribution in Annular UV Reactors. *Journal of Food Science* **2004**, 69(1), E14–E22.

Koutchma, T.; Keller, S.; Chirtel, S.; Parisi, B. Ultraviolet Disinfection of Juice Products in Laminar and Turbulent Flow Reactors. *Innovative Food Science and Engineering Technologies* **2004**, 5, 179-189.

Koutchma, T.; Parisi, B.; Patazca, E. Validation of UV Coiled Tube Reactor for Fresh Fruit Juices. *Journal of Environmental Engineering* **2007**, 6, 319–328.

Koutchma, T.; Parisi, B.; Unluturk, S. Evaluation of UV Dose in Flow Through Reactors for Fresh Apple Juice and Cider. *Chemical Engineering Communications* **2006**, 193(6), 715-728.

Koutchma, T.N.; Forney, L.J.; Moraru, C.I. *Ultraviolet Light in Food Technology: Principles and Applications* (1st ed. 13-17). **2009**, New York, United States,

Kuhn, H.J.; Braslavsky, S.E.; Schmidt, R. Chemical Actinometry. *Pure and Applied Chemistry* **1989**, 76(12), 187-210.

Kuhn, H.J., Braslavsky, S.E.; and Schmidt, R.; Chemical Actinometry (IUPAC Technical Report). *Pure and Applied Chemistry* **2004**, 76(12), 2105-2146.

Kumar, A., Numerical Investigation of Secondary Flows in Helical Heat Exchangers. *Institute of Food Technologists Annual Meeting* **1995**, Anaheim, CA, USA. 148.

Lage, C.; Teixeira, P.C.N; Leitao, A.C. Non-Coherent Visible and Infrared Radiation Increase Survival to UV (254 nm) in *Escherichia coli* K12. *Journal of Photochemistry and Photobiology B: Biology* **2003**, 54, 155-161.

Lazarova, V.; Janex, M.L.; Fiksdal, L.; Oberg, C.; Barcina, I.; Pommepuy, M. Advanced Wastewater Disinfection Technologies: Short and Long Term Efficiency. *Water Science and Technology* **1998**, 38(12) 109-117.

Le, H.; Moin, P.; Kim, J. Direct Numerical Simulation of Turbulent Flow Over a Backward-Facing Step. *Journal of Fluid Mechanics* **1997**, 330, 349-374

Lee, W.C.; Lee, M.J.; Kim, J.S.; Park, S.Y. Foodborne Illness in Korea and Japan Studied Retrospectively. *Journal of Food Protection* **2001**, 64, 899-902.

Lee, Y.; Nam, S. Reflection of Kinetic Models to the Chlorine Disinfection for Drinking Water Production. *The Journal of Microbiology* **2002**, 40(2), 119-124.

Lehtola, M. J.; Miettinen, I.T.; Lampola, T.; Hirvonen, A.; Vartiainen, T.; Martikainen, P.J. Pipeline Materials Modify the Effectiveness of Disinfectants in Drinking Water Distribution Systems. *Water Research* **2004**, 39, 1962-1971.

Lewis, S.; McIndoe, A. Cleaning, Disinfection and Sterilization of Equipment. *Anaesthesia and Intensive Care Medicine* **2004**, 5(11), 360-363.

Li, C.; Deng, B.; Nyung, C. A Numerical Prediction on the Reduction of Microorganisms with UV Disinfection. *Journal of Mechanical Science and Technology* **2010**, 24(7), 1465-1473.

Liltved, H.; Landfald, B. Effects Of High Intensity Light on Ultraviolet-Irradiated and Non-Irradiated Fish Pathogenic Bacteria. *Water Research* **2000**, 34(2), 481-486.

Linden, K.; Darby, L. Ultraviolet Disinfection of Marginal Effluents: Determining UV Absorbance and Subsequent Estimation of UV Intensity. *Water Environment Research* **1998**, 70, 214-223.

Liu, D.; Ducoste, J.; Shanshan, J.; Linden, K. Evaluation of Alternative Fluence Rate Distribution Models. *Journal of Water Supply: Research and Technology-AQUA* **2004**, 53(6), 391-408.

Liu, D.; Wu, C.; Linden, K.; Ducoste, J. Numerical Simulation of UV Disinfection Reactors: Evaluation of Alternative Turbulence Models. *Applied Mathematical Modelling* **2007**, 31, 1753-1769.

Lu, G.; Li, C.; Liu, P.; Cui, H.; Xia, Y.; Wang, J. Inactivation of Microorganisms in Apple Juice using an Ultraviolet Silica-Fiber Optical Device. *Journal of Photochemistry and Photobiology*. *B, Biology* **2010**, 100(3), 167-172.

Lumley, L.C. The Mathematical Nature of the Problem of Relating Eulerian and Lagrangian Statistical Functions in Turbulences, in *Mecanique de* la *Turbulence,* Edition due CNRS, Paris, 17-26. A. Favre *(ed.)* **1962**, English edition: *The mechanics of turbulence,* Gordon and Breach, New York.

Luse, R.A.; McLaren, A.D. Mechanism of Enzyme Inactivation by Ultraviolet Light and Photochemistry of Amino Acids (at 2537 Å). **1963**, 2(3), 343-360.

Lyn, D.A.; Blatchley III, E.R. Numerical Computational Fluid Dynamics-Based Models of Ultraviloet Disinfection Channels. *Journal of Environmental Engineering* **2005**, 131(6), 838-849.

Ma, L.; Chang, F.J.; Barbosa-Canovas, G.V.; Swanson, B.G. Inactivation of *E.coli* in Liquid Whole Eggs using Pulsed Electric Fields Technology. In: Barbosa-Canovas (Ed.) *New Frontiers in Food Engineering* **1994**, New York, AIChE.

Malley, J.P.; Snicer, G.A.; Doucette. A.M. Alternative Disinfection Strategies for Small Systems. In *Small Systems Water Treatment Technologies: State of the Art Workshop*. **1998,** NEWWA Joint Regional Operations Conference and Exhibition: Marlborough, Massachusetts.

Mañas, P.; Pagán, R.; Alvarez, I.; Usón, S.C. Survival of *Salmonella senftenberg* 775 W to Current Liquid Whole Egg Pasteurization Treatments. *Food Microbiology* **2003**, 20(5), 593-600.

Marsellés-Fontanet, À.R.; Martín-Belloso, O. Optimization and Validation of PEF Processing Conditions to Inactivate Oxidative Enzymes of Grape Juice. *Journal of Food Engineering* **2007**, 83, 452-462.

Marsellés-Fontanet, À.R.; Puig, A.; Olmos, P.; Mínguez-Sanz, S.; Martín-Belloso, O. Optimising the Inactivation of Grape Juice Spoilage Organisms by Pulse Electric Fields. *International Journal of Food Microbiology* **2009**, 130, 159-165.

Marugán, J.; Van Grieken, R.; Sordo, C.; Cruz, C. Kinetics of the Photocatalytic Disinfection of *Escherichia coli* Suspensions. *Applied Catalysis B: Environmental* **2008**, 82(1-2), 27-36.

Masschelein, J.; Debacker, E.; Chebak, S. "Laboratory Investigations on the Disinfection of Water by UV-Light. *Revue des Sciences de L'eau* **1989**, 2, 29-41.

Matak, K.E.; Churey, J.J.; Worobo, R.W.; Sumner, S.S.; Hovingh, E.; Hackney, C.R.; Pierson, M.D. Efficacy of UV light for the Reduction of *Listeria monocytogenes* in Goat's Milk. *Journal of Food Protection* **2005**, 68, 2212-2216.

Matak, K.E.; Sumner, S.S.; Duncan, S.E.; Hovingh, E.; Worobo, R.W.; Hackney, C.R.; Pierson, M.D. Effects of Ultraviolet Irradiation on Chemical and Sensory Properties of Goat Milk. *Journal of Dairy Science* **2007**, 3178-3186

McDonnell G. Glutaraldhyde and Other Aldehyde Resistant Bacteria Associated with the Use of Washer Disinfectors. *Society for Healthcare Epidemiology of America (SHEA) 19th Annual Scientific Meeting* **2009**, San Diego, CA, USA

McDonnell, G.; Burke, P. Disinfection: Is It Time to Reconsider Spaulding? *Journal of Hospital Infection* **2011**, 78, 163-170

Miller, R.; Jeffrey, W.; Mitchell, D.; Elasri, M. Bacterial Responses to Ultraviolet Light. *ASM news* **1999**, 65, 534-541.

Mills, D. Development and Validation of a Preliminary Model for Optimisation of Baking Ovens. *The Food and Packaging Cooperative Research Centre Annual Report* **1998-1999**, Australia.

Moan, J. 1989. Effects of UV Radiation on Cells. *Journal of Photochemistry and Photobiology B: Biology* **1989**, 4(1), 21-34

Montenegro, J.; Ruan, R.; Ma, H.; Chen, P. Inactivation of *E.coli* O157:H7 using a Pulsed Nonthermal Plasma System. *Journal of Food Science* **2002**, 67, 646–48.

Morowitz, H.J. 1950. Absorption Effects in Volume Irradiation of Microorganisms. *Science* 1950, 111, 229-230.

Moyer, J.C.; Aitken, H.C. Apple juice. In Nelson, P.E. and Tressler, D.K. (Eds). *Fruit and vegetable juice processing* **1980**, 212-267. USA: AVI Publishing Co., Inc.

Munoz, A.; Craik S.; Kresta, S. Computational Fluid Dynamics for Predicting Performance of Ultraviolet Disinfection-Sensitivity to Particle Tracking Inputs. *Journal of Environmental Engineering and Science* **2007**, 6, 285-301.

Murakami, E.G.; Jackson, L.; Madsen, K.; Schickedanz, B. Factors Affecting the Ultraviolet Inactivation of *Escherichia coli* K12 in Apple Juice and a Model System. *Journal of Food Process Engineering* **2006**, 29(1), 53–71.

Muriana, P.M. Effect of pH and Hydrogen Peroxide on Heat Inactivation of *Salmonella* and *Listeria* in Egg White. *Food Microbiology* **1997**. 14, 11-19.

National Research Council. *Drinking water and health* **1980**, National Academy of Sciences Press, Washington, D.C.

Ngadi, M.; Smith, J.P.; Cayouette, B. Kinetics of Ultraviolet Light Inactivation of *Escherichia coli* O157:H7 in Liquid Foods. *Journal of the Science of Food and Agriculture* **2003**, 83, 1551-1555.

Noci, F.; Riener, J.; Walkling-Ribeiro, M.; Cronin, D.A.; Morgan, D.J.; Lyng, J.G. Ultraviolet Irradiation and Pulsed Electric Fields (PEF) in a Hurdle Strategy for a Preservation of Fresh Apple Juice. *Journal of Food Engineering* **2008**, 85(1), 141-146.

Norton, T.; Sun, D. Computational Fluid Dynamics (CFD)-An Effective and Efficient Design and Analysis Tool for the Food Industry: A Review. *Trends in Food Science & Technology* **2006**, 17, 600-620

Norton, T.; Sun, D.; Grant, J.; Fallon, R.; Dodd, V. Applications of Computational Fluid Dynamics (CFD) in the Modelling and Design of Ventilation Systems in the Agricultural Industry: A Review. *Bioresource Technology* **2007**, 98, 2386-2414.

Ochoa-Velasco, C.E.; Guerrero-Beltran, J.Á. (2012). Ultraviolet-C Light Effect on Pitaya (*Stenocereus griseus*) Juice. *Journal of Food Research* **2012**, 1(2), 60-70.

Oppenheimer, J.A.; Montgomery, W.; Pasadena, C.A.; Hoagland, J.E.; Laine J.M.; Jacangelo, J.G.; Bhamrah, A. Microbial Inactivation and Characterisation of Toxicity and by Products Occurring in Reclaimed Wastewater Disinfected with UV Radiation. *Alit Water Environmental Federation Planning of Desalination Operations of Effluent Disinfection Systems* **1993**, Whippany, NJ, 23-25 May, p. 13.

Ortuño, C.; Martínez-Pastor, M.T.; Mulet, A., Benedito, J. Supercritical Carbon Dioxide Inactivation of *Escherichia coli* and *Saccharomyces cerevisiae* in Different Growth Stages. *Journal of Supercritical Fluids* **2012**, 63, 8-15.

Oteiza, J.M.; Giannuzzi, L.; Zaritzky, N. Ultraviolet Treatment of Orange Juice to Inactivate *E.coli* O157:H7 as Affected by Native Microflora. *Food Bioprocess Technology* **2010**, 3, 603-614.

Ozkan, M.; Kırca, A.; Cemeroglu, B. Effects of Hydrogen Peroxide on the Stability of Ascorbic Acid During Storage in Various Fruit Juices. *Food Chemistry* **2004**, 88, 591-597.

Pala, C.U.; Toklucu, A.K. Effects of UV-C Light Processing on Some Quality Characteristics of Grape Juices. *Food and Bioprocess Technology* **2013**, 6, 719-725

Palgan, I.; Caminiti, I.M.; Muñoz, A.; Noci, F.; Whyte, P.; Morgan, D.J.; Cronin, D.A.; Lyng, J.G. Combined Effect of Selected Non-Thermal Technologies on *Escherichia coli* and *Pichia fermentans* Inactivation in an Apple and Cranberry Juice Blend and on Product Shelf Life. *International Journal of Food Microbiology* **2011**, 151, 1-6.

Parker, C.A. A new sensitive chemical actinometer. I. Some Trials with Potassium Ferrioxalate. *Proceedings of the Royal Society A* **1953**, 220(1440), 104-116.

Parker, J.A.; Darby, J.L. Particle-Associated Coliform in Secondary Effluents: Shielding from Ultraviolet Light Disinfection. *Water Environment Research* **1995**, 67, 1065-1072.

Parrotta, M.J.; Bekdash, F. UV Disinfection of Small Groundwater Supplies. *Journal of the American Water Works Association* **1998**, AWWA: Denver.

Patras, A.; Brunton, N.; Pieve, S.D.; Butler, F.; Downey, G. Effect of Thermal and High Pressure Processing on Antioxidant Activity and Instrumental Colour of Tomato and Carrot Purees. *Innovative Food Science and Emerging Technologies* **2009**, 10, 16-22.

Peldszus, S.; Andrews, S.A.; Souza, R.; Smith, F.; Douglas, I.; Bolton, J. Huck, P. M. Effect of Medium-Pressure UV Irradiation on Bromate Concentrations in Drinking Water, A Pilot-Scale Study. *Water Research* **2003**, 38, 211-217.

Petrasek, A. C.; Wolf, H.R.; Esmond, S.E.; Andrews, D.C. Ultraviolet Disinfection of Municipal Wastewater Effluents. *EPA-600/ 2-80-102, PB81-111049, U.S.* **1998**, Environmental Protection Agency, Cincinnati.

Piper, P.; Calderon, C.O.; Hatzixanthis, K.; Mollapour, M. Weak Acid Adaptation: The Stress Response that Confers Yeasts with Resistance to Organic Acid Food Preservatives. *Microbiology* **2001**, 147, 2635-2642.

Plaza, L.; Sánchez-Moreno, C.; Elez-Martínez, P.; De Ancos, B.; Martín-Belloso, O.; Pilar Cano, M. Effect of Refrigerated Storage on Vitamin C and Antioxidant Activity of Orange Juice Processed by High-Pressure or Pulsed Electric Fields with Regard to Low Pasteurization. *European Food Research and Technology A* **2006**, 223, 487-493.

Ponce, E.; Pla, R.; Sendra, E. Destruction of *Salmonella enteritidis* Inoculated in Liquid Whole Egg by High Hydrostatic Pressure: A Comparative Study in Selective and Non Selective Media. *Food Microbiology* **1999**, 16, 357-365.

Predicala, B.Z.; Maghirang, R.G., Numerical Simulation of Particulate Matter Emissions from Mechanically Ventilated Swine Barns. *Transactions of the American Society of Agricultural Engineering* **2003,** 46, 1685–1694.

Qiu, X.; Sharma, S.; Tuhela, L.; Jia, M.; Zhang, Q.H. An Integrated PEF Pilot Plant for Continuous Non-thermal Pasteurization of Fresh Orange Juice. *Transactions of the American Society of Agricultural Engineering* **1998**, 41, 1069-1074.

Qualls, R.G.; Johnson, J.D. Bioassay and Dose Measurement in UV Disinfection. *Applied and Environmental Microbiology* **1983**, 45(3), 872-877

Qualls, R.G.; Osseff, S.F.; Chang, J.C.H.; Dorfman, M.H.; Dumais, D.C.; Johnson, J.D. Factors Controlling Sensitivity in Ultraviolet Disinfection of Secondary Effluents. *Journal of Water Pollution. Control Federation* **1985**, 57, 1006-1011.

Quarini, J.; 1995. Applications of Computational Fluid Dynamics in Food and Beverage Production. *Food Science and Technology* Today 9 (4), 234–237.

Quek, P.H.; Hu, J.Y. Indicators for Photoreactivation and Dark Repair Studies for Following Ultraviolet Disinfection. *Journal of Industrial Microbiology and Biotechnology* **2008**, 35, 533.

Quintero-Ramos, A.; Churey, J.J.; Hartman, P.; Barnard, J.; Worobo. R.W. Modeling of *Escherichia coli* inactivation by UV Irradiation at Different pH Values in Apple Cider. *Journal of Food Protection* **2004**, 67,1153-1156.

Rahn, R.O. Potassium Iodide as a Chemical Actinometer for 254 nm Radiation: Use of Iodate as an Electron Scavenger. *Photochemistry and Photobiology* **1997**, 66(4), pp. 450-455.

Rahn, R.O.; Echols, S. 2010. Iodide/Iodate Chemical Actinometry Using Spherical Vessels for Radiation Exposure as Well as for Monitoring Absorbance Changes. *Photochemistry and Photobiology* **2010**, 86, 990-993.

Rahn, R.O.; Stefan, M.I.; Bolton, J.R.; Goren, E.; Shaw, P.; Lykke, K.R. Quantum Yield of the Iodide-iodate Chemical Actinometer: Dependence on Wavelength and Concentration. *Photochemistry and Photobiology* **2003**, 82, 611-615.

Rahn, R.O.; Bolton, J.R.; Stefan, M.I. The Iodide/Iodate Actinometer in UV Disinfection: Determination of the Fluence Rate Distribution in UV reactors. *Photochemistry and Photobiology* **2006**, 78(2), 146-152.

Rahn, R.O.; Gerstenberg, H.M.; Vavrina, G.A. "Dosimetry of Ionizing Radiation using an Iodide/Iodate Aqueous Solution. *Applied Radiation and Isotopes* **2002**, 56, 525-534.

Rahn, R.O.; Xu, P.; Miller, S.L. Dosimetry of Room-Air Germicidal (254 nm) Radiation Using Spherical Actinometry. *Photochemistry and Photobiology* **1999,** 70 (3), 314-318.

Reichl, C.; Buchner, C.; Hirschmann, G.; Sommer, R.; Cabaj, A. Development of a Simulation Method to Predict UV Disinfection Reactor Performance and Comparison to Biodosimetric Measurements in *Conference on Modelling Fluid Flow (CMFF'06) The 13th International Conference on Fluid Flow Technologies* **2006,** Budapest, Hungary,

Richardson, L.F. The Approximate Arithmetical Solution by Finite Differences of Physical Problems Involving Differential Equations, with an Application to the Stresses in a Masonry Dam. *Phil Trans R Soc London* **1910**, Series A; 210, 307-57.

Sahu, A.K.; Kumar, P.; Patwardhan, A.W.; Joshi, J.B. CFD Modelling and Mixing in Stirred Tanks. *Chemical Engineering Science* **1999**, 54 (13-14), 2285-2293.

Sanchez-Moreno, C.; Plaza, L.; Elez-Martinez, P.; Ancoz, B.D.; Martin-Belloso, O.; Cano, M.P. (2005). Impact of High Pressure and Pulsed Electric Fields on Bioactive Compounds and Antioxidant Activity of Orange Juice in Comparison with Traditional Thermal Processing. Journal of Agricultural and Food Chemistry **2005**, 53, 4403-4409.

Schaldach, G.; Berger, L.; Razilov, I.; Berndt, H. Computer Simulation for Fundamental Studies and Optimisation of ICP Spray Chambers. *ISAS (Institute of Spectrochemistry and Applied Spectroscopy) Current Research Reports* **2000**, Berlin, Germany.

Scheible O. K.; Bassel C.D. Ultraviolet Disinfection of a Secondary Wastewater Treatment Plant Effluent. *EPA publ. no. 600/S2-81-52. U.S.* **1981**, Environmental Protection Agency, Washington, D. C.

Scott, C.M. Computational Fluid Dynamics for the Food Industry. *Food Technol. Int Eur*. **1994**, 49-51

Scott, G.; and Richardson, P. The Application of Computational Fluid Dynamics in the Food Industry. *Trends in Food Science & Technology* **1997**, 81, 119-124

Scott, G.M. Computational Flud Dynamics-Modelling the Flow of Newtonian Fluids in Pipelines. *Campden Chorleywood Food Research Association RD Report No. 24,* **1996**, Chipping Campden, UK

Scott, G.M. Simulation of the Flow of Non-Newtonian Foods Using Computational Fluid Dynamics. Campden *Chorleywood Food Research Association RD Report No. 34* **1997**, Chipplng Campden, UK

Seliger, H.H. Chemiluminescence of H_2O_2-NaOCl Solutions. *Journal of Chemical Physics* **1964**, 40, 3133-3134

Sethian, J.A., Computational fluid dynamics. In: From Desktop to Teraflop: Exploiting the US Lead in High Performance Computing. NSF Publications, *National Science Foundation* **1993**, Washington, DC, USA.

Severin, B.F. Disinfection of Municipal Wastewater Effluents with Ultraviolet Light. *Journal of the Water Pollution Control Federation* **1980**, 52, 2007-2018.

Shama, G. Process Challenges in Applying Low Doses of Ultraviolet Light to Fresh Produce for Eliciting Beneficial Hormetic Responses. *Postharvest Biology and Technology* **2007**, 44, 1-8.

Shang, J.S. Three Decades of Accomplishments in Computational Fluid Dynamics. *Progress in Aerospace Sciences* **2004**, 40, 173-197.

Shaw, P.E.; Moshonas, M.; Nisperos-Carriedo, M.O.; Controlled Atmosphere Storage Effects on the Composition of Volatile Components in Dancy Mandarin and Mandarin Hybrid Fruit. *LWT* **1992a**, 25, 346-349.

Shaw, P.E.; Moshonas, M.; Nisperos-Carriedo, M.; Carter, R.D. Controlled-Atmosphere Treatment of Freshly Harvested Oranges at Elevated Temperature to Increase Volatile Flavor Components. *Journal of Agricultural and Food Chemistry* **1992b**, 40, 1041-1045.

Sommer, R.; Cabaj, A.; Pribil, W.; Haider, T. Influence of Lamp Intensity and Water Transmittance on the UV Disinfection of Water. *Water Science and Technology* **1998**, 35(11-12). 113-118.

Sosnin, E.A.; Oppenländer, T.; Tarasenko, V.F. Applications of Capacitive and Barrier Discharge Excilamps in Photoscience. *Journal of Photochemistry and Photobiology C: Photochemistry Reviews* **2006**, 7, 145-163.

Sozzi, D.A.; Taghipour, F. Experimental Investigation of Flow Field in Annular Ultraviolet Reactors Using Particle Image Velocimetry. *Industrial & Engineering Chemistry Research* **2005**, 44, 9979-9988.

Sozzi, D.A; Taghipour, F. UV Reactor Performance Modeling by Eulerian and Lagrangian Methods. *Environmental Science Technology* **2006**, 40, 1609-1615.

Stone, G.; Chapman, B.; Lovell, D. Development of a Log-Quadratic Model to Describe Microbial Inactivation, Illustrated by Thermal Inactivation of *Clostridium botulinum*. *Applied and Environmental Microbiology* **2009**, 75(22), 6998-7005.

Sun, S.H.; Keener, R.; Towell, R.; Michel, F.C. Two-Dimensional Computational Fluid Dynamics (CFD) Modeling of Air and Ammonia Distribution in a High-RiseTM Hog Building (HRHB). *Transactions of the ASAE*. **2002**, 45(5),1559-1568.

Taghipour, F. Ultraviolet and Ionizing Radiation for Microorganism Inactivation. *Water Resources* **2004**, 38, 3940-3948.

Taghipour, F.; Sozzi, A. Modeling and Design of Ultraviolet Reactors for Disinfection by-Product Precursor Removal. *Desalination* **2001**, 176, 71-80.

Tchobanoglous, G.L.F.; Darby, J.; Devries, M. UV Design: Comparison of Probabilistic and Deterministic Design Approaches. *Water Science and Technology* **1996**, 33(10-11), 251-260.

Telis-Romero, J.; Thomas, C.E.P.; Bernardi, M.; Telis, V.R.N.; Gabas, A.L. Rheological Properties and Fluid Dynamics of Egg Yolk. *Journal of Food Engineering* **2006**, 74, 191-197.

Templeton, M.R.; Andrews, R.C.; Hofmann, R. Impact of Iron Particles in Groundwater on the UV Inactivation of Bacteriophages MS2 and T4. *Journal of Applied Microbiology*, **2006**, 101, 732-741.

Thayer, D.W.; Boyd, G. Effect of Irradiation Temperature in Inactivation of *Escherichia coli* O57:H7 and *Staphylococcus aureus*. *Journal of Food Protection* **2001**, 64(10), 1624-1626

Timmermans, R.A.H.; Mastwijk, H.C.; Knol, J.J.; Quataert, M.C.J.; Vervoort, L.; Van der Plancken, I.; Hendrickx, M.E.; Matser, A.M. Comparing Equivalent Thermal, High Pressure and Pulsed Electric Field Processes for Mild Pasteurization of Orange Juice. Part I: Impact on Overall Quality Attributes. *Innovative Food Science and Emerging Technologies* **2011**, 12, 235-243.

Tiwari, B.K.; O'Donnel, C.P.; Muthukumarappan, K.; Cullen, P.J. Anthocyanin and Colour Degradation in Ozone-Treated Blackberry Juice. *Innovative Food Science and Emerging Tehnology* **2009a**, 10(1), 70-75.

Tiwari, B.K.; O'Donnel, C.P.; Muthukumarappan, K.; Cullen, P.J. Effect of Ozone Processing on Anthocyanins and Ascorbic Acid Degradation of Strawberry Juice. *Food Chemistry* **2009b**, 113(4), 1119-1126.

Torkamani, A. E.; Niakousari, M. Impact of UV-C Light on Orange Juice Quality and Shelf Life. *International Food Research Journal* **2011**, 18(4), 1265-1268.

Tornaletti S. Transcription Arrest at DNA Damage Sites. *Mutation Research* **2005**, 577, 131-145.

Tran, M.T.; Farid, M. Ultraviolet Treatment of Orange Juice. *Innovative Food Science Emerging Technology* **2004**, 5, 495-502.

Triassi, M.; Di Popolo, A.; Ribera D'Alcalà, G. Clinical and Environmental Distribution of *Legionella pneumophila* in a University Hospital in Italy: Efficacy of Ultraviolet Disinfection *Journal of Hospital Infection* **2006**, 6(4), 494-501.

U.S. Environmental Protection Agency. *Ultraviolet Light Disinfection Technology in Drinking Water Application-An Overview* **1996**, Office of Water: Washington, D.C. EPA/811-R-96-002.

U.S. Environmental Protection Agency. *Small System Compliance Technology List for the Surface Water Treatment Rule and Total Coliform Rule* **1998**, Office of Water: Washington,

Ugarte-Romero, E.; Feng, H.; Martin, S.E.; Cadwallader, K.R.; Robinson, S.J. Inactivation of *Escherichia coli* with Power Ultrasound in Apple Cider. *Journal of Food Science* **2006**, 71(2), E102-108.

Ukuku, D.O.; Geveke. D.J. A Combined Treatment of UV-Light and Radio Frequency Electric Field for the Inactivation of *Escherichia coli* K-12 in Apple Juice. *International Journal of Food Microbiology* **2010**, 138, 50-55.

Unluturk, S. K.; Arastoopur, H.; Koutchma, T. Modeling of UV Dose Distribution in a Thin-Film UV Reactor for Processing of Apple Cider. *Journal of Food Engineering* **2004**, 65(1), 125-136.

Unluturk, S.; Atilgan, M.R.; Baysal, A.H.; Tari, C. Use of UV-C Radiation as a Non-Thermal Process for Liquid Egg Products (LEP). *Journal of Food Engineering* **2008**, 85(4), 561-568.

Unluturk, S.; Atilgan, M.R.; Baysal, A.H.; Unluturk, M.S. Modeling Inactivation Kinetics of Liquid Egg White Exposed to UV-C Irradiation. *International Journal of Food Microbiology* **2010**, 142(3), 341-347.

USFDA. Hazard Analysis and Critical Control Point (HACCP): Procedures for the Safe and Sanitary Processing and Importing of Juice-Final Rule. *Federal Register* **2001**, U.S. Food and Drug Administration, Washington, DC, 66, 13.

Van Boekel, M.A.J.S. On the use of the Weibull Model to Describe Thermal Inactivation of Microbial Vegetative Cells. *International Journal of Food Microbiology* **2002**, 74, 139-159.

Versteeg, H.K.; Malalasekera, W. Solution Algoriths for Pressure-Velocity Coupling in Steady Flows" In: Versteeg (Ed.). *An Introduction to Computational Fluid Dynamics The Finite Volume Method* **1995**, England, Longman Scientific Technical, 135-154.

Walking-Ribeiro, M.; Noci, F.; Cronin, D.A.; Riener, J.; Lyng, J.G.; Morgan. D.J. Reduction of *Staphylococcus aureus* and Quality Changes in Apple Juice Processed by Ultraviolet Irradiation, Pre-Heating and Pulsed Electric Fields. *Journal of Food Engineering* **2008**, 89, 267-273.

Wang, L.; Sun, D.W. (2003). Recent Developments in Numerical Modelling of Heating and Cooling Processes in the Food Industry: A Review. *Trends in Food Science and Technology* **2003**, 14, 408-423.

Wareing, P.; Davenport, R.R., *Microbiology of Soft Drinks and Fruit Juices, in Chemistry and Technology of Soft Drinks and Fruit Juices* **2007**, Blackwell, Publishing Ltd, Oxford, UK.

Watson, H.E. A Note on the Variation of the Rate of Disinfection with Change in the Concentration of the Disinfectant. *The Journal of Hygiene* **1908**, 8(4), 536-542.

Welti-Chanes, J.; Ochoa-Velasco, C.E.; Guerrero-Beltrán, J.Á. High-Pressure Homogenization of Orange Juice to Inactivate Pectinmethylesterase. *Innovative Food Science & Emerging Technologies* **2009**, 10(4), 457-462

Wols, B.A.; Shao, L.; Uijttewaal, W.S.J.; Hofman, J.A.M.H.; Rietveld, L.C.; Van Dijk, J.C. Evaluation of Experimental Techniques to Validate Numerical Computations of the Hydraulics inside a UV Bench-Scale Reactor. *Chemical Engineering Science* **2010**, 65(5), 4491–4502

Wong, E.; Linton, R.H.; Gerrard, D. E. Reduction of *E.coli* and *S. seftenberg* on Pork Skin and Pork Muscle Using Ultraviolet Light. *Food Microbiology* **1998**, 15(4), 415-423.

Wong, W.C.; Pui, C.F.; Chai, L.C.; Lee, H.Y.; Ghazali, F.M.; Tang, J.Y H.; Ponniah, J.; Tuan-Zainazor, T.C.; Cheah, Y.K.; Son, R. Biosafety Assessment of *Listeria monocytogenes* in Vegetarian Burger Patties in Malaysia. *International Food Research Journal* **2011**, 18, 459-464

Worley, M.S.; Manbeck, H.B. Modelling Particle Transport and Air Flow in Ceiling Inlet Ventilation Systems. *Transactions of the ASAE* **1995**, 38(1), 231-239.

Wright, N.G; Hargreaves, D.M. The Use of CFD in the Evaluation of UV Treatment. Systems. *Journal of Hydroinformatics* **2001**, 3,(2), 59-70.

Wright, J.R.; Sumner, S.S.; Hackney, C.R.; Pierson, M.D.; Zoecklein, B.W. "Efficacy of Ultraviolet Light for Reducing *Escherichia coli* O157:H7 in Unpasteurized Apple Cider. *Journal of Food Protection* **2000**, 63, 563-567.

Wrigley, D.M.; Llorca, N.G. Decrease of *Salmonella typhimurium* in Skim Milk and Egg by Heat and Ultrasonic Wave Treatment. *Journal of Food Protection* **1992**, 55, 678-680.

Wyckomar UV Purification Systems' web site, (Accessed in **2007**). http://www.wyckomaruv.com/Ultraviolet%20Sterilization%20Technology.pdf

Wu, Y.G.S.; Griffiths, M.W. Effect of Pulsed Electric Field on the Inactivation of Microorganisms in Grape Juices with and without Antimicrobials. *Biosystems Engineering* **2005**, 90(1), 1-7.

Xia, B.; Sun, D. Applications of Computational Fluid Dynamics (CFD) in the Food Industry: A Review. *Computers and Electronics in Agriculture* **2002**, 34, 5-24

Yaun, B.R.; Sumner, S.S.; Eifert, J.D.; Marcy, J.E. Response of *Salmonella* and *Escherichia coli* O157:H7 to UV Energy. *Journal of Food Protection* **2003**, 66(6), 1071-1073.

Ye, Z.; Forney, L.J.; Koutchma, T.; Giorges, A.T.; Pierson, J.A. Optimum UV Disinfection between Concentric Cylinders. *Industrial Engineering Chemistry* **2008**, 47(1), 3444-3452.

VITA

Mehmet Reşat Atılgan was born on December 22 1981 in İzmir, Turkey. He graduated from Buca Anatolian Technical High School (İzmir, Turkey), Department of Mechanic in 1999. Then he started İzmir Institute of Technology, Department of Chemical Engineering (İzmir, Turkey) in fall semester of 1999. He graduated with a Bachelor of Science degree as chemical engineer in spring semester of 2004. He worked as chief of ready-to eat foods in Tesco-Kipa shopping center (Balçova, Turkey) on June-September of 2004. He was approved to İzmir Institute of Technology, Graduate School from Engineering and Science, Biotechnology and Bioengineering Master of Science program and started in fall semester of 2004. Also he worked as cashier in Tansaş shopping center between September 2004-April 2005. He was admitted as research assistant in fall semester of 2005. He has studied non-thermal UV-C inactivation of liquid egg products in master of science period. He graduated Biotechnology and Bioengineering MSc program in spring semester of 2007. Then he was approved to İzmir Institute of Technology, Food Engineering PhD program in fall semester of 2007. He has worked as research assistant in Graduate School of Engineering and Science since 2005 November. He is a citizen of Turkey and married.